May 2021

Modeling the Abrasion and Transport of Mud Aggregates in the James River, Virginia

Jonathan C. Hollingsworth
Clemson University, Joncrofthollingsworth@gmail.com

MODELING THE ABRASION AND TRANSPORT OF MUD AGGREGATES IN THE JAMES RIVER, VIRGINIA

A Thesis
Presented to
the Graduate School of
Clemson University

In Partial Fulfillment
of the Requirements for the Degree
Master of Science
Civil Engineering

---

by
Jonathan C. Hollingsworth
May 2021

Accepted by:
Dr. Abdul Khan, Committee Chair
Dr. Earl Hayter
Dr. Nigel Kaye
Dr. Jarrell Smith

ABSTRACT

Recent research has found that dredged material placed in rivers and estuaries tends to erode as aggregated particles as opposed to individual particles. These aggregated particles, or mud aggregates, are then observed to undergo abrasion during bedload transport. Testing of these mud aggregates in an aggregate tumbler and a flume suggested that the aggregates could only travel a few kilometers before losing over approximately 90% of their effective diameter due to abrasion (Perkey *et al.,* 2019). Current sediment transport models do not simulate the process of abrasion.

An aggregate abrasion routine was derived from existing research and then added to a one-dimensional (1-D) sediment transport model developed during this research and to an existing three-dimensional (3-D) sediment transport model. The abrasion routine was developed to simulate the abrasion of mud aggregates that were being transported as bedload. Instead of changing the diameter of the aggregate as it is transported and undergoes abrasion, abrasion was simulated by transferring mass from aggregates moving as bedload to the next smallest aggregate size class as well as to a 20 μm aggregate size class representing the byproduct of abrasion. As the 1-D and 3-D sediment transport models use a Eulerian grid, transferring mass between size classes allowed the abrasion routine to be used in a Eulerian grid, as opposed to using a Lagrangian time frame where the diameter of each individual aggregate would decrease while being transported as bedload.

Using the 1-D sediment transport model, the simulations involving the abrasion routine increased the total mass of suspended load of the mud aggregates by 0.5% to 1% and decreased the total bedload mass of the aggregates by 0.25% to 0.5% over an hour-long simulation in a closed system.

Using a 3-D sediment transport model of the James River, the inclusion of the abrasion routine to the simulation resulted in the bedload concentrations of the two largest mud aggregate size classes, analyzed at 1.2 km and 2.2 km away from the center of area of the placement site, to be less than 5% of the bedload concentrations given by the model simulation without abrasion when compared at each time step during a 15-day simulation. This indicated that the mud aggregates in bedload were losing over 95% of their mass within the first few kilometers of transport due to abrasion, which was expected based on prior research by Perkey *et al.* (2019).

In the portions of the navigation channel that were analyzed, all within 11 km of the placement site, the inclusion of the abrasion routine to the simulation resulted in approximately a 55% to 75% decrease in total mass of mud aggregates in the sediment bed compared to the simulation without abrasion when using a 15-day, 3-D sediment transport model of the James River. This was due to the abrasion routine transferring mass from larger mud aggregates in bedload to smaller mud aggregates, primarily in suspension, that were less likely to deposit.

ACKNOWLEDGMENTS

I would like to thank Dr. Khan and Dr. Kaye for challenging me in your classes and supporting me throughout my time at Clemson. I would like to thank the U.S. Army Engineer Research and Development Center for providing me the opportunity to pursue this research and work with some great people. I would like thank Dr. Jarrell Smith and David Perkey for introducing me to their research on the erosion, transport, and abrasion of mud aggregates and for guiding me throughout my research on the topic. Lastly, I would like thank Dr. Hayter for all his support, time, and guidance during my time in graduate school. His work ethic and dedication to his craft will always be something that I will strive to match in my career.

TABLE OF CONTENTS

Page

Table of Contents (Continued)

LIST OF TABLES

List of Tables (Continued)

Table Page

LIST OF FIGURES

List of Figures (Continued)

Figure Page

List of Figures (Continued)

Figure Page

List of Figures (Continued)

Figure Page

List of Figures (Continued)

Figure Page

CHAPTER ONE

INTRODUCTION

Maintaining waterways and ports in coastal areas is an essential mission to the United States Army Corp of Engineers (USACE). Removing sediment accumulated in these waters, dredging, is facilitated by the USACE and is considered to be their main strategy to maintain navigation lanes and waterways. While the need for dredging is essential, dredging sediment does increase the difficulty of predicting sediment transport in waterways. Numerical models are frequently used for the prediction of sediment transport over several years. Understanding where and when sediment will eventually deposit is crucial knowledge to the USACE in order to plan and budget dredging operations. The sediment beds in these waterways and ports are made up of fine and coarse material such as clay, silt, sand, and gravel. Additionally, the presence of cohesive material, such as clay and fine silt, are also present, increasing complexity of the simulation of sediment transport in waterways and ports. Existing models consider sediment being transported to remain a constant size. However, recent research has shown that cohesive sediment aggregated together, which will be henceforth referred to as mud aggregates, do in fact decrease in size when traveling as bedload due to abrasion (Perkey *et al.,* 2020). This thesis will focus on simulating the abrasion and subsequent transport of mud aggregates and identifying if adding the simulation of abrasion to current sediment transport models is necessary.

PROBLEM STATEMENT

Maintaining navigable waterways and ports by dredging is a crucial responsibility of the USACE. Further, the USACE is always trying to find ways to decrease the costs of dredging. For example, in the case of the James River, one of the major tributaries of the Chesapeake Bay, the cheapest and most efficient strategy to dredge the navigation channel is to place the dredged material along the channel in selected dredged material placement sites.

Estuaries are naturally a setting where large amounts of cohesive sediments can settle due to sediment transported by ebb and flood tides (Guillou *et al*., 2011). During periods of slack water, the sediments can settle to the bed and consolidate. Observations over time show that erosion from consolidated beds is often eroded as "chunks." These "chunks" will be referred to as mud aggregates and the type of this erosion will be referred to as mass erosion. This is significant because transport of mud aggregates is vastly different than that of disaggregated particles. These differences include frequency of erosion and whether it is transported as bedload or suspended load (Perkey *et al.,* 2019). Prior research has shown that mud aggregates could only travel 10-100's of meters after mass erosion occurred, but recent research has demonstrated that the distanced traveled could be kilometers (Perkey *et al.,* 2019). Concern regarding beds eroding as mud aggregates originated since current numerical models do not represent sediment as mud aggregates, only individual sediment particles, thus potentially leading to inaccurate predictions about sediment transport in estuaries and navigation waterways. The USACE uses these predictions to assist in planning and budgeting future dredging and locations of

placement sites, so accurate models of sediment transport are essential to the mission of the USACE. While current models are considered accurate, incorporating the modeling of mud aggregates and abrasion of these aggregates could potentially increase the accuracy further.

GOALS AND OBJECTIVES

- Goal: To simulate the transport and abrasion of mud aggregates in the James River.
    - Objective: Develop an algorithm to represent the abrasion of mud aggregates.
    - Objective: Verify the algorithms by developing a 1-dimensional sediment transport model.
    - Objective: Perform multi-tidal cycle simulations using the James River model to compare differences between the existing model and the new model.

JAMES RIVER

The James River is located on the eastern coast of the United States of America. The mouth of the James River is located in Chesapeake Bay, off the coast of Virginia, as shown in Figure 1.1 and Figure 1.2. The area of interest is located in the red box in each figure.

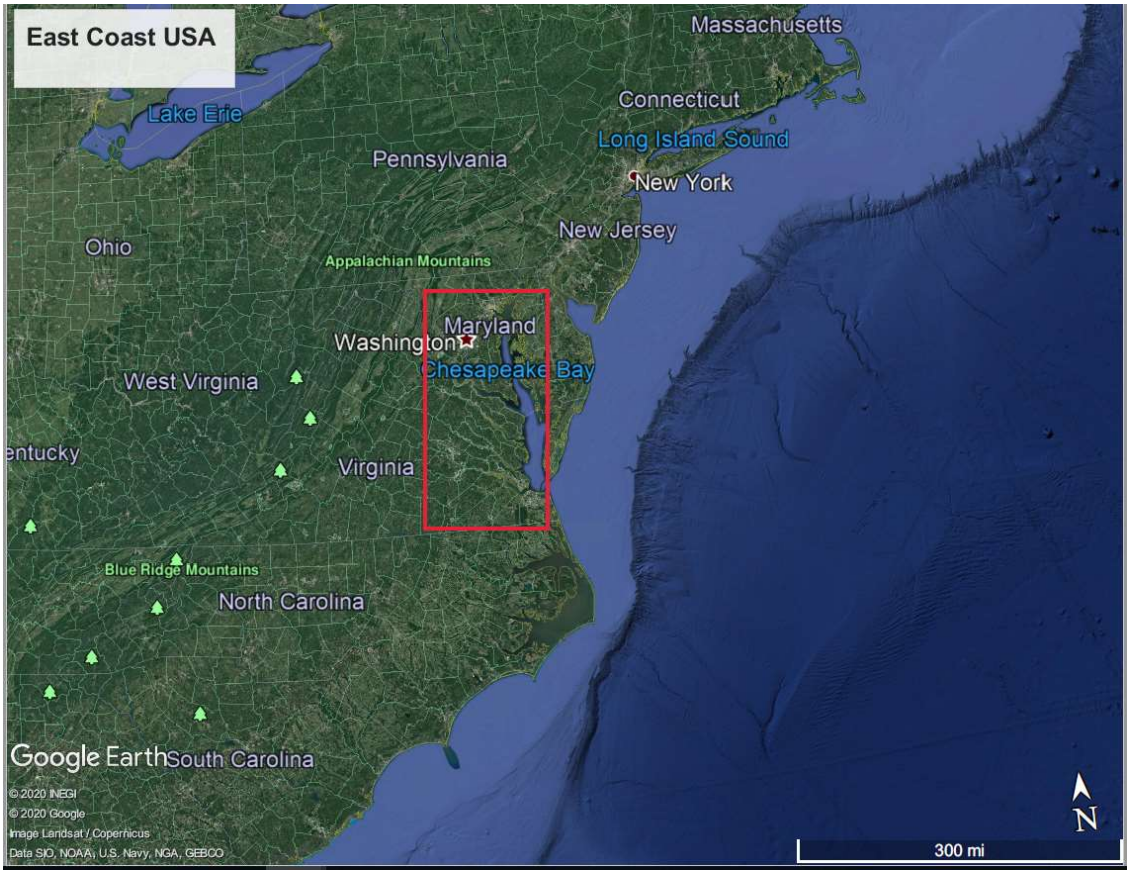

Figure 1.1: East Coast of United States

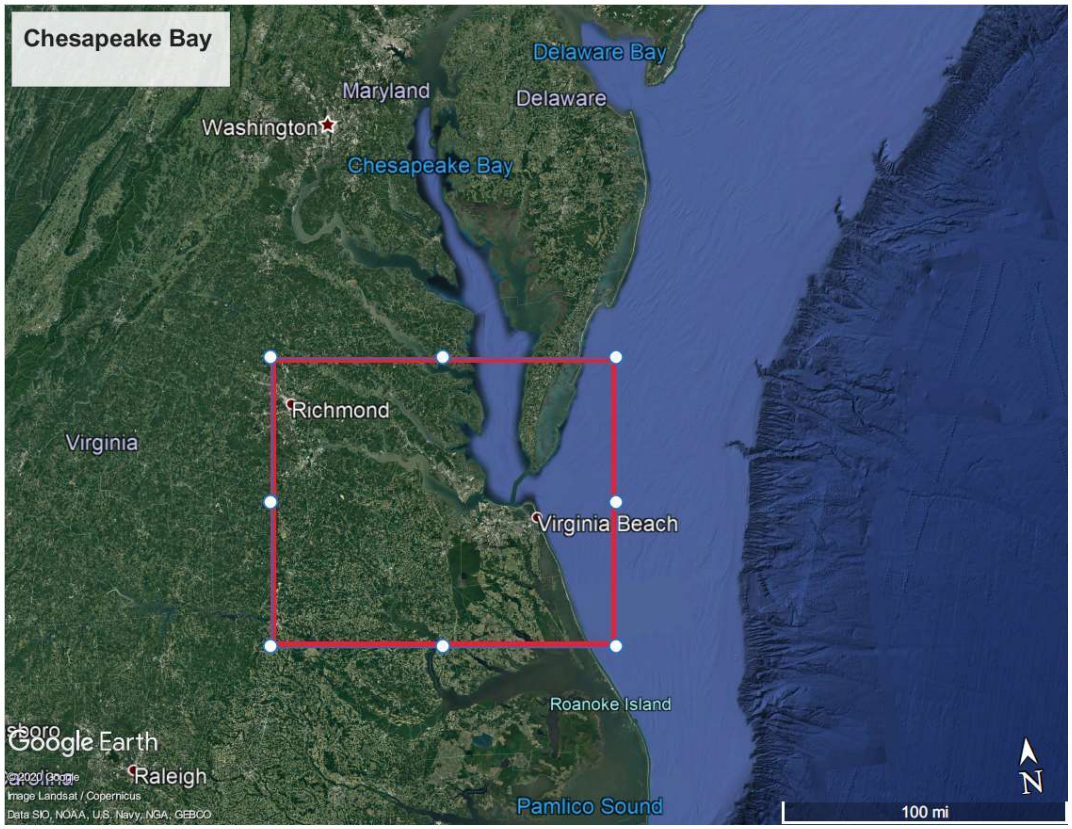

Figure 1.2: Chesapeake Bay

The section of James River that is being researched in this thesis is the portion of the river influenced by the tide. The James River federal navigation channel is maintained by the USACE is 90 miles long, running from Richmond to the Chesapeake Bay (Perkey *et al.,* 2019). Figure 1.3 shows where the new dredged material placement site will be located which will also be the location of the dredged material placement site in this thesis. This study site is classified as a partially mixed estuary, meaning there is mixing due to density differences of fresh water and salt water. Since the study reach of the James River is classified as an estuary, the hydrodynamic and sediment transport models needed to simulate flow and transport are more complex because the models must

simulate the density differences over the water column due to vertical salinity, temperature differences and most importantly, the tidal cycles. Partially mixed estuaries are also water bodies where sediment tends to settle. In the case of the area of interest in the James River, sediment transported downstream in the James River will deposit on top on sediment transported upstream from the Chesapeake Bay due to the tidal cycles (Perkey *et al.,* 2020). Accumulation rates in the estuary are as high as 11 cm/yr, and on average are around 0.5 cm/yr and the discharge of the James River is usually between 150 m^3/s and 270 m^3/s. The sediment bed in the study reach in the middle James River is primarily made up of mixed gravel, sand, silt, and clay, and has depths ranging from 0.5 m to 30 m, with an average of 6 m (Perkey *et al.,* 2020).

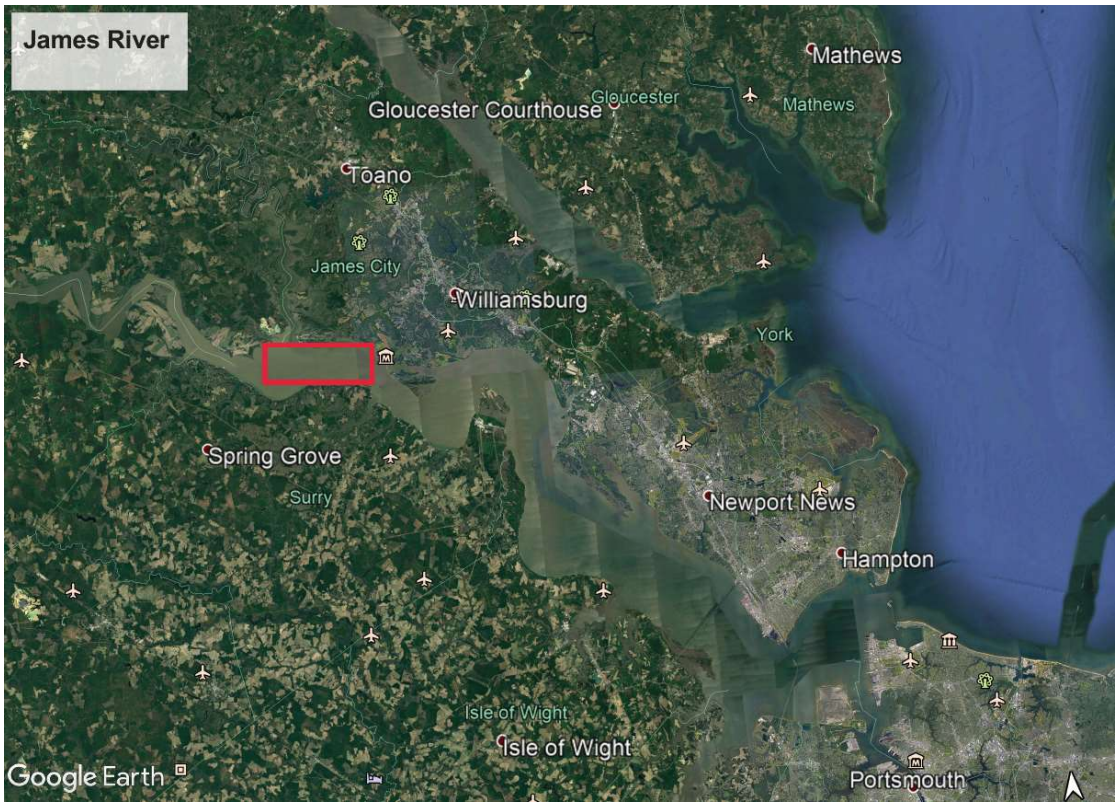

Figure 1.3: James River Placement Site Location

CHAPTER TWO

LITERATURE REVIEW

AGGREGATE RESEARCH

Before a sediment transport model can be created, there needs to be an understanding of the materials and processes that the model is attempting to simulate. In the case of the James River, an understanding of cohesive sediment transport is essential in the creation of the model. This literature review of aggregates will first analyze cohesive sediments and then give an overview of the properties of mud aggregates that are composed of mostly cohesive sediments. After the overview of cohesive sediments, research that is relevant to the new aggregate abrasion model is reviewed.

A limitation of current sediment transport models is that they do not simulate abrasion of mud aggregates. Mud aggregates are pieces of the riverbed that have eroded in chunks instead of as individual particles. Researchers and modelers have been aware that erosion can occur as mud aggregates, but not much has been done to incorporate abrasion of mud aggregates into existing sediment transport models. This is because, up until recently, there has not been sufficient research to predict the frequency that mud aggregates will erode, how long they can travel before being fully abraded, and how they will be transported. David Perkey and Dr. Jarrell Smith, Research Hydraulic Engineers at the USACE Engineer Research and Development Center's Coastal and Hydraulics Laboratory, have recently completed research involving mud aggregates (Perkey *et al.,* 2020). They researched the frequency that erosion of mud aggregates would take place.

They then researched the durability of mud aggregates to see how far they could travel before eroding down to particles small enough that are only transported as suspended load. In their research, there were two different sets of "sub-experiments." One experiment set uses sediment specific to the James River, and the other set uses sediment from different sites across the United States to see if the results were location dependent.

The research specific to the James River began with taking sediment cores directly from the river. These cores were then run through a variety of different tests. A visual description of the uses of the core samples can be seen in Figure 2.1. An explanation of these tests will be discussed next.

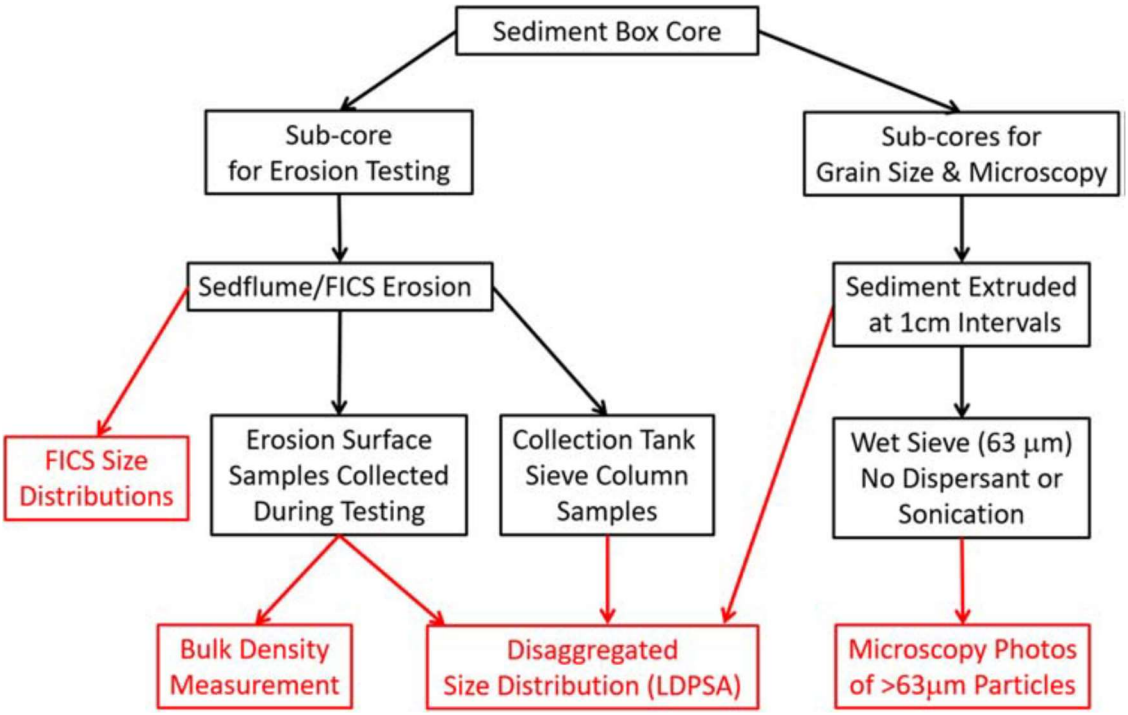

Figure 2.1: Visual Description of Uses of Sediment Cores from James River (Perkey *et al.,* 2020).

The main equipment used in these experiments is a USACE developed Sedflume (Perkey *et al.,* 2020). A Sedflume is a device that can measure erosion rates by varying flows through the flume and observing the erosion of sample cores that are slowly eroded in the flume. There were three different techniques used to obtain a grain size distribution of the eroded sediment: a flume imaging camera system (FICS), laser diffraction particle size analysis (LDPSA) and microscopy imaging. FICS distributions were obtained by videos taken of the eroded material by high performance cameras placed above the Sedflume and sediment core. The LDPSA analysis was completed once the eroded material was transported through the flume into a collection container. Microscopy imaging was done by observing and taking pictures of the mud aggregates that were collected by the sieves shown in Figure 2.2 (Perkey *et al.,* 2020). A schematic drawing of the Sedflume is also given in Figure 2.2.

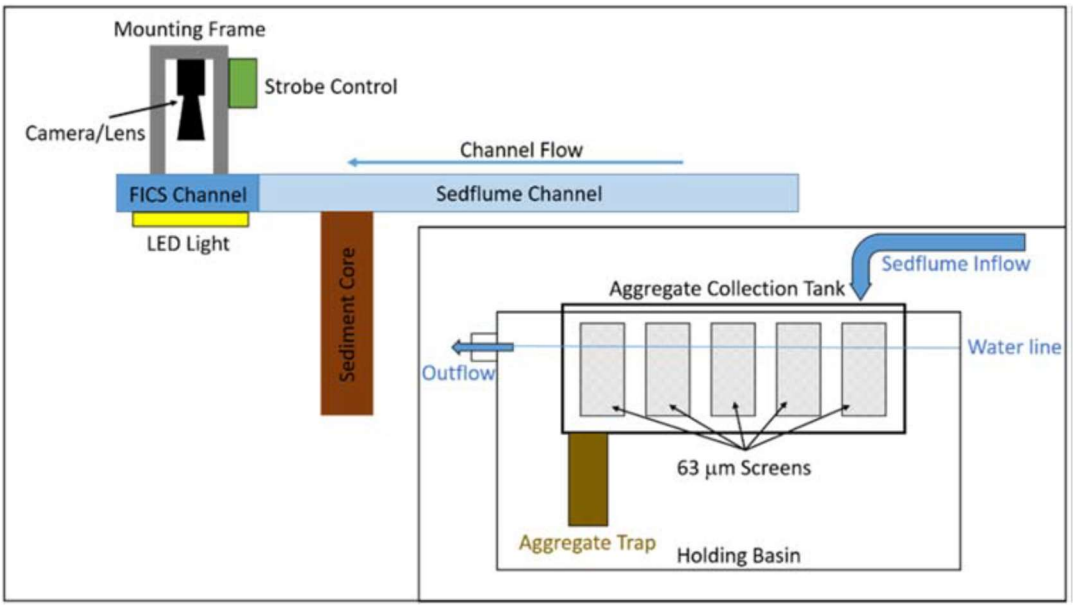

Figure 2.2: USACE Sedflume (Perkey *et al.,* 2020).

After data were collected from the Sedflume experiments, the research continued by obtaining simulated velocities and depths, using the Geospatial Scale Transport Multi-Block Modeling System (GSMB), which will be discussed in more depth later in this thesis, to predict sediment transport modes of both mud aggregates found in the Sedflume tests as well as individual sediment particles (Perkey *et al.,* 2020). The mud aggregates were typically between 50 to 10,000 μm and the individual particles were between 4 to 63 μm (Perkey *et al.,* 2020). Using the modified Shields criterion, the modified Stokes particle-settling relationship, and results from the CH3D model, a non-dimensional Rouse number, *P*, was calculated which classified sediment or mud aggregates into different states of motion. The four transport modes simulated were immobile, bedload, incipient suspension, and full suspension (Perkey *et al.,* 2020). Table 2.1 shows the relationships between *P*, bed shear stress τ_b, and critical shear stress τ_c.

Table 2.1: Relationship between *P*, τ_b, and τ_c

Classification	Condition Requirements
Immobile	$\tau_b <= \tau_c$ & $P > 2.5$
Mobile, bedload	$\tau_b >= \tau_c$ & $P > 2.5$
Mobile, incipient suspension	$1 < P <= 2.5$
Mobile, full suspension	$P <= 1$

The research concluded that erosion from the bed does in fact erode as mud aggregates rather than as individual particles. A comparison between FICS and LDPSA grain size distributions confirmed these findings. As stated earlier, FICS grain size distributions are generated by a camera recording the sizes of the eroded mud aggregates and LDPSA grain size distributions are created using the disaggregated particles after the sediment is transported through the flume. The median diameter of the FICS grain size distribution ($D50_F$) was between 50 and 270 times larger than the median diameter of the LDPSA grain size distribution ($D50_L$), indicating that the sample was eroding as mud aggregates which were then disaggregated once they left the flume (Perkey *et al.,* 2020). A plot of the differences of volume fraction between FICS and LDPSA grain size distributions is given in Figure 2.3.

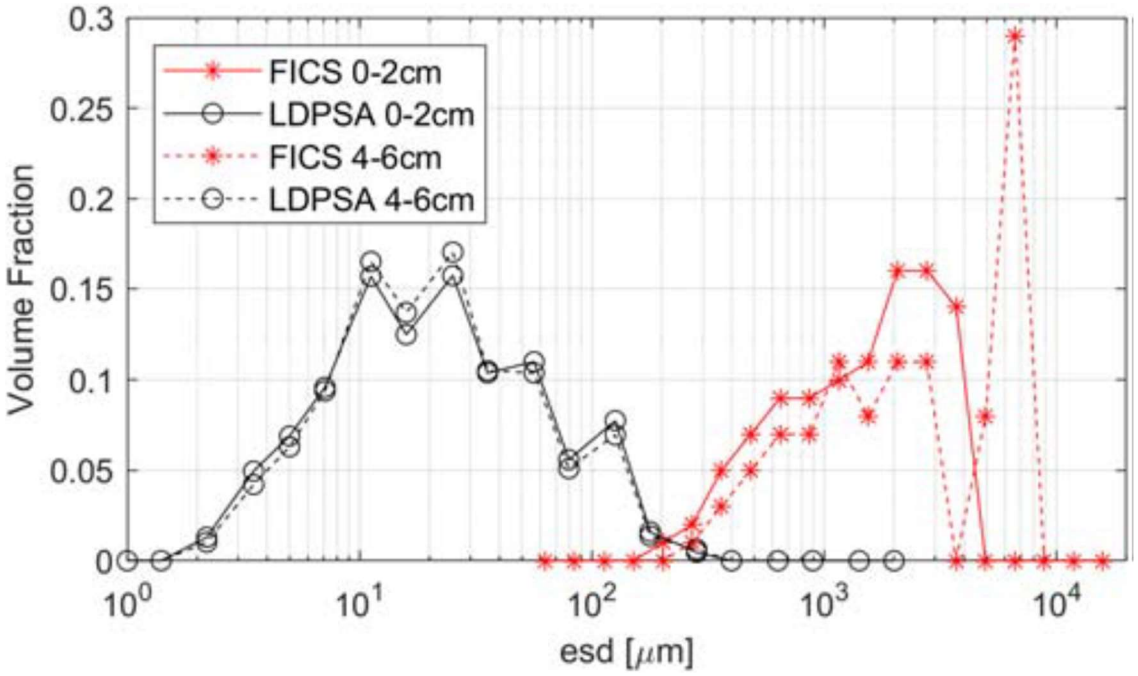

Figure 2.3: Plot of Size Distribution (Perkey *et al.,* 2020).

From the experiments and observations, it was clear that erosion primarily occurred as mud aggregates as opposed to individual particles. What was not clear, however, was the frequency and size of mud aggregates that had eroded from the sediment bed. In the experiment using James River cores by Perkey and Smith, data were plotted for $D50_F$ versus shear stress to see if there was a correlation between $D50_F$ and shear stress. When shear stresses ranging from 0 Pascal's (Pa) to 9 Pa were plotted, there was no significant correlation between these two parameters. However, when the data were plotted for shear stresses under 2 Pa, there was a positive correlation and the R^2 value was 0.17 and the p-value was 0.0006. Since the p-value was less than 0.001, there technically was a statistically significant correlation, but it was a very weak correlation (Perkey *et al.,* 2020). Figure 2.4 shows these two plots.

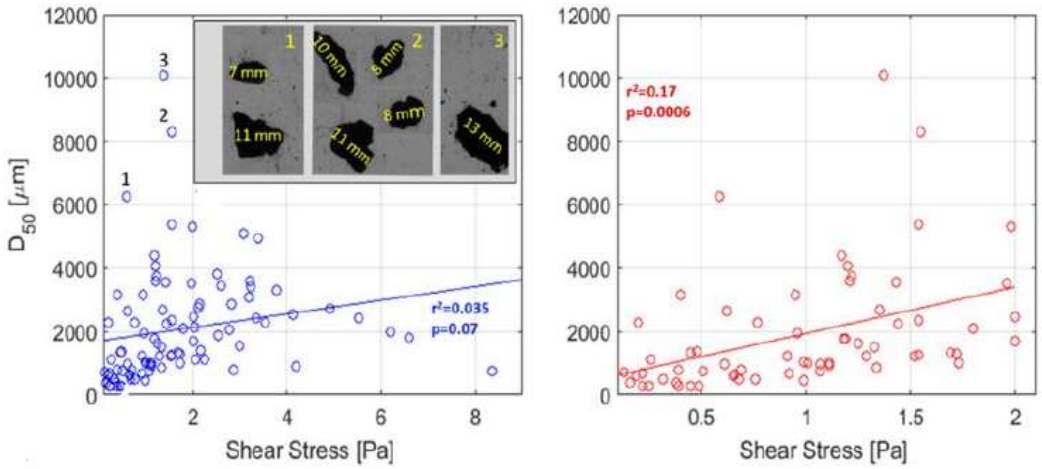

Figure 2.4: Plots of $D50_F$ and Shear Stress (Perkey *et al.,* 2020).

Perhaps the most important result of the James River experiment were the differences in results of sediment transport model runs when modeling mud aggregates compared to individual particles. Using the previously calculated Rouse number, an adjustment was made to the sediment transport model in terms of mode of transport. Figure 2.5 shows the modes of transport of individual particles versus modes of transport of mud aggregates. In the left graph in Figure 2.5, all the individual particles are at most 63 µm in diameter and the vast majority of the particles are transported as suspended load. When the particles are aggregated together, as the graph on the right in Figure 2.5 represents, the mode of transport changes drastically. All the aggregates have a diameter greater than 63 µm, are far more likely to be immobile, are far less likely to be transported as suspended load and may be transported as bedload. Notice that the bulk density of the sediment also changes. 2.65 g/cm^3 is the density of individual sediment particles while 1.25 g/cm^3 is the bulk density of the mud aggregates.

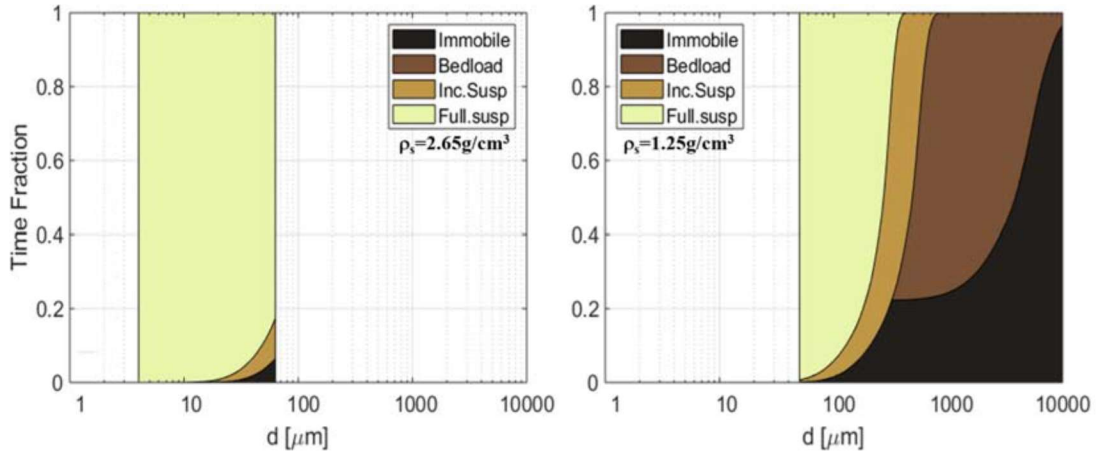

Figure 2.5: Mode of Transport of Individual Particles Versus Mud Aggregates (Perkey *et al.,* 2020).

The differences between the modes of transport of the two models can significantly alter the results from the simulations of sediment transport in the estuary. This could cause issues for the USACE, who relies on the accuracy of these models for life cycle analysis of deposit sites, frequency of dredging, or several other projects in the James River (Perkey *et al.,* 2020).

While the experiments on sediment samples in the James River provided much needed information and data on the erosion of mud aggregates for that location, Perkey and Smith also researched sediment samples across the country. They wanted to observe if there was a better way to predict the erosion size and frequency of mud aggregates in rivers as well as how far these mud aggregates could travel before they break apart due to abrasion. Similar to the James River experiment, the samples taken in other estuaries were tested in a multitude of ways. The samples were tested for properties such as percent clay, percent sand, water content, density, plasticity index, etc. (Perkey *et al.,* 2020). The sample cores were then eroded in the Sedflume where FICS and LDPSA grain size distributions were assembled.

The James River experiment gave the result that mass erosion from a sediment bed does occur and while the correlation between $D50_F$ and bed shear stress was statistically significant, the correlation was not strong enough to use in a model. For the next experiment, the ratio $D50_F/D50_L$ was plotted versus various sample core sediment properties to determine if there was any correlation. This ratio was used because $D50_L$, which is the median diameter of individual particles after they have disaggregated, is a precise measurement that can be easily repeated (Perkey *et al.,* 2020). Table 2.2 shows

the correlation of $D50_F/D50_L$ and different sample core sediment properties, and Figure 2.6 is a plot of $D50_F/D50_L$ versus clay content which had the best correlation.

Table 2.2: $D50_F/D50_L$ Correlation with Different Sediment Properties (Perkey *et al.,* 2020).

Physical Parameter	**r^2**	**p-value(s)**
% Clay	0.82	2.2e-05
% Sand	0.63	0.001
Water content	0.63	0.001
Density	0.48	0.009
Plasticity Index	0.40	0.07
Volume fraction mud	0.07	0.30

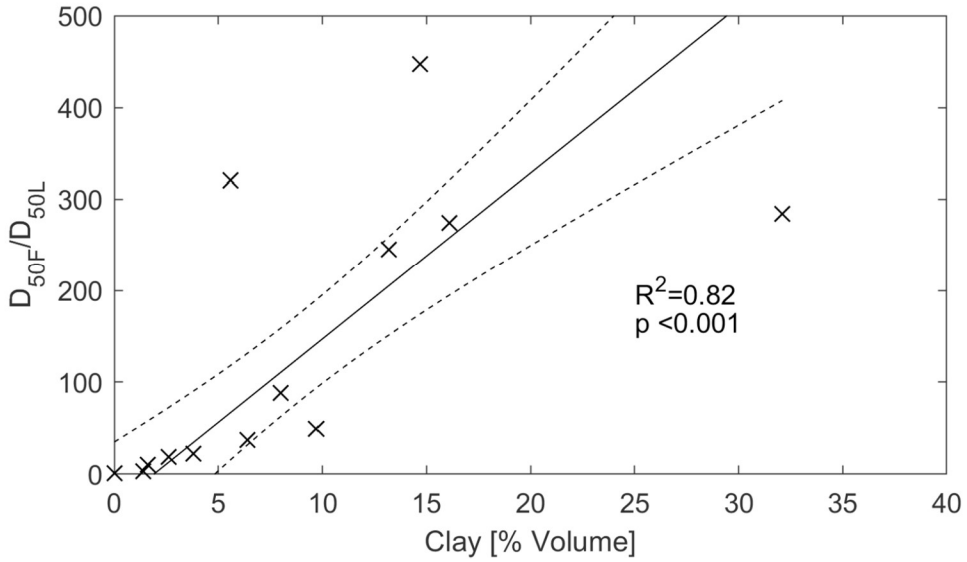

Figure 2.6: $D50_F/D50_L$ Versus Clay Content (Perkey *et al.,* 2020).

In the future, sediment cores from different locations can be tested for properties such as clay content, sand content and water content (the physical parameters with the best correlation to $D50_F/D50_L$) to determine the approximate size of aggregates that erode from the bed. The second experiment that Perkey and Smith completed on mud aggregates from different locations, aggregate durability, will be discussed later in the abrasion section of this chapter.

As mentioned earlier, the James River contains a navigation channel that must be maintained by dredging by the USACE. Dredging the river, while achieving the goal of deepening the channel, can cause unintended consequences such as complications predicting the transport of the dredged material. Dredging can also increase sediment concentration around the dredging and disposal site (Fettweis *et al.,* 2011). Fettweis *et al.,* (2011) wanted to determine if there was a significant increase in suspended particulate matter (SPM) around the disposal sites of dredged material. Their findings, along with the previously reviewed research that sediment beds may erode as mud aggregates, as opposed to individual particles, and then abrade during bedload transport, will give background information to aid in the creation of an aggregate abrasion model that could be added to sediment transport models.

The goal of the research by Fettwies *et al.,* (2011) was to determine if SPM concentrations were affected by dredging. This was accomplished by monitoring SPM concentrations at a location close to the location of the dredging activity and at a location 5 km from the disposal site. Since the variability of SPM concentrations was high,

statistical techniques were used to determine if dredging did increase SPM concentrations (Fettweis *et al.,* 2011). The variability of SPM concentrations is high because there are numerous factors that can cause changes in SPM concentrations such as seasonal changes in river flows, tides, storms, or human activities such as dredging. Statistical outliers would hopefully determine if dredging did cause an increase of SPM concentrations. Measurements of concentration were taken at 0.2 meters above the bed (mab) and 2.0 mab (Fettweis *et al.,* 2011).

To begin, measurements were taken at random times at a specific location to obtain SPM concentrations. A fitted lognormal distribution was then developed for the probability of SPM concentration values at these specific locations at 0.2 mab and 2.0 mab. Visual results from location near the dredging activity showed that a crater that had formed during dredging was now filled in by sediment that had transported into the crater. SPM concentration from the location 5 km away from the disposal site showed that maximum concentrations were 50 times higher than the minimum concentrations, and the peaks in concentration were dominated by the tidal cycle. Statistical analysis showed that there were higher SPM concentrations during disposal, and the mean maximum concentration was 1.7 times higher during disposal than it was during normal monitoring. At 0.2 mab, the median SPM concentration was twice as high during the dredging case compared to the results with no dredging. This could be caused by erosion of mud aggregates, which tend to be transported closer to the bed than disaggregated particles (Fettweis *et al.,* 2011). The increase in concentration of aggregates at 0.2 mab is

potentially significant because all bedload would be transported below 0.2 mab, and this bedload would be undergoing abrasion during transport, which is discussed next.

ABRASION

Previously reviewed research included how aggregates are eroded from the bed and the size of the eroded aggregates. After erosion, mud aggregates are suspected to undergo abrasion during transportation. Along with their research of erosion of the bed as mud aggregates as discussed earlier, David Perkey and Dr. Jarrell Smith also experimented on durability of mud aggregates. Durability of aggregates were tested by running aggregates in a Slake Durability tumbler which can be seen in Figure 2.7.

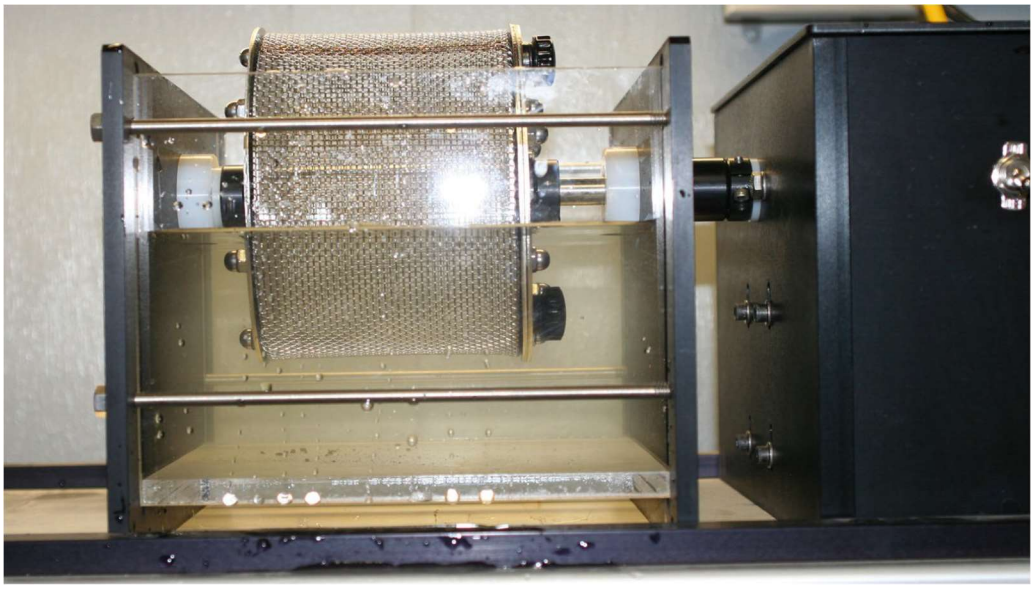

Figure 2.7: Slake Durability Tumbler (Perkey *et al.,* 2020).

The aggregates, all originally greater than 250 µm, were left in the tumbler for 20 minutes and the aggregated mass fraction greater than 250 µm was measured after 2.5 minutes, 5 minutes, 10 minutes, and 20 minutes. The data were then fitted using Equation (2.1) where A is a constant, δ is the tumbling abrasion rate and t is tumbling time (Perkey *et al.,* 2020).

$$F_{MA>} = Ae^{-\delta t} \quad (2.1)$$

An example of a plot of tumble time vs the mass fraction greater than 250 µm can be seen in Figure 2.8 where the mass fraction of aggregates from the James River and aggregates from Seven Mile Island were plotted.

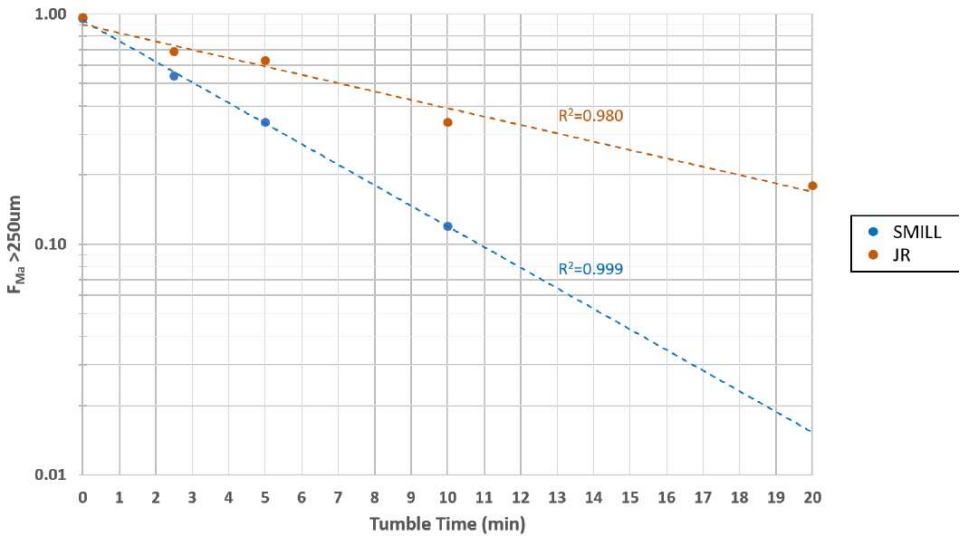

Figure 2.8: Example Plot of Tumble Time vs Mass Fraction Greater than 250 µm (Perkey *et al.,* 2020).

Different δ, in units of 1/time, can be seen in Table 2.3 along with the corresponding water content, *w*. A larger magnitude δ value means the aggregate sample from the different locations abraded faster in the aggregate tumbler. Table 2.4 shows the locations of the sampled cores. Notice the samples were taken from a variety of locations in the United States.

Table 2.3: δ Values from Different Aggregate Samples (Perkey *et al.,* 2020).

Sample Name	**Water content**	**Fraction of Wet Sieve (>250µm)**	**δ**
DH	0.74	0.05	-0.195
ARE45	0.68	0.01	-0.229
ARE60	0.25	0.07	N/A
SMILL	1.02	0.04	-0.206
JR	1.20	0.03	-0.084
MS100	0.99	N/A	-0.217
MS029	0.19	0.01	-0.042
MS021	0.18	0.02	-0.129
MS011	0.13	0.02	N/A
MS003	0.19	0.02	N/A
GP	1.96	N/A	-0.093
CSC	1.27	0.14	-0.231
HSC	0.85	N/A	-0.107

Table 2.4: Locations of Different Samples (Perkey *et al.,* 2020).

Sample Name	Preparation Method	Location	Material Description
DH	Poured Slurry	Duluth Harbor	Dredged Sediment
ARE45	Poured Slurry	Inner Ashtabula Harbor	Native Bottom Sediment
ARE60	Poured Slurry	Outer Ashtabula Harbor	Native Bottom Sediment
SMILL	Poured Slurry	Seven Mile Island	Native Bottom Sediment (Composite)
JR	Poured Slurry	James River	Dredged Sediment
MS100	Poured Slurry	Mississippi River	Lab Prepared Mixture
MS029	Tamped Lifts	Mississippi River	Lab Prepared Mixture
MS021	Tamped Lifts	Mississippi River	Lab Prepared Mixture
MS011	Tamped Lifts	Mississippi River	Lab Prepared Mixture
MS003	Tamped Lifts	Mississippi River	Lab Prepared Mixture
GP	Poured Slurry	Gulfport Entrance Channel	Native Bottom Sediment
CSC	Poured Slurry	Calcasieu Shipping Channel	Native Bottom Sediment (Composite)
HSC	Poured Slurry	Houston Shipping Channel	Dredged Sediment

This aggregate durability experiment can be compared to the research by Parker (1991) that examines the abrasion of gravel. Although Parker's research was related to gravel, it is hypothesized that the same concept can be used with mud aggregates. Parker found that gravel undergoes abrasion as it is transported as bedload, and the byproduct of

the abrasion is silt (Parker 1991). Conservation laws can be used to determine the size of the gravel after a certain distance traveled and how much mass has been converted into silt, which would be transported in suspension.

The transport velocity of aggregates moving as bedload will be calculated using van Rijn's equation for particle velocity given in Equation (2.2):

$$\frac{u_b}{[(s-1)gD]^{0.5}} = 1.5T^{0.6} \tag{2.2}$$

in which u_b is the aggregate velocity, s is the specific gravity, D is the aggregate diameter, and T is a transport stage parameter given by Equation (2.3)

$$T = \frac{(u_*')^2 - \left(u_{*,cr}\right)^2}{\left(u_{*,cr}\right)^2} \tag{2.3}$$

in which:

$$u_*' = \frac{g^{0.5}}{C'}\overline{u} \tag{2.4}$$

where u_*' is the bed shear velocity, $u_{*,cr}'$ is the critical bed shear velocity, C' is Chezy's coefficient, and $\overline{u}$ is the depth averaged flow velocity (van Rijn 1987).

A combination of the research completed by Perkey and Smith, the van Rijn bedload transport equations and the abrasion theory by Parker will be used in the abrasion routine developed in this thesis. A more detailed explanation of the creation of the abrasion algorithm will be discussed in the next chapter.

The next section of the literature review will discuss existing sediment transport models. Reviewing the literature of mud aggregates, dredging impacts and current hydrodynamic and sediment transport models will help in developing a new sediment transport model that includes the transport and abrasion of mud aggregates.

REVIEW OF MODELS

Numerical modeling of hydrodynamics and transport in estuaries and rivers is a complex process that combines models of interdependent processes. Estuaries, such as where the James River enters the Chesapeake Bay, can be complicated to model because of the added effect of both barotropic and baroclinic transport. The need for accurate models of estuaries has become increasingly more important based on the locations of ports and population centers near the estuaries (Hayter 2013). All major estuaries have natural and human impacts that need to be accounted for in models as well.

The U.S Army Engineer Research and Development Center (ERDC) uses a 3-D Geospatial Scale Transport Multi-Block Modeling System (GSMB) to model stratified water bodies such as the Chesapeake Bay, which is classified as a partially stratified estuary. GSMB combines models of different processes into one large, interdependent modeling system. A schematic diagram of GSMB can be seen in Figure 2.9. The arrows in Figure 2.9 show the dependencies of each model. For example, CE-QUAL-ICM receives necessary results from CH3D and SEDZLJ to solve its equations (Hayter *et al.,* 2020).

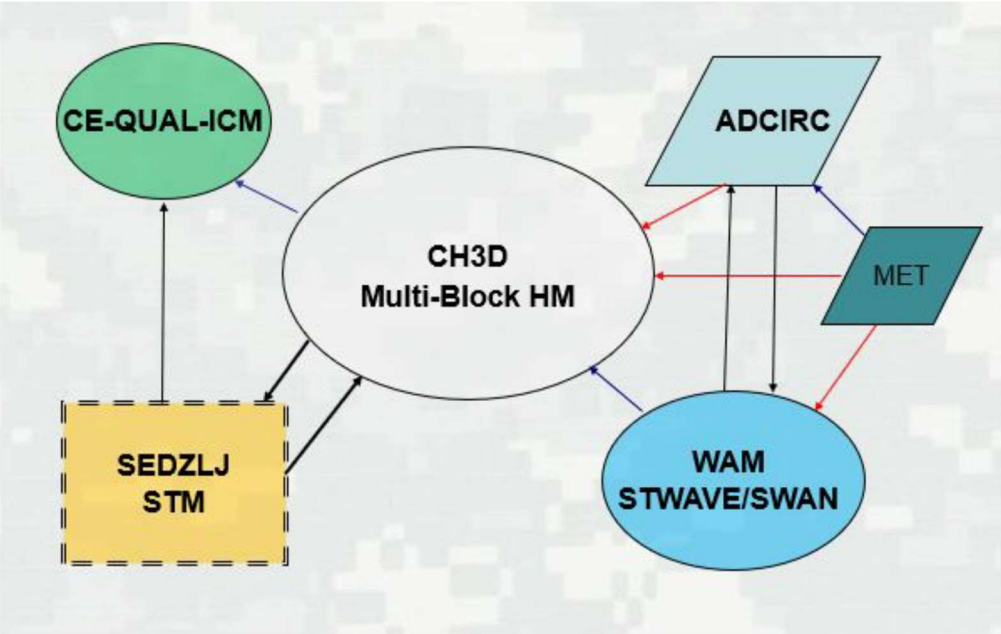

Figure 2.9: Schematic of GSMB Model (Hayter *et al.,* 2020).

The centerpiece of the GSMB model is a 3-D hydrodynamic model, the Curvilinear Hydrodynamics in 3-Dimensions or CH3D. CH3D solves the equations of motion to obtain a flow field in a curvilinear grid. The results from CH3D give outputs of velocities and water depths over time as well as other parameters, e.g., salinity, water temperature (Hayter *et al.,* 2020). CE-QUAL-ICM is a water quality model that can represent biogeochemical cycles such as the aquatic carbon cycle and nitrogen cycle (ERDC). CE-QUAL-ICM also simulates physical factors such as salinity and temperature (ERDC). ADCIRC is another time dependent model that incorporates the effects of tides and wind into the model. ADCIRC is also used for storm surges (ADCIRC). WAM is a 2-Dimensional (2D) deep water wave model (Hayter *et al.,* 2020). SEDZLJ is the sediment transport model that is dynamically linked to CH3D. Figure 2.10 is the grid

used for the Chesapeake Bay model, and Figure 2.11 is an enlarged view of the grid used to represent the James River. The entire model domain is split up into 33 different grid blocks so each grid block can be run on a different processor, thereby decreasing the time for each model simulation.

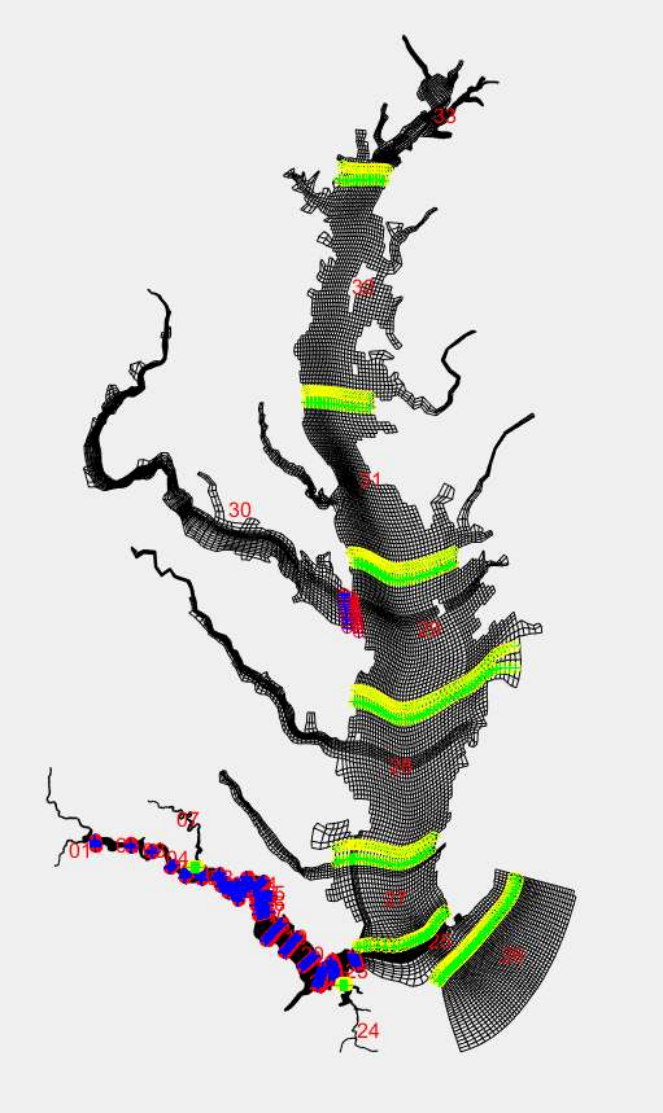

Figure 2.10: Chesapeake Bay Grid (Hayter *et al.,* 2020).

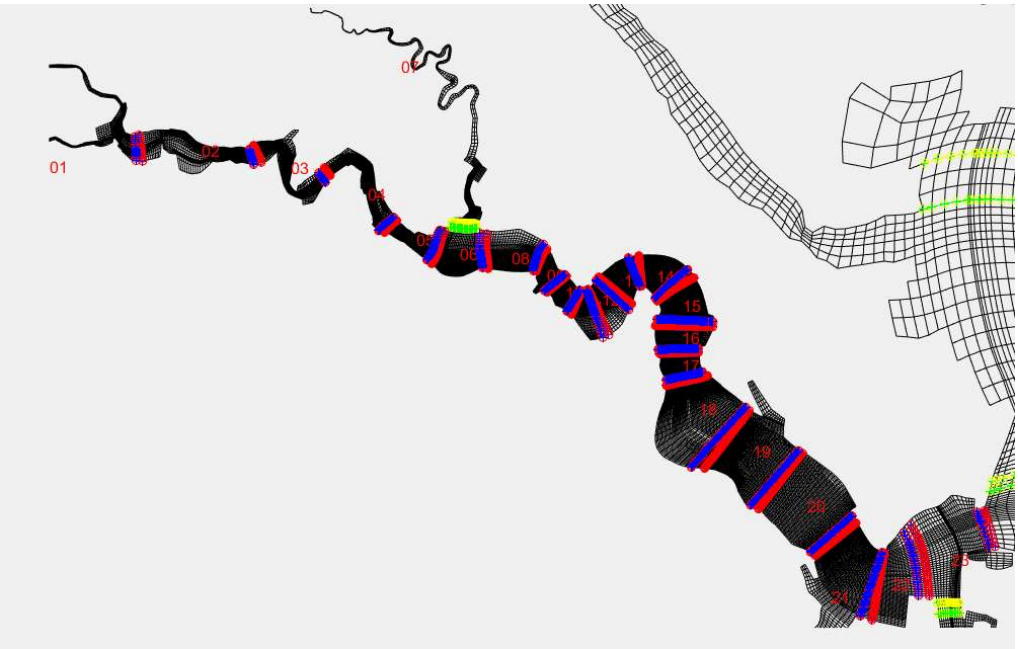

Figure 2.11: Grids for James River (Hayter *et al.,* 2020).

SEDZLJ, the mixed sediment transport model, is where the new abrasion routine will be located, so a more in-depth description of SEDZLJ will be given. Before SEDZLJ is discussed, the fundamentals of modeling sediment transport will be summarized.

FUNDAMENTALS OF MODELING SEDIMENT TRASNPORT

The transport of sediment has increasingly become an important topic for researchers and modelers. With waterways being an important part of the coastal economy, an accurate sediment transport model of sediment erosion, deposition, and transport is essential (Hayter 2013). Sediment transport can be a simple process such as sand being transported in a flume, or a complicated process such as cohesive sediment

transport in an estuary. There are many different parameters that can affect the transport of sediment, but a few key parameters that are used in all sediment transport models need to be understood.

Perhaps the most important property of sediment is its size. Size of sediment is a good predictor of how the sediment will behave. For instance, sediment smaller than 63 μm is typically classified as a cohesive sediment and will transport primarily in suspension while a sediment that is 2 cm in diameter may not be transported at all unless the magnitude of the bed shear stress is large. Modelers will normally have a grain size distribution (GSD) to develop initial conditions for the sediment bed (Hayter 2013).

Another important property of sediment is the composition of the sediment. In this thesis, mainly clay material will be modeled. Clay is classified as a cohesive sediment, which will be explained next.

Cohesion of sediment refers to how sediment particles interact with one another. Cohesive sediment tends to "bond" together such as mud. The main reason that particles exhibit cohesive properties is that their ratio of surface area to bulk volume is very large. The gravitational forces acting on cohesive sediment are very small relative to attractive and repulsive forces between the sediment particles themselves. The attractive forces are the van der Waal forces which are additive between particles. Repulsive forces between cohesive sediment particles are due to unbalanced cations on the surface of the particles. In environments with a small amount of salt, such as estuaries, individual cohesive sediment particles will bond together, known as flocculation, because the presence of salt diminishes the effect of the repulsive force (Hayter 2013).

The last important property that will be discussed is the settling speed of sediment. The settling speed is dependent on size, shape, and density of the particle. Settling speeds are used in models to determine the probability that a particle of a certain size class will be transported in suspension in each time step. A particle with a high settling speed has a higher chance to deposit or be transported in bedload than a particle with a low settling speed which would more likely be transported in suspension (Hayter 2013)

Next, SEDZLJ, the sediment transport model used in GSMB, will be summarized. SEDZLJ uses the fundamental properties discussed above to calculate net erosion of the bed.

SEDZLJ

SEDZLJ is an advanced sediment transport model that is used in this thesis. In the results section of this thesis, two simulations using SEDZLJ will be run, a 1-D simplified model and a 3-D model of the James River – Chesapeake Bay estuary. The main purpose of SEDZLJ, or any sediment transport model, is to calculate three values: erosion of sediment, deposition of sediment, and transport rate of sediment. By calculating those three values over the simulation time and at the grid cells in the model domain, the change in bed elevation and the sediment composition of the sediment beds can be obtained.

An equilibrium between erosion and deposition naturally occurs in steady-state flow after some time. Equation (2.5) gives this equilibrium where E is equal to erosion rate, p is equal to probability of deposition, w_s is equal to the settling speed and C is equal to the near-bed sediment concentration.

$$E - pw_sC = 0 \tag{2.5}$$

The second term on the left-hand side of Equation (2.5) represents the deposition rate. This equilibrium will be seen in the steady state 1-D model in the next chapter (Jones *et al.,* 2001).

Erosion of the sediment bed occurs when the bed shear stress is greater than the critical shear stress of erosion for a particular sediment size class. For instance, for a given shear stress, a small sediment size class may be eroded and subsequently transported either as bedload or suspension, while a larger size class may not be eroded. The critical shear stress for erosion of cohesive sediments is experimentally found and that data are input in the sediment transport model for each sediment size class. Another important parameter experimentally found is the critical shear stress for suspension which is the required shear stress for a particular sediment size class to be transported in suspension. The bed shear stress in SEDZLJ is calculated by Equation (2.6)

$$\tau = \frac{\rho_w * fc * u^2}{8} \tag{2.6}$$

where rho is the density of water, *u* is the flow velocity and *fc* is a roughness parameter calculated by Equation (2.7)

$$fc = \frac{0.24}{\log\left(\frac{12 * depth}{kn^2}\right)} \tag{2.7}$$

where *kn* is calculated by $\frac{30*d50a}{10000}$, where d_{50avg} is the median sediment diameter of the bed (Jones *et al.,* 2001). Another parameter that is normally found experimentally for cohesive sediment is the erosion rate. The erosion rate is found by eroding a sediment core in a Sedflume. Results are fitted using Equation (2.8)

$$E = A\tau^n \tag{2.8}$$

where *E* is the erosion rate of cm/s, τ is the bed shear stress in units of Pa, and *A* and *n* are empirical constants. If the bed shear stress is greater than the critical shear stress for erosion for the given size classes, the amount of erosion for the given size classes will be calculated at each time step.

Once sediment is eroded from the bed and is in transport, the sediment may begin to deposit. Each sediment size class being transported as bedload or suspension has a probability that it will deposit, and once the probability of deposition is calculated, the deposition rate per time step is calculated by Equation (2.9)

$$d = p * C * w_s * dt \tag{2.9}$$

where d is mass of the sediment deposited per unit bed area (g/cm^2), C is the concentration of bedload or suspended load, w_s is the sediment settling velocity and dt is the time step. The deposited sediment will be placed in the top layer of the sediment bed. Similar to the erosion rate, the deposition rate differs for each size class at each time step (Jones *et al.,* 2001).

The transport of bedload and suspended load are calculated using two separate differential equations. In both bedload and suspended load, the transport of sediment in bedload or suspended load is due to the flow of fluid. For the transport of suspended sediment, the 2-D vertically integrated transport equation is given by the advection-diffusion equation derived from the conservation of mass, as shown in Equation (2.10).

$$\frac{\partial hC}{\partial t} + \frac{\partial UC}{\partial x} + \frac{\partial VC}{\partial y} = D_H \left[\frac{\partial}{\partial x}\left(h\frac{\partial C}{\partial x}\right) + \frac{\partial}{\partial y}\left(h\frac{\partial C}{\partial y}\right)\right] + Q_s \qquad (2.10)$$

where C is the suspended sediment concentration, h is the depth of water, U and V are the flow velocities in the x and y directions, D_H is a horizontal eddy diffusivity constant (Fischer 1979) which is given in Equation (2.11).

$$D_H = 0.15hu_* \qquad (2.11)$$

where u_* is the shear velocity = $\sqrt{\frac{\tau}{\rho}}$. In Equation (2.10), Q_s is the source/sink term given in Equation (2.12) which represents net erosion.

$$Q_s = p_{sus} * E - D \qquad (2.12)$$

E represents the mass eroded per unit bed area, *D* represents the mass deposited per unit bed area and p_{sus} represents the probability of suspension. The probability that a sediment size class is transported in suspension is given by Equation (2.13)

$$p_{sus} = \frac{\frac{\log(usw) - \log(\sqrt{\tau_{cs}})}{w_s}}{\frac{\log(4) - \log(\sqrt{\tau_{cs}}}{w_s}} \tag{2.13}$$

where p_{sus} is the probability of suspension, τ_{cs} is the critical shear stress for suspension, and *usw* is a parameter calculated by $\frac{\sqrt{\tau}}{w_s}$ (Jones *et al.,* 2001).

Bedload transport is calculated by a 2-D advection equation derived using the conservation of mass and is given by Equation (2.14).

$$\frac{\partial C}{\partial t} + u\frac{\partial C}{\partial x} + v\frac{\partial C}{\partial y} = Q_b \tag{2.14}$$

where *C* is the bedload concentration, *u* and *v* are velocities in the *x* and *y* direction, and Q_b is a source/sink term given by Equation (2.15) which represents net erosion.

$$Q_b = (1 - p_{sus}) * E - D \tag{2.15}$$

The bedload velocities are calculated by Equation (2.16)

$$v = 1.5 * T^{0.6} * \sqrt{(SG - 1) * g * \frac{d}{10000}} \tag{2.16}$$

where *SG* is the specific gravity of the sediment, *g* is the acceleration due to gravity and *d* is the diameter of the size class. *T* is a transport parameter calculated by equation 2.17.

$$T = \frac{\tau - \tau_c}{\tau_c} \tag{2.17}$$

where τ_c is the critical shear stress for erosion (Jones *et al.,* 2001).

CHAPTER THREE

DESCRIPTION OF ALGORITHMS

TRANSPORT, EROSION AND DEPOSITION OF MUD AGGREGATES

To confirm that the proposed aggregate abrasion model would simulate abrasion of mud aggregates, a one-dimensional (1-D) finite difference flow and sediment transport model was developed. The new 1-D model was developed using MATLAB using a simplified version of SEDZLJ. To determine the effects that the aggregate abrasion model has on the results of the sediment transport model, the aggregate abrasion model was added to the 1-D model, and results were compared to a sediment transport model simulation without using the abrasion routine.

To begin, the initial conditions for the model are stated. The simplified model simulated flow in a hypothetical one-meter-long flume, where flow values were calculated at nodes every 10 cm, creating a 1-D grid. The sediment transport model simulation in the hypothetical flume was considered to be open to the atmosphere and of a constant slope for uniform flow to be established. Four mud aggregate size classes and three sediment bed layers were included in the 1-D sediment transport model. The initial bed layer thickness was 10 cm and was placed in the third, i.e., bottom most layer. There were no aggregates placed in the top two layers at the beginning of the simulation. The grain size distribution in the third bed layer was set at 1/3 for each of the largest three aggregates size classes. Table 3.1 is a summary of the physical properties of the four size classes of bed aggregates.

Table 3.1: Sediment Size Class Characteristics

Size Class (μm)	Critical shear stress for erosion (dyne/cm^2)	Critical shear stress for suspension (dyne/cm^2)	Specific Gravity	Settling Velocity (cm/s)
3,500	3.2	180	2.65	13.7
300	0.4	0.7	2.65	0.84
80	0.3	0.3	2.65	0.07
20	0.1	0.1	2.65	0.01

Before the time integration loop in the finite difference sediment transport model, the initial sediment mass per unit sediment bed area for each layer of the sediment bed was calculated as well as a sediment flag array, indicating which sediment bed layers had aggregates present. This sediment flag array was updated after each time step during the sediment transport model run to identify which layers had sediment present.

After the initial conditions were defined, the time integration loop began. The bedload velocity for each aggregate size class was the first parameter solved in the time loop using Equation (2.2).

The next step was to calculate mass of deposition per unit sediment bed area for the four aggregate size classes. Deposition can occur from suspended load or from bedload, depending on flow conditions and the aggregate's physical properties such as settling velocity. The current mass of aggregates per unit sediment bed area was then

calculated for the first layer, i.e., active layer, which is the layer where deposited material was placed. The maximum mass of aggregates per unit sediment bed area of the active layer was also calculated. Using Equation (2.9), the mass of aggregates deposited per unit sediment bed area was calculated for each aggregate size class. Note that not every aggregate size class necessarily had sediment depositing every time step. Once the deposited sediment was added to the active layer, new percentages of each size class in the first layer were calculated.

Next, when the bed shear stress was greater than the critical shear stress of erosion for a given aggregate size class, the probability that an aggregate of a given size will be transported in suspension was calculated for each aggregate size class. For example, if the bed shear stress is greater than the critical stress for erosion for an aggregate size class but less than the critical shear stress for suspension of the same aggregate size class, the probability of suspension will be zero. Erosion of the sediment bed and the sink/source terms for suspended and bedload transport will both be calculated using the probability of suspension.

The next section of code in sediment transport model prepared the model for erosion of the sediment bed. First, it was determined if aggregates had moved from the first layer to the second layer after deposition. If the mass of aggregates deposited per unit sediment bed area was larger than the mass of aggregates per unit sediment bed area of the active layer, aggregate mass per unit sediment bed area was transferred from the active layer to layer two until the mass of aggregates per unit sediment bed area of deposited aggregates were equal to the mass of aggregates per unit sediment bed area of

the active layer. If the mass of aggregates deposited per unit sediment bed area in the active layer was less than the maximum mass per unit area of the active layer, then there were no aggregates present in layer two and layer three was the layer below the active layer. Then, using newly calculated post-deposition median aggregate sizes in the surface layer, the aggregate mass per unit sediment bed area of the active layer was calculated.

Once the amount of aggregate mass per unit sediment bed area for each size class in each layer were updated for the current time step, erosion of the aggregates from the sediment bed was calculated. First, the median diameter of the aggregates in the surface layer were recalculated. Then, the erosion rate (cm/s) was calculated for the experienced bed shear stress as well as the eroded aggregate mass per time step. If the bed shear stress was less than the critical shear stress for erosion for a given aggregate size class, no erosion of the given aggregate size class occurred for that time step. If the bed shear stress was greater than the critical shear stress for erosion for a given aggregate size class, erosion of the given aggregate size class occurred. Erosion of each aggregate size class at each node per time step, erosion of each layer of each aggregate size class per time step, and mass of each aggregate size class per sediment bed area per time step were calculated. Total aggregate erosion at each node and total aggregate erosion for each layer were calculated from summing the previously calculated values for all aggregate size classes. The new aggregate mass per unit sediment bed area for each layer was then recalculated by subtracting the aggregate mass per unit sediment bed area eroded from the sediment bed from the aggregate mass per unit sediment bed area.

Once rates of deposition and erosion were calculated, sediment transport equations were used to determine suspended sediment concentrations and bed load concentrations at the nodes in the model grid. Suspended sediment transport was calculated by the 1-D advection-diffusion equation that is based on the principle of conservation of mass and given by Equation (3.1).

$$\frac{dC}{dt} + u\frac{dC}{dx} = D_H\frac{d^2C}{dx^2} + Q_s \tag{3.1}$$

Discretizing this equation using forward difference in time and backward difference in space gives Equation (3.2).

$$C_x^{t+1} = C_x^t - \frac{u\Delta t}{\Delta x}(C_x^t - C_{x-1}^t) + \frac{D_H\Delta t}{\Delta x^2}(C_{x-1}^t - 2C_x^t + C_{x+1}^t) + Q_s\Delta t \tag{3.2}$$

where u is equal to the depth averaged flow velocity, Q_b is equal to the suspended sediment source term which was calculated in Equation (2.12), and D_H is the diffusion coefficient calculated by Equation (2.11).

Bed load transport was calculated using the 1D advection equation that represents conservation of mass and is given by Equation (3.3)

$$\frac{dC}{dt} + \frac{dC}{dx} = Q_b \tag{3.3}$$

Discretizing this equation using forward difference in time and backward difference in space gives Equation (3.4).

$$C_x^{t+1} = C_x^t - \frac{u_b \Delta t}{\Delta x}(C_x^t - C_{x-1}^t) + Q_b \Delta t \quad (3.4)$$

where u_b is the bedload velocity, and Q_b is the bedload source term calculated in Equation (2.15).

All variables at the next time step were set equal to the values of the variables at the current time step and then were recalculated for the remaining time steps.

ABRASION OF MUD AGGREGATES

In existing sediment transport models, aggregates that are transported as bedload do not undergo abrasion. This was also the case for the 1-D finite difference sediment transport model developed in this research. The next step was to create a model that simulates abrasion of aggregates being transported as bedload. The derivations were developed using a theory by Parker (1991). Parker's theory states that the abrasion of aggregates in transport could be represented by a transfer of mass from a sediment size class "A" to the next smallest sediment size class "B" as well as a transfer of mass from sediment size class "A" to the smallest sediment size class "C" where size class "C" represents the silt sized sediment created as the product of abrasion. In deriving the abrasion routine, a Lagrangian time frame was used because a single aggregate can be "followed," and the aggregate can be simulated to decrease in diameter as it travels along the bed. Lagrangian time frames can be effective for deriving equations that follow singular points, but these equations would not work in a Eulerian grid used in GSMB. To

account for this, the derived formulas were changed from a Lagrangian time frame to a Eulerian time frame. By doing this, the decrease in diameter from an aggregate being transported on the bed was represented by changing its mass, instead of its size. This allowed a Eulerian grid to be used in the simulation of abrasion of four aggregate size classes while using constant aggregate diameters.

To better explain this process an example will be given. In the 1-D sediment transport model, four size classes of aggregates, 3,500 µm, 300 µm, 80 µm and 20 µm, were modeled. Figure 3.1 shows the 3,500 µm aggregate undergoing abrasion in a Lagrangian time frame, as the aggregate's diameter decreases to a diameter of 300 µm after a distance of *DX*. As the 3,500 µm aggregate moves along the bed, abrasion causes its diameter decreases, and silt is the byproduct of the abrasion. Figure 3.1 shows the 20 µm aggregate, representing silt, in suspended load (there would be numerous 20 µm aggregates abrading from the larger aggregates over the distance *DX*). The representation of aggregate abrasion in a 1-D Eulerian grid is shown in Table 3.2 where the aggregate is moving as bedload from x = 1 to x = 2.

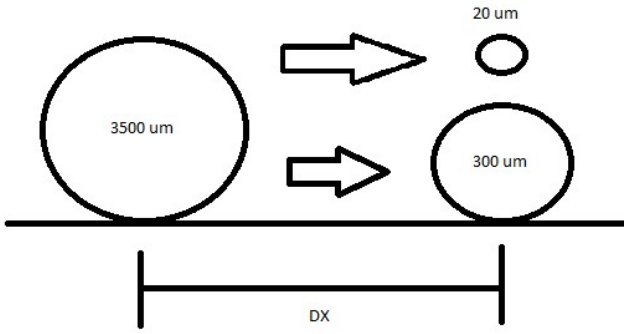

Figure 3.1: Aggregate Abrasion Representation in Lagrangian Time Frame

Table 3.2: Representation of Abrasion in Eulerian Grid

	Mass @ x=1	Mass @ x=2
3,500 µm	A	A-B-C
300 µm	0	B
80 µm	0	0
20 µm	0	C

ABRASION ROUTINE DERIVATION

Equation (3.5) states that the mass of a given size class of aggregate will decrease with distance at a rate equal to the product of an abrasion coefficient, α, times the mass,

$$\frac{dM_i}{dx} = -\alpha_i M_i \tag{3.5}$$

where *i* represents the sediment size class. Equation (3.6) calculates the distance traveled by an aggregate moving as bedload during a time step (Smith 2020).

$$dx = dt * u_b \tag{3.6}$$

Substituting Equation (3.6) into Equation (3.5) gives

$$\frac{dM_i(sink)}{dt} = -\alpha_i M_i u_b \tag{3.7}$$

Equation (3.7) is the first of two sink terms for the largest three size classes. The mass lost due to abrasion from Equation (3.7) will be added to the mass of the 20 μm aggregate size class, which represents the silt created from the process of abrasion.

The source and sink terms for the mass transfer between the largest three aggregate size classes is derived now. To calculate the source and sink terms, the change in volume over time was first calculated in the Lagrangian time frame as described below.

The eroded bed aggregate was assumed to be spherical, so the volume was calculated by

$$V_i = \frac{\pi}{6} D_i^3 \tag{3.8}$$

Multiplying Equation (3.8) by the density of the aggregate results in a mass value, and inserting the new mass equation into Equation (3.7) gives

$$\frac{d\frac{\pi}{6}\rho D_i^3}{dt} = -\alpha_i \frac{\pi}{6} \rho D_i^3 u_b \tag{3.9}$$

Simplifying Equation (3.9) gives

$$\frac{dD_i^3}{dt} = -\alpha_i D_i^3 u_b \tag{3.10}$$

Evaluating the derivative on the left-hand side of Equation (3.10) gives

$$3D_i^2 \frac{dD_i}{dt} = -\alpha_i D_i^3 u_b \tag{3.11}$$

Simplifying Equation (3.11) gives

$$\frac{dD_i}{dt} = -\frac{1}{3}\alpha_i D_i u_b \tag{3.12}$$

Equation (3.12) represents the change in diameter of the eroded bed aggregate with time. In order to use a Eulerian grid, Equation (3.13) was used (Smith 2020).

$$\frac{dM_i}{dt} = \frac{d}{dD_i}\left(M_i \frac{dD_i}{dt}\right) \tag{3.13}$$

By inserting Equation (3.12) into Equation (3.13) the right-hand side simplifies to

$$\frac{dM_i}{dt} = \frac{d}{dD_i}(-\frac{1}{3}\alpha_i D_i u_b M_i) \tag{3.14}$$

Taking the constants out of the derivative gives

$$\frac{dM_i}{dt} = -\frac{1}{3}\alpha \frac{d}{dD_i}(D_i u_b M_i) \tag{3.15}$$

Discretizing the derivative using backward difference gives

$$\frac{dM_i}{dt} = -\frac{1}{3}\alpha \frac{\left(D_i u_{b,i} M_i - D_{i-1} u_{b,i-1} M_{i-1}\right)}{D_i - D_{i-1}} \tag{3.16}$$

By splitting Equation (3.16) into two separate equations, a source and sink term were developed (Smith 2020).

$$dM_i(source) = \frac{1}{3}\frac{\alpha D_{i-1} u_{b,i-1} M_{i-1} dt}{D_i - D_{i-1}} \tag{3.17}$$

$$dM_i(sink) = -\frac{1}{3}\frac{\alpha D_i u_{b,i} M_i dt}{D_i - D_{i-1}} \tag{3.18}$$

The 3,500 μm size class only has sink terms given by Equations (3.7) and (3.18) and does not have any sources being the largest size class. The 300 μm and 80 μm size classes have sink terms given by Equations (3.7) and (3.18) and a source term given by Equation (3.17). The 20 μm size class only inherits mass through the abraded silt of the aggregates, so the only source term for that size class is given by Equation (3.7). The 20 μm size class does not have a sink term being the smallest size class and only transported in suspension (Smith 2020).

ABRASION COEFFICIENT

The aggregate abrasion routine derived in the previous section will not properly simulate the physical process of abrasion of aggregates transported as bedload unless accurate abrasion coefficients are used. To determine the abrasion coefficient that best represents the abrasion of aggregates in the James River, sediment samples were taken from the James River and analyzed (Perkey *et al.,* 2019). The liquidity index, given in Equation (3.19), was calculated for each sediment core taken,

$$LI = \frac{w - PL}{LL - PL} \tag{3.19}$$

where w is the water content of the sample, PL is the plastic limit of the sample and LL is the liquid limit of the sample. The plastic limit and liquid limit are two of the three Atterberg limits, with the other being the shrinkage limit. The plastic limit is defined as when the water content of a sediment sample increases such that the sample changes from a semisolid state to a plastic state. The liquid limit is defined as when a sediment

sample's water content increases such that the sample changes from a plastic state to a liquid state (Mehta 2014). The water content is defined as the ratio of mass of water to mass of solid in each sediment sample. The liquidity index is correlated to the abrasion of an aggregate because of the effects that water content and Atterberg limits has on the abrasion of an aggregate. Figure 3.2 shows the breakup rate of aggregate samples from the James River at different flow speeds and liquidity indexes in an aggregate tumbler. The data shows that aggregates with smaller liquidity indexes tend to have little variation of size after the first 500 seconds of the experiment while there is more variation in change of aggregate's diameter with larger liquidity indexes. Figure 3.2 also suggests that aggregates with low liquidity indexes can travel longer distances as bedload before completion of abrasion occurred.

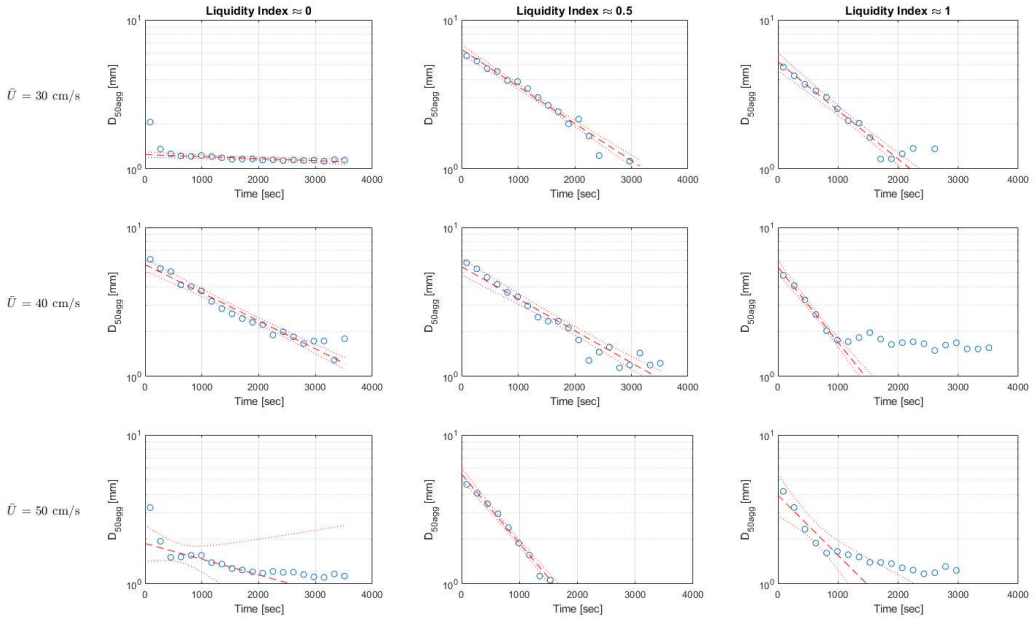

Figure 3.2: Breakup Rate of Aggregates from the James River in a Flume (Smith *et al.,* 2020)

Sediment abrasion tests were conducted in a constant slope enclosed flume as well as an aggregate tumbler. Based on abrasion testing, the flume results showed a higher abrasion coefficient compared to the aggregate tumbler, which was determined to be the result of more varied transport of bedload, such as saltation, in the flume. According to Smith (2020), the results from the flume experiment were determined to be a better representation of abrasion of mud aggregates since the transport of aggregates in a flume more closely resembled the transport of aggregates compared to the aggregate tumbler. Figure 3.3 gives a comparison of abrasion coefficients observed when running experiments with a flume and aggregate tumbler.

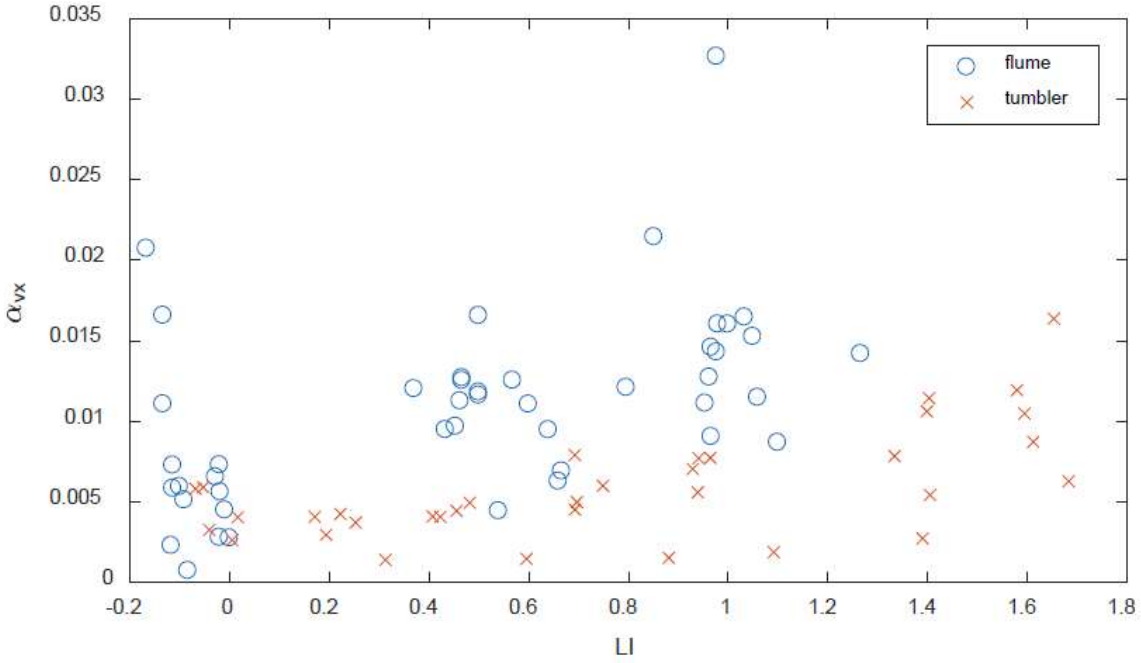

Figure 3.3: Comparison of Abrasion Coefficients between Flume and Aggregate Tumbler (Smith *et al.,* 2020)

Samples collected from the dredge placement site in the James River showed a liquidity index between 0.5 and 1.0. Testing of aggregates in the flume suggested that an abrasion coefficient between $0.01\frac{1}{m}$ and $0.015\frac{1}{m}$ would accurately represent abrasion of the mud aggregates in the James River. The abrasion coefficient used in the James River GSMB model was $0.0125\frac{1}{m}$, or an average of the range of appropriate abrasion coefficients. In the 1-D sediment transport model, an abrasion coefficient of $0.05\frac{1}{m}$ was also used to compare the effects of two different abrasion coefficients (Smith 2020). To simulate the amount of abrasion that occurs for a singular aggregate being transported as bedload, Equation (3.12) was plotted in Figure 3.4 using the two abrasion coefficients

that were tested in the 1-D sediment transport model. Note that the abrasion coefficients were converted to $\frac{1}{cm}$, as cm is the unit of length used in the 1-D and 3-D sediment transport models. The aggregate plotted was the 3,500 µm sized aggregate which is converted to 0.35 cm. The bedload velocity used was 15 cm/s and the time step was one second. The simulation was for one hour.

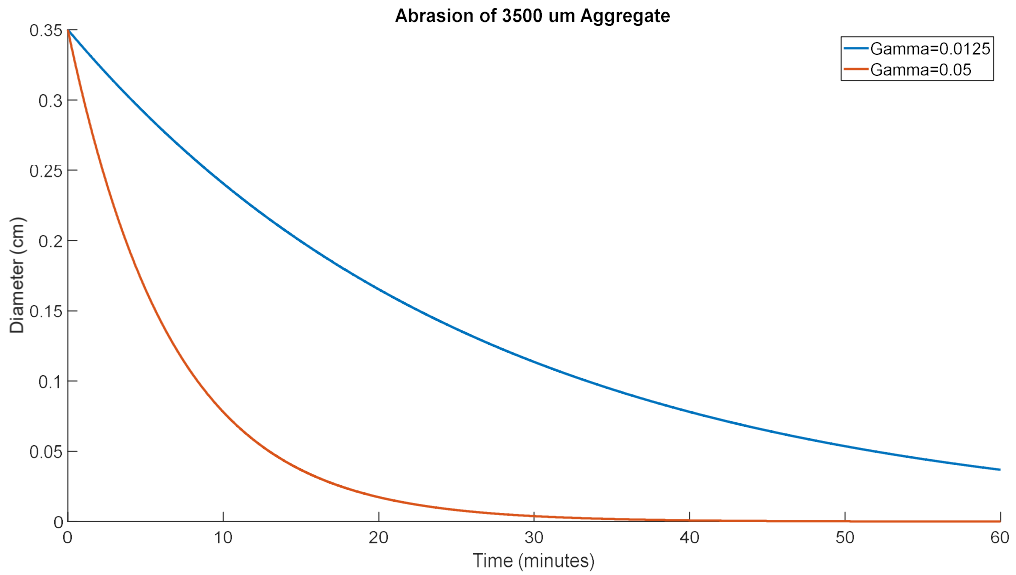

Figure 3.4: Abrasion of a Singular 3,500 µm Aggregate

The results from Figure 3.4 are similar to the observed values from Figure 3.2, although a constant interval y-axis was used in Figure 3.4. After one hour, when the abrasion coefficient was equal to $0.0125\frac{1}{m}$, the aggregate had lost most of its size, but still was around 0.05 cm in diameter. When $0.05\frac{1}{m}$ was used as the abrasion coefficient, the aggregate was almost completely abraded after 30 minutes. Traveling as bedload for one

hour at 15cm/s, the aggregate would have traveled 540 meters. Although this simple simulation was completed in a Lagrangian time frame, by tracking a single particle, the simulation provided an early insight on how far an aggregate undergoing abrasion can travel before its diameter is decreased by over 85%.

INPUT DATA FOR THE SEDIMENT TRANSPORT MODELS

To accurately simulate sediment transport in the James River, the sediment properties input into the sediment transport model must be as similar to the sediment from the area of interest as possible. This was achieved by taking sediment core samples from the dredged material placement sites and testing those sediment cores to determine bed properties such as the erosion rate and bulk density. For this thesis, sediment cores were taken and analyzed by David Perkey and Dr. Jarrell Smith (2019) and the area of interest modeled in this thesis is the placement area for dredged material in the James River just downstream of the confluence with the Chickahominy River. Perkey and Smith took five sediment core samples from the placement site and eroded them in a Sedflume. Photographs of the top of the cores can be seen in Figure 3.5.

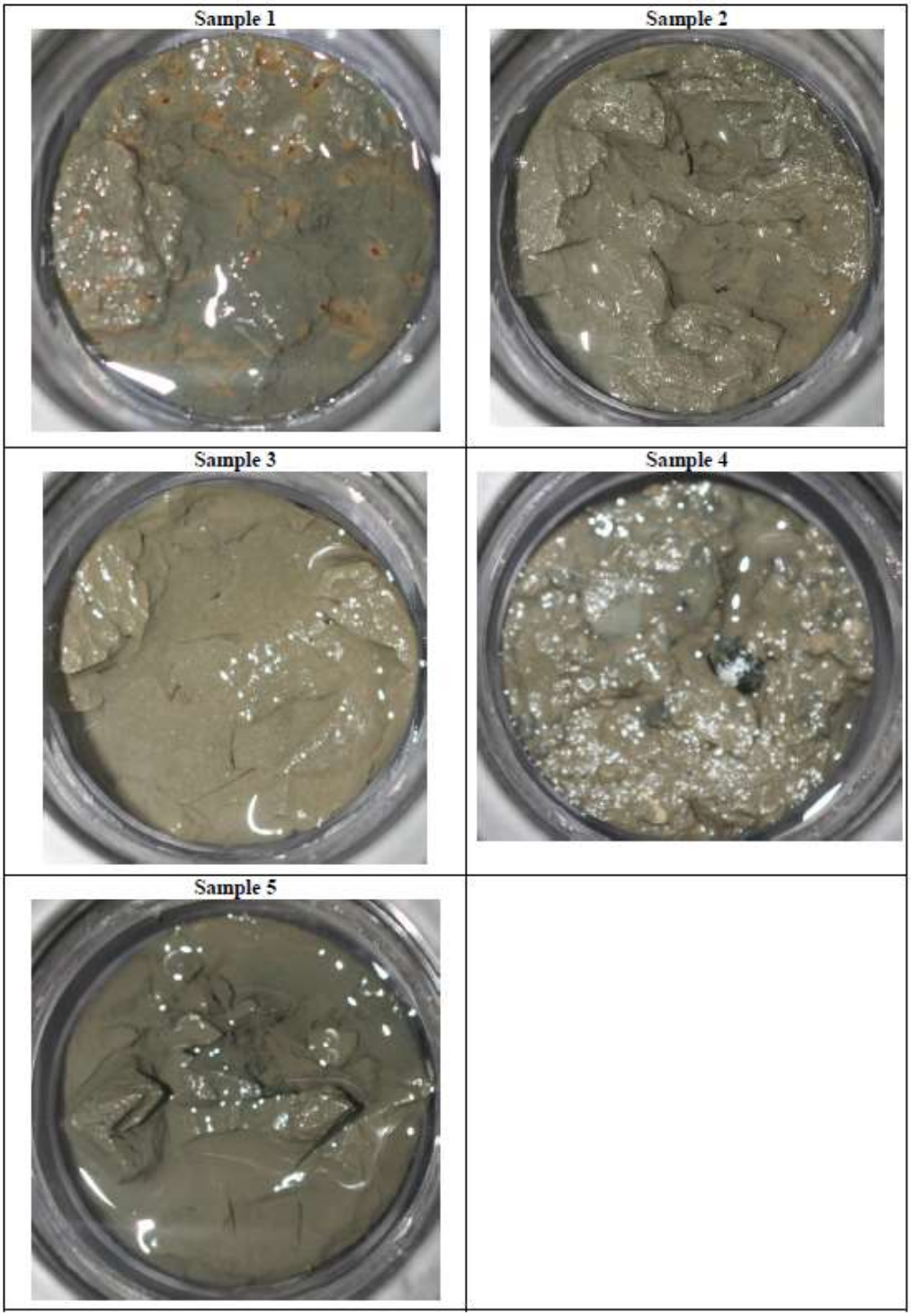

Figure 3.5: Core samples from James River (Perkey *et al.,* 2019).

Once eroded in the Sedflume, a grain size distribution for each core was measured. Samples from the cores were sized by a laser-particle sizer which records sizes from 0.02 µm to 2000 µm. A cumulative grain size distribution graph and a probability density graph from the samples taken from the dredged material placement site, labeled as core 14, can be seen in Figure 3.6 and Figure 3.7 (Perkey *et al.,* 2019).

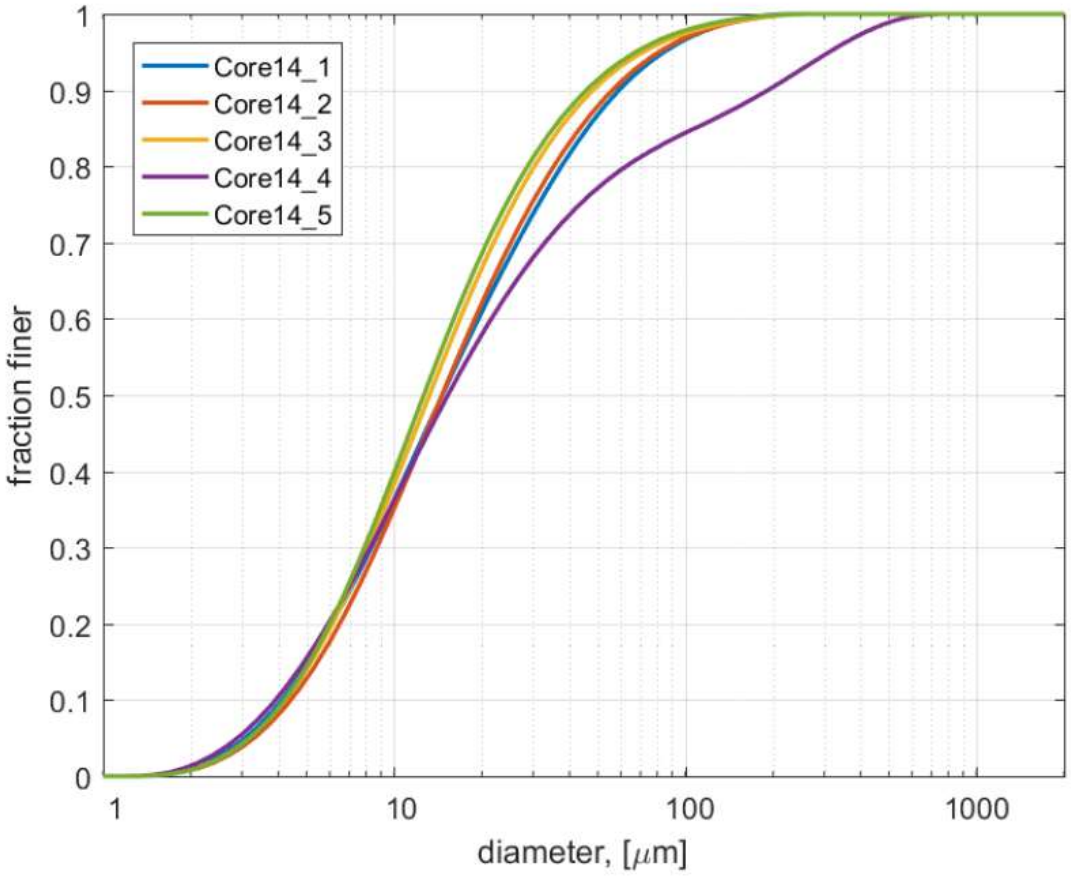

Figure 3.6: Cumulative Grain Size Distribution (Perkey *et al.,* 2019).

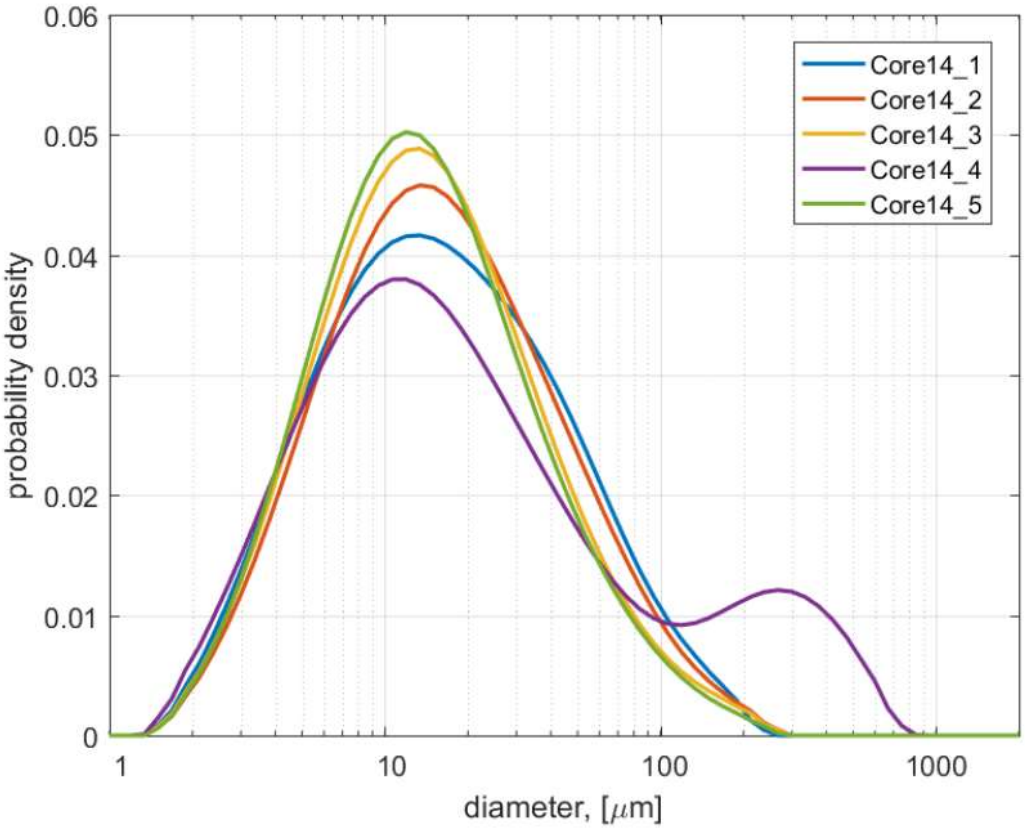

Figure 3.7: Probability Density Grain Size Distribution (Perkey *et al.,* 2019).

The last input data used for the sediment transport model was the erosion rate of sediment from the bed. The erosion rate was found using a Sedflume, where the core is slowly pushed up into the flume as the top of the core erodes in the flume. The erosion rates in the tested core are shown in Figure 3.8 (Perkey *et al.,* 2019).

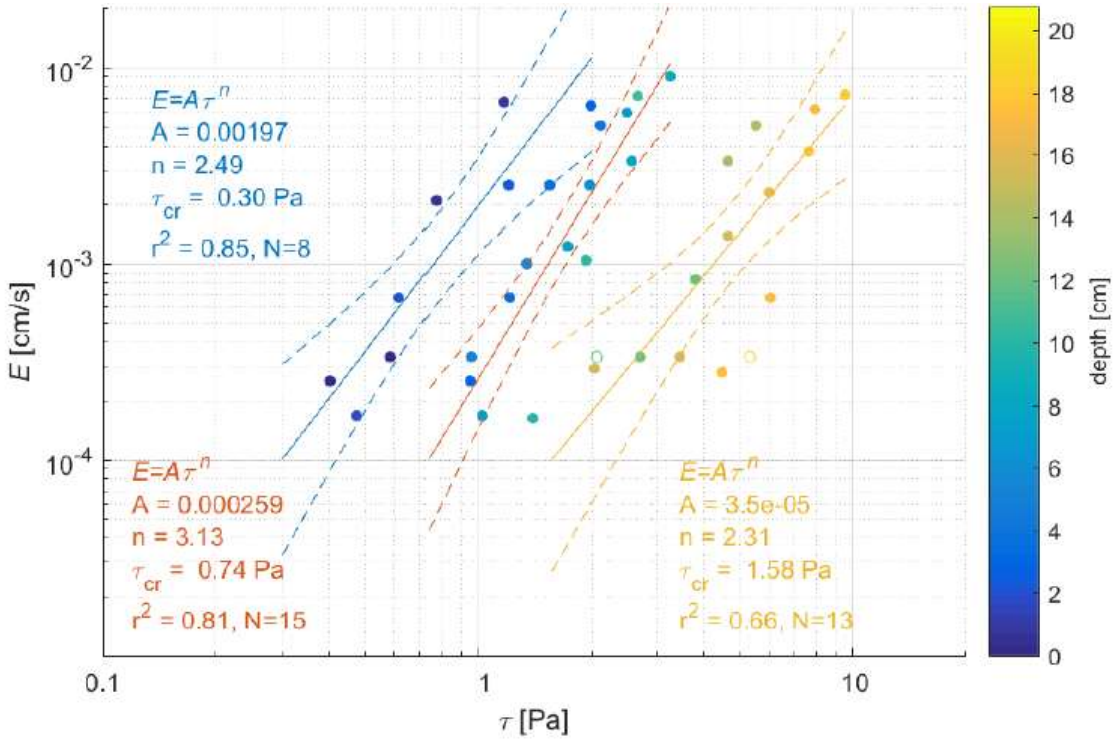

Figure 3.8: Erosion rate in sample core (Perkey *et al.,* 2019).

The color of the data points represents the initial depth of the top of the core at the time of recording the data, as shown on the right-side y-axis of Figure 3.8. For example, a data point that is yellow in color indicates that when that data point was taken, the top of the core in the Sedflume was initially 16-20 cm deep in the core. Data points of similar color were grouped and fitted together because they are representative of similar depths and their erosion rates are similar. The x axis shows the shear stress in Pa and it was found that for sediment initially deeper in the core, a greater shear stress is needed to erode that sediment when it reaches the sediment bed (Perkey *et al.,* 2019).

For the 1D sediment transport model, the only input data used from this section will be the erosion rate. The James River GSMB model will use all the input data from this section.

CHAPTER 4

ONE-DIMINSIONAL SEDIMENT TRANSPORT MODEL

ONE-DIMINSIONAL SEDIMENT TRANSPORT MODEL DESCRIPTION

To test and verify the aggregate abrasion routine before incorporating it into the GSMB model of the James River, the aggregate abrasion routine was input in a 1-D sediment transport model developed for this thesis. In a 3-D model, such as GSMB, it could be difficult to interpret the effects of adding abrasion of mud aggregates to the model, which was why a steady state 1-D sediment transport model was developed and analyzed first. The sediment transport model simulated flow and sediment transport in a one-meter-long flume using 11 nodes separated 10 cm apart. This model was run using a constant flume slope and two different abrasion coefficients. The total simulation time for each run was one hour. The flow in the flume was uniform, and the velocity was calculated using Equation 4.1 (Manning's equation).

$$v = \left(\frac{1}{n}\right) * R^{\frac{2}{3}} * S^{0.5} \tag{4.1}$$

where n is the Manning roughness coefficient, R is the hydraulic radius given by $\frac{Area}{Wetted\ Perimeter}$, and S is the slope of the flume. Table 4.1 summarizes the sediment transport model setup and initial conditions.

Table 4.1: Flume Setup

Parameter	Value
Slope	0.015
Flow Velocity	31.71 cm/s
Depth of Flow	25 cm
Width of Flume	10 cm
Dx	10 cm
Dt	0.05 seconds
Abrasion coefficient (1/m)	0.05 & 0.0125
Initial Sediment Bed Depth	10 cm
Initial Sediment Bed Composition	$\frac{1}{3}$ →3,500 µm size class $\frac{1}{3}$ →300 µm size class $\frac{1}{3}$ →80 µm size class
Simulation Time	1 hour

The erosion rate was calculated by Equation (4.2), where A and n are empirical constants.

$$E = A\tau^n \tag{4.2}$$

Since the sediment bed depth of the simulated 1-D flume was 10 cm, the constants chosen in Equation (4.2) were to represent sediment near the surface of the sediment bed in the James River. Based on Sedflume erosion experiments with results shown in Figure 3.5, the value of *A* used was 0.00197 and the value of *n* was 2.49 (Perkey *et al.,* 2019).

The 1-D flow and sediment transport model used a circular boundary condition, meaning sediment that flows out of the flume at node 11 will be added as a boundary condition at node 1 as given in Equation (4.3)

$$C_1^{t+1} = C_{11}^t \tag{4.3}$$

The downstream boundary condition is given by Equation (4.4).

$$C_{11}^t = C_{10}^t \tag{4.4}$$

The circular boundary condition was introduced because if sediment could leave the flume at node 11, the maximum distance travelled by an aggregate would be one meter. By using a circular boundary condition, aggregates could travel as suspended load or as bedload for the entire length of the simulation, as they would never leave the flume. The sediment transport model simulated three different conditions:

1. No abrasion
2. Abrasion with a coefficient = 0.0125 $\frac{1}{m}$ = 0.000125 $\frac{1}{cm}$
3. Abrasion with a coefficient = 0.05 $\frac{1}{m}$ = 0.0005 $\frac{1}{cm}$

The abrasion coefficients were converted to $\frac{1}{cm}$ as cm is the unit of length for the 1D and 3D sediment transport models.

RESULTS FROM THE 1-D SEDIMENT TRANSPORT MODEL

The model was run for one hour for these three conditions. Many of the figures in this chapter start at 20 minutes to better show the differences between the three conditions.

Figure 4.1 shows the thickness of the bed at node 5 as a function of time for the three model runs. Node 5 was chosen to show these results because there were little differences between the nodes due to the circular boundary condition. Between 0.16 cm and 0.17 cm of sediment was eroded from the bed after an hour for all three conditions. When aggregate abrasion was not being simulated, the thickness of the bed reached an equilibrium thickness of approximately 9.83 cm. In a steady state model, without abrasion, most parameters such as thickness, bed shear stress, suspended sediment concentration and bedload concentration reached equilibrium. As shown in Figure 4.1, the thickness of the bed at node 5 was also function of the value of the abrasion coefficient when abrasion was simulated. The difference between the two abrasion simulations was 0.01% after one hour with the simulation of the largest abrasion coefficient resulting in the smallest thickness of the three simulations. It was not immediately obvious why this was the case, but further investigation provided the explanation.

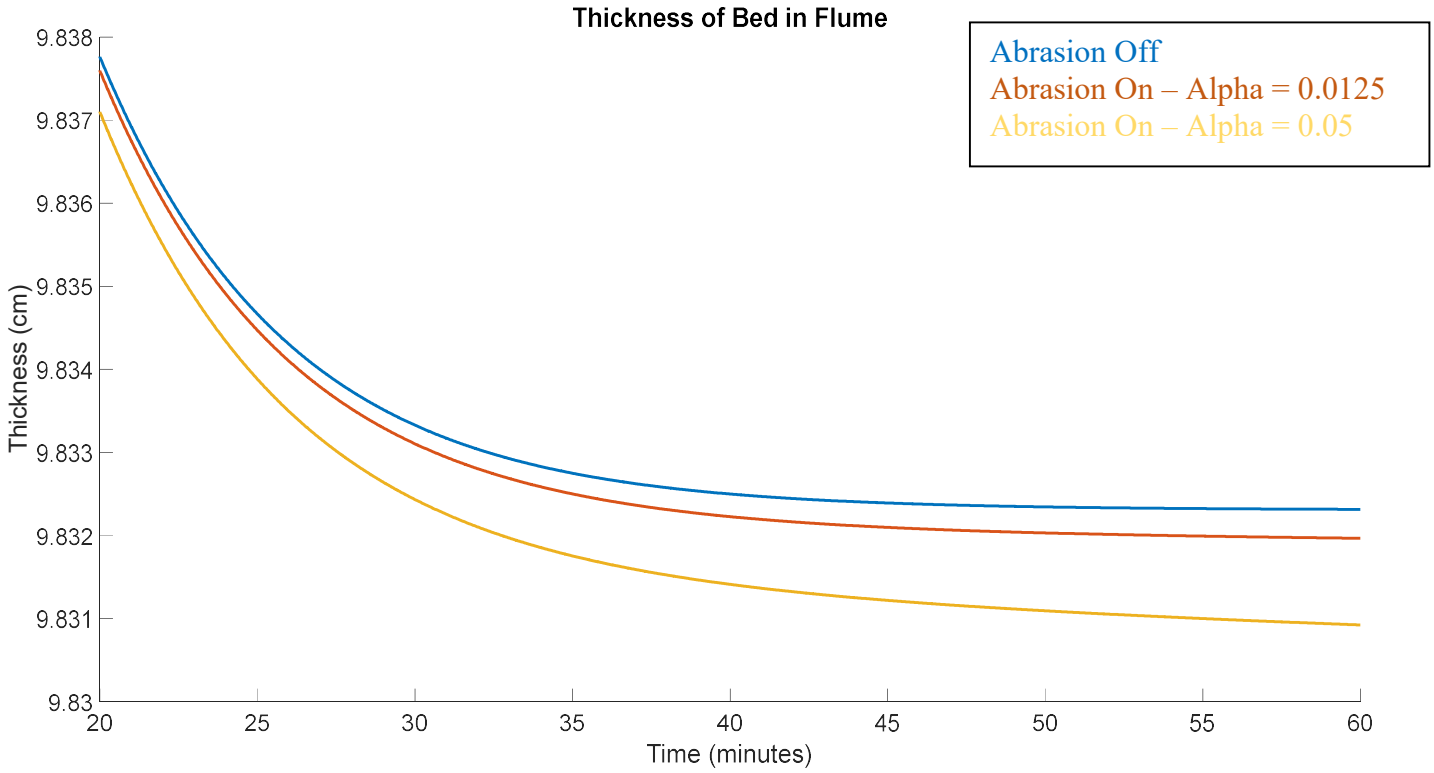

Figure 4.1: Thickness of Sediment Bed in Flume at Node 5

Figure 4.2 shows the changes in the median diameter of the aggregates in the surface layer of the bed over the hour-long simulation at node 5. For the run when abrasion was not being simulated, the median aggregate diameter of the bed immediately began to increase when the flow began and then reached an equilibrium aggregate diameter of around 1,313.7 µm between 35 and 45 minutes. The initial increase of the median bed aggregate diameter in the bed surface, for all three simulations, was due to a process known as bed armoring. Bed armoring is when smaller sediment in the sediment bed erodes more rapidly than larger sediment simply because it takes less force to move

smaller sediment. Since the smaller sediments are eroding more rapidly than larger sediment, some of which may not erode at all, the median diameter of the aggregates in the surface bed layer increases. As shown in Figure 4.2, the increase was relativity small, increasing from the initial 1,313.1 μm to around 1,313.7 μm, a 0.046% difference. The two runs with aggregate abrasion being simulated had an initial increase in median diameter of the sediment bed layer due to bed armoring, but after 25 to 45 minutes the median aggregate diameter of the sediment bed layer started to decrease, with the run involving the larger abrasion coefficient decreasing at a faster rate. The decrease of the median aggregate diameter in the sediment bed layer after 25 to 45 minutes occurred because when the abrasion of aggregates was simulated, a portion of the mass was transferred to the 20 μm aggregate size class, as described in the abrasion routine derivation in Chapter 3 and calculated by Equation (3.7). There was deposition of the 20 μm size class, therefore decreasing the median aggregate dimeter of the sediment bed. Also, as described in the abrasion routine derivation in Chapter 3, there was abrasion of the 3,500 μm and 300 μm size classes in bedload, with mass being transferred to the next smallest size class and then depositing thus also attributing to a decrease in median aggregate diameter of the sediment bed layer.

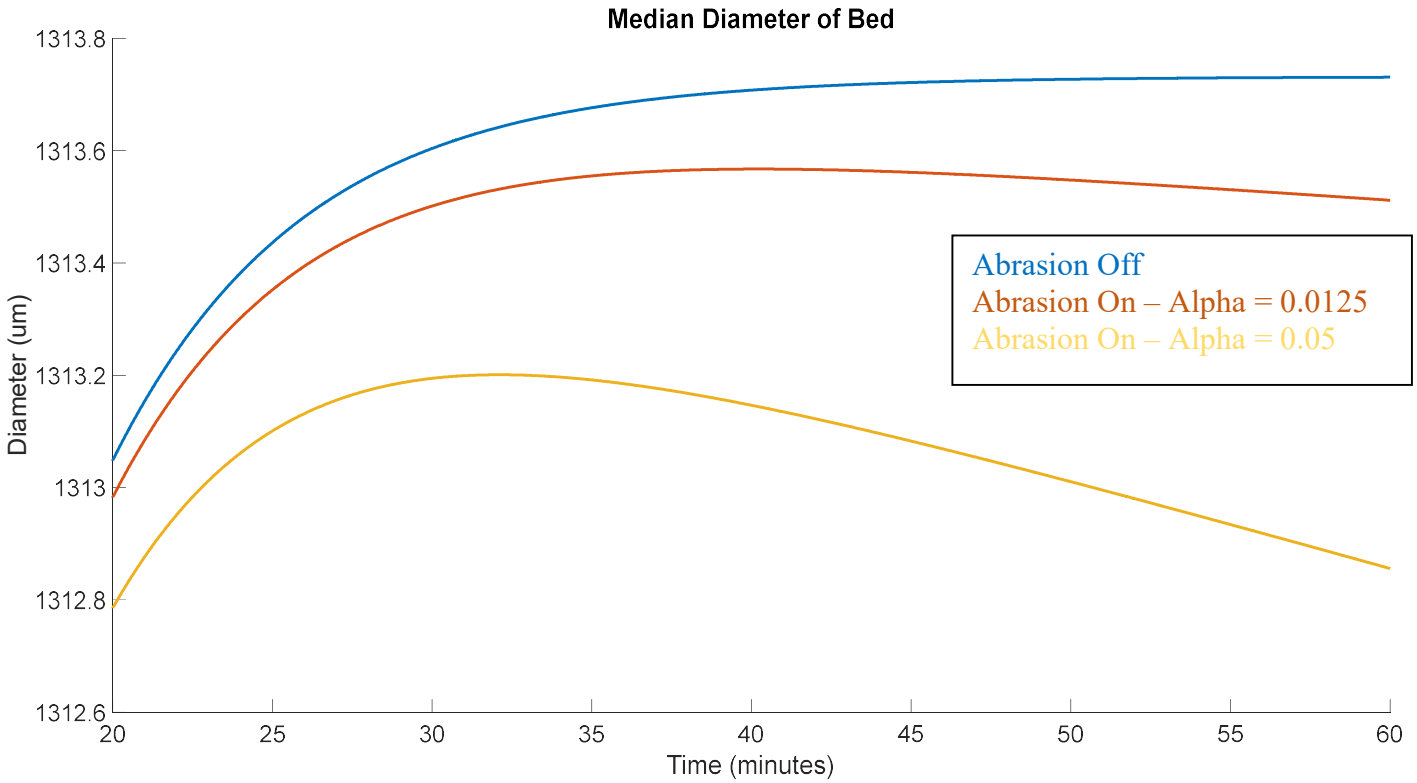

Figure 4.2: Median Diameter of Aggregates in Sediment Bed Layer at Node 5

As can be observed in Figure 4.3, the bed shear stress is directly correlated the median aggregate diameter of the sediment bed. Equation (2.6) gives the equation for the bed shear stress where f_c is calculated by Equation (2.7), and k_n in Equation (2.7) is calculated by $\frac{30*d50avg}{10000}$. These equations show that when the median diameter of the bed increases, the bed shear stress also increases due to the increase in value of k_n which decreases the value of f_c, as shown in Equation (2.7), which then decreases the value of the bed shear stress, as shown in Equation (2.6). Also, after 25 to 45 minutes of simulation time, the decrease in the median aggregate diameter of the sediment bed layer caused by abrasion

results in the decrease in bed shear stress for the runs simulating abrasion as shown in Figure 4.3.

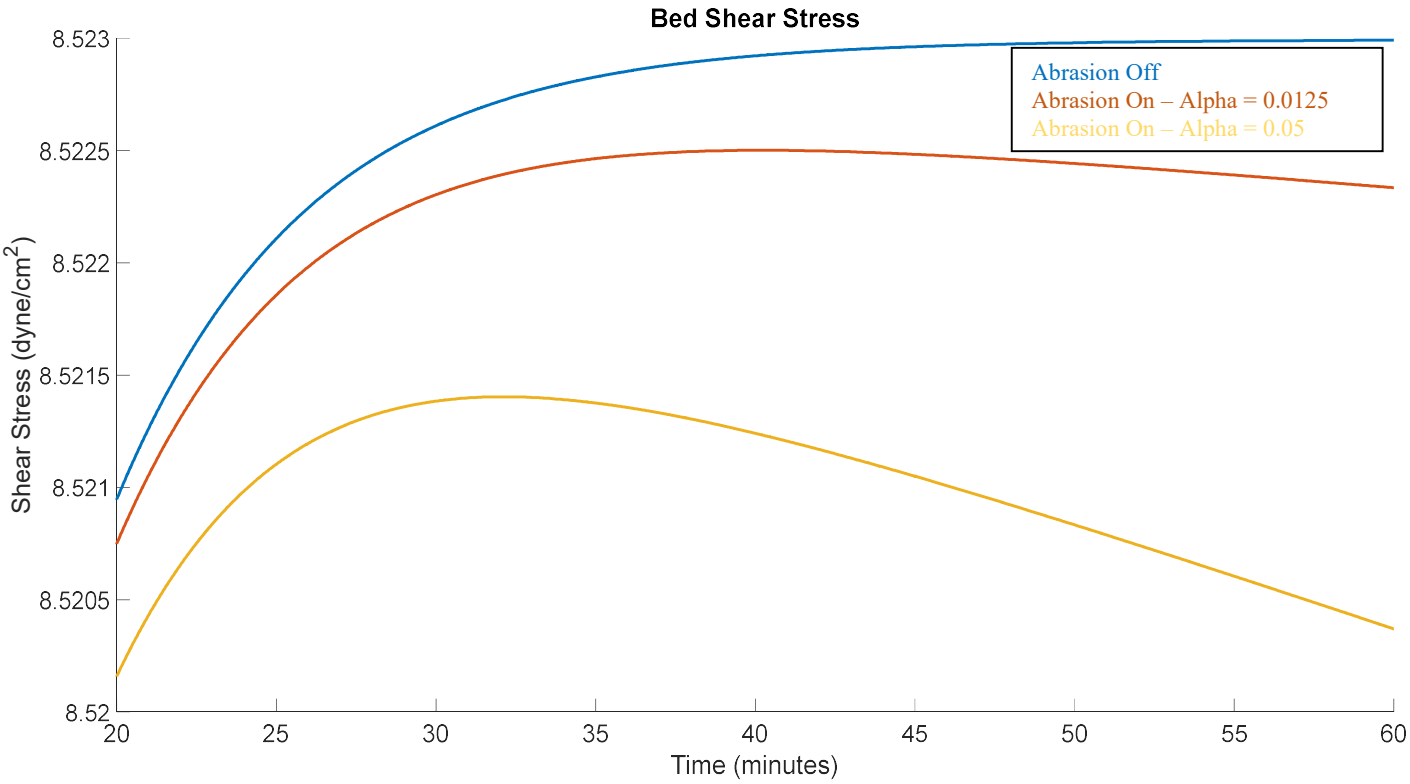

Figure 4.3: Bed Shear Stress Time Series at Node 5

The first individual aggregate size class and transport mode analyzed was the 3,500 µm size class that was transported as bedload. In fact, the 3,500 µm size class was only transported as bedload because its critical shear stress for suspension was 180 $\frac{dyne}{cm^2}$ and the bed shear stress was only around 8.52$\frac{dyne}{cm^2}$. Figure 4.4 shows the concentration of the 3,500 µm size class aggregate in bedload for all three simulations. In all three simulations there was initially a quick increase in bedload concentration, because there

was initially no flow in the flume, so the x-axis starts at 20 minutes to better show the differences between the three simulations for the last 40 minutes of the simulations. The simulation without abrasion reached an equilibrium bedload concentration which was expected due to the steady flow in the hypothetical flume. There was a 0.07% difference between maximum bedload concentrations of the simulation without abrasion and the simulation using an abrasion coefficient of $0.0125\frac{1}{m}$, and a 0.27% difference between maximum bedload concentrations of the simulation without abrasion and the simulation using an abrasion coefficient of $0.05\frac{1}{m}$. The 3,500 μm bedload concentrations of the simulations involving abrasion started decreasing after 30 to 40 minutes which was due to the simulation of abrasion of the aggregates during bedload transport. The simulation using the $0.05\frac{1}{m}$ abrasion coefficient resulted in a 0.2% smaller maximum bedload concentration compared to the $0.0125\frac{1}{m}$ abrasion coefficient. This is simply because, as defined in the sink terms of the aggregate abrasion routine, Equations (3.7) and (3.18), a larger abrasion coefficient results in a larger decrease in mass per time step compared to a smaller abrasion coefficient.

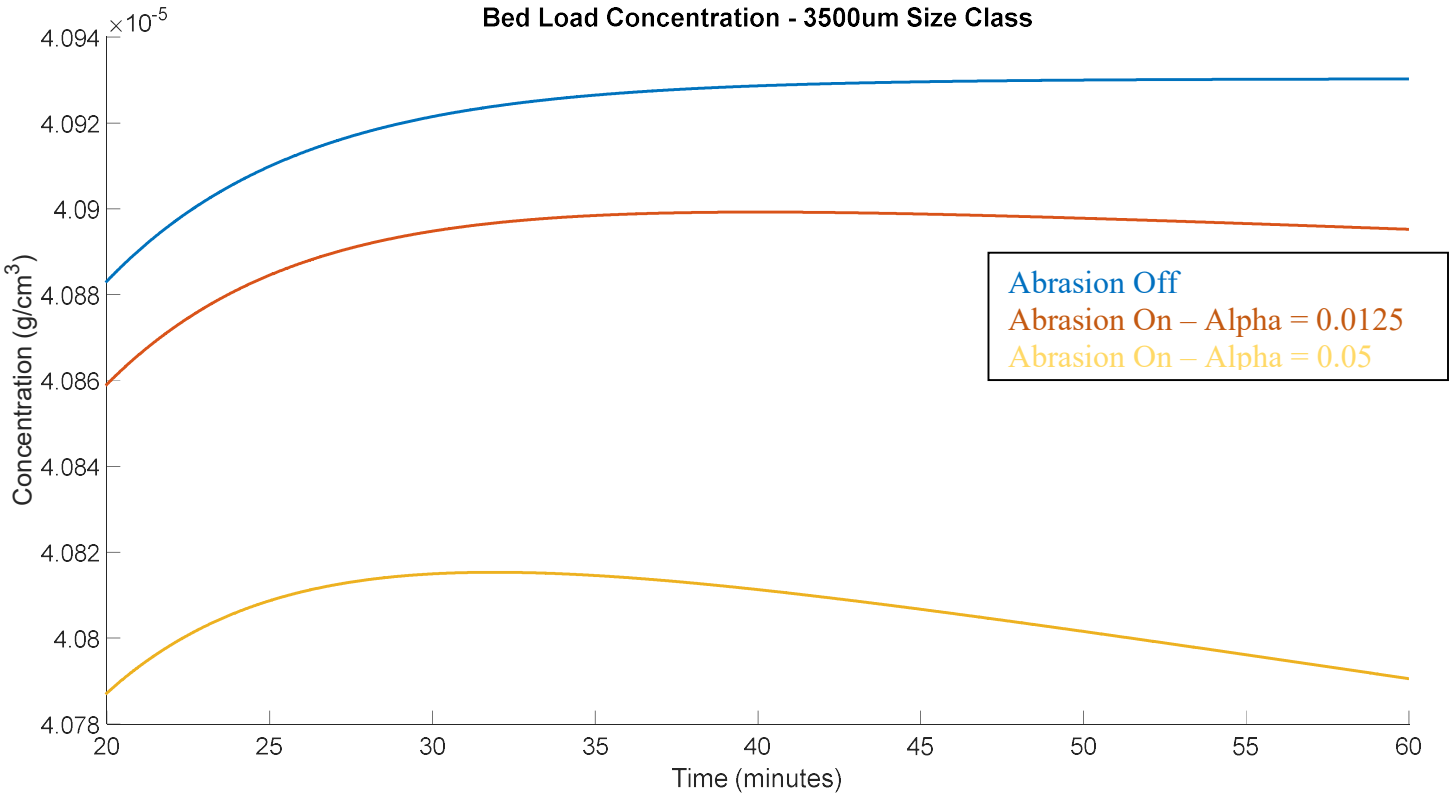

Figure 4.4: Bed Load Concentration for 3,500 µm size class at Node 5

Figure 4.5 shows the bedload concentration of the 300 µm aggregate size class in the hour-long simulation. The bedload concentrations were slightly larger than the bedload concentrations of the 3,500 µm aggregate size class. This was simply because the 300 µm size class took less force, i.e., shear stress, to erode and was less likely to deposit, due to a slower settling velocity, compared to the larger 3,500 µm size class. Similar to the bedload concentration of the 3,500 µm aggregate size class, the bedload concentration of the 300 µm aggregate size class reached equilibrium when abrasion was not being simulated. As opposed to the 3,500 µm aggregate size class, the 300 µm aggregate size class bedload concentrations continually increased when abrasion was being simulated.

This was due to the source term for the 300 μm aggregate size class, calculated by Equation (3.17), being greater than the sink term, calculated by Equation (3.18). The bedload concentration increased at a higher rate with the $0.05\frac{1}{m}$ abrasion coefficient due to more mass being transferred from the 3,500 μm size class to the 300 μm aggregate size class per time step, compared to the simulation with the $0.0125\frac{1}{m}$ abrasion coefficient, as calculated in Equation (3.17).

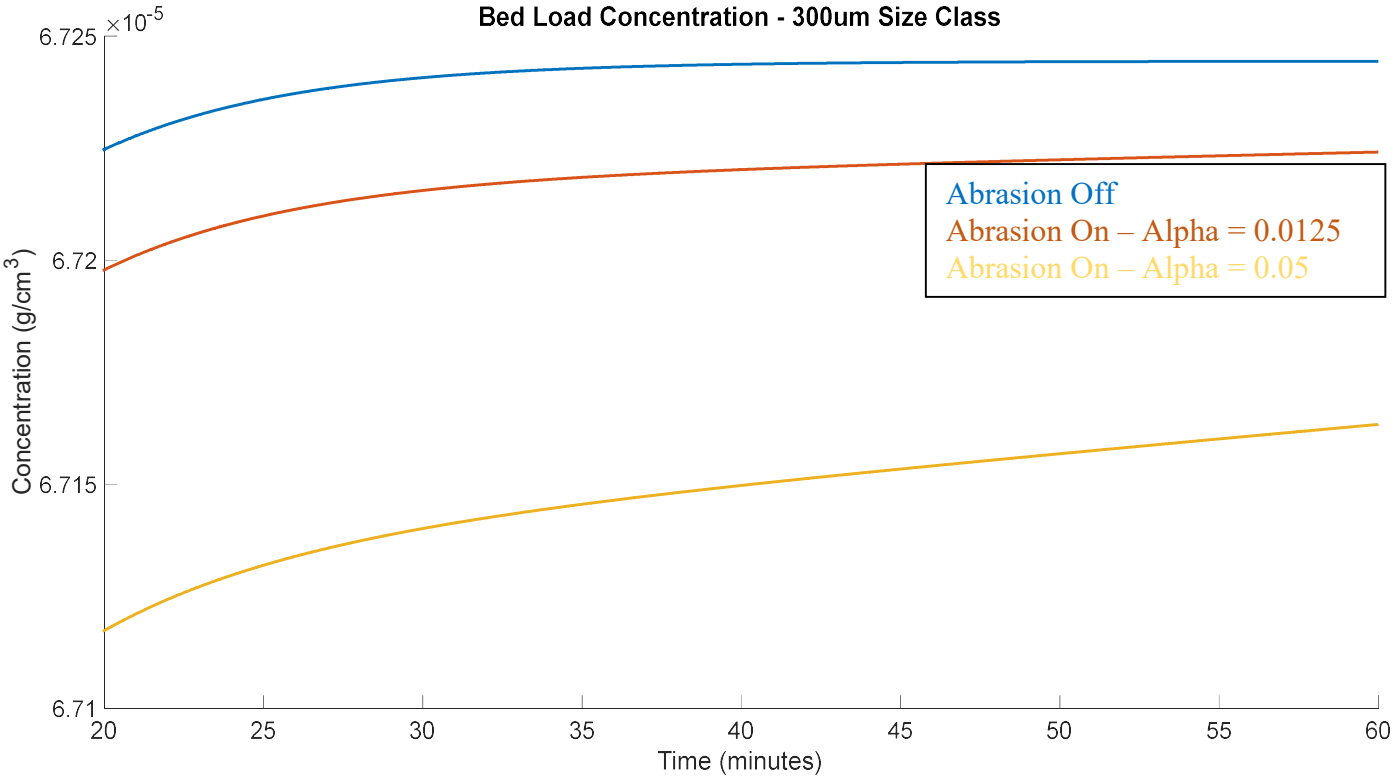

Figure 4.5: Bed Load Concentration for 300 µm Size Class at Node 5

The suspended sediment concentration time series for the 300 µm aggregate size class, the largest aggregate size class that was transported in suspension, is shown in Figure 4.6. Just as with bedload, the model not simulating abrasion reached an equilibrium concentration. When studying Figure 4.6, the first questions that came to mind were 1) why are the suspended load concentrations greater for the simulations with abrasion in the first 50 minutes of the simulation and 2) why do the runs simulating abrasion have decreases in concentration after 35-45 minutes? The first answer comes from Equation (3.17) which is repeated below.

$$dM_i(source) = \frac{1}{3}\frac{\alpha D_{i-1} u_{b,i-1} M_{i-1} dt}{D_i - D_{i-1}} \tag{3.17}$$

As described in Chapter 3, if aggregates were being transported as bedload and abrasion of the sediment was being modeled, then a calculated amount of mass of that aggregate size class would be transferred to the smallest aggregate size class in suspension and to the next aggregate size class. Equation (3.17) represents the change of mass transferred from the aggregate size class moving as bedload to the next smallest aggregate size class. In this case, the 3,500 μm aggregate size class was moving as bedload, and the mass lost due to abrasion was transferred to the 300 μm aggregate size class. Another addition to the abrasion routine was that not 100% of the mass transferred from the 3,500 μm size class was transferred to the 300 μm size class in bedload, but some mass was transferred to the 300 μm size class in suspension as the probability of suspension of the 300 μm aggregate size class was nonzero. To determine how much of the abraded mass was transferred to the next aggregate size class that was moving as bedload and how much was transferred to the smallest aggregate size class that was transported in suspension, the probability of suspension was calculated using Equation (2.13) (repeated below).

$$p = \frac{\frac{\log(usw) - \log\left(\sqrt{\tau_{cs}}\right)}{w_s}}{\frac{\log(4) - \log\left(\sqrt{\tau_{cs}}\right)}{w_s}} \tag{2.13}$$

Equation (4.5) and Equation (4.6) give how the probability of suspension was used to determine how much of the abraded mass was transferred to the aggregate size class in bedload or suspension.

$$M_{1\to 2}^{sus} = p_{sus} * M_{1\to 2} \tag{4.5}$$

$$M_{1\rightarrow 2}^{bed} = (1 - p_{sus}) * M_{1\rightarrow 2} \quad (4.6)$$

The probability of suspension for the 300 µm size class for the conditions in the three simulation was approximately 0.89 but varied slightly with bed shear stress. The addition of mass to the suspended sediment concentration of the 300 µm aggregate size class from the 3,500 µm size class was why the concentration was greater in the first 50 minutes of the simulation when abrasion was being modeled compared to when abrasion was not being modeled. As for the second question, why the suspended sediment concertation decreased when abrasion was being simulated; that can be explained by Figures 4.1 and 4.2. As stated earlier, when abrasion was being simulated the average aggregate diameter of the sediment bed layer decreased which also decreased the bed shear stress. When the bed shear stress decreased, the erosion rate of the sediment bed layer decreased which in turn decreased the concentrations of aggregates in transport. This was confirmed in Figure 4.7 which is a time series plot of mass eroded per sediment bed area for the 300 µm aggregate size class when the abrasion coefficient was equal to $0.05\frac{1}{m}$. After approximately 35 to 40 minutes, the addition of mass (converted to concentration) to the 300 µm aggregate size class in suspension from the 3,500 µm aggregate size class in bedload per time step was less than source concentration term for the 300 µm aggregate size class in suspension per time step, as given by Equation 2.12, hence the decrease in suspended load concentration shown in Figure 4.6 for both runs simulating abrasion.

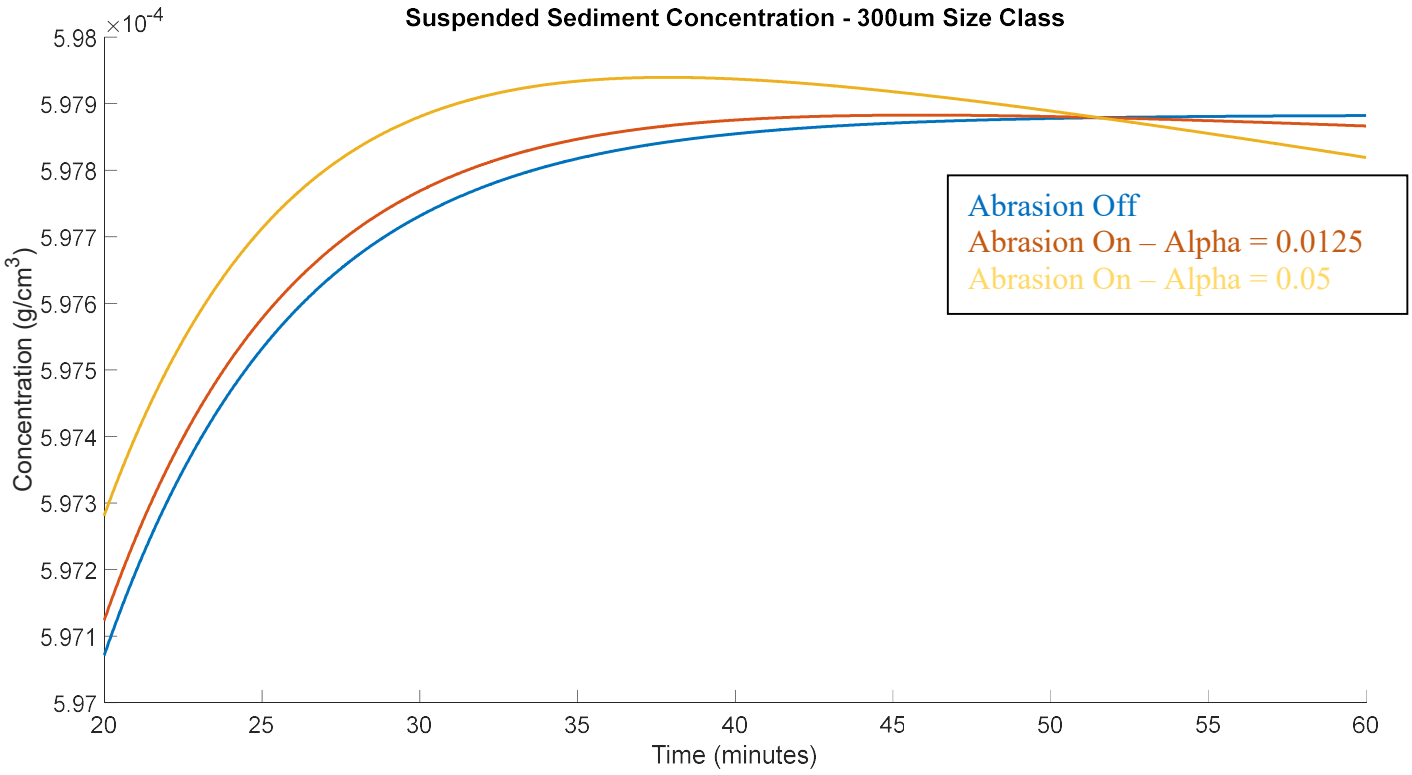

Figure 4.6: Suspended Sediment Concentration for 300 µm Size Class at Node 5

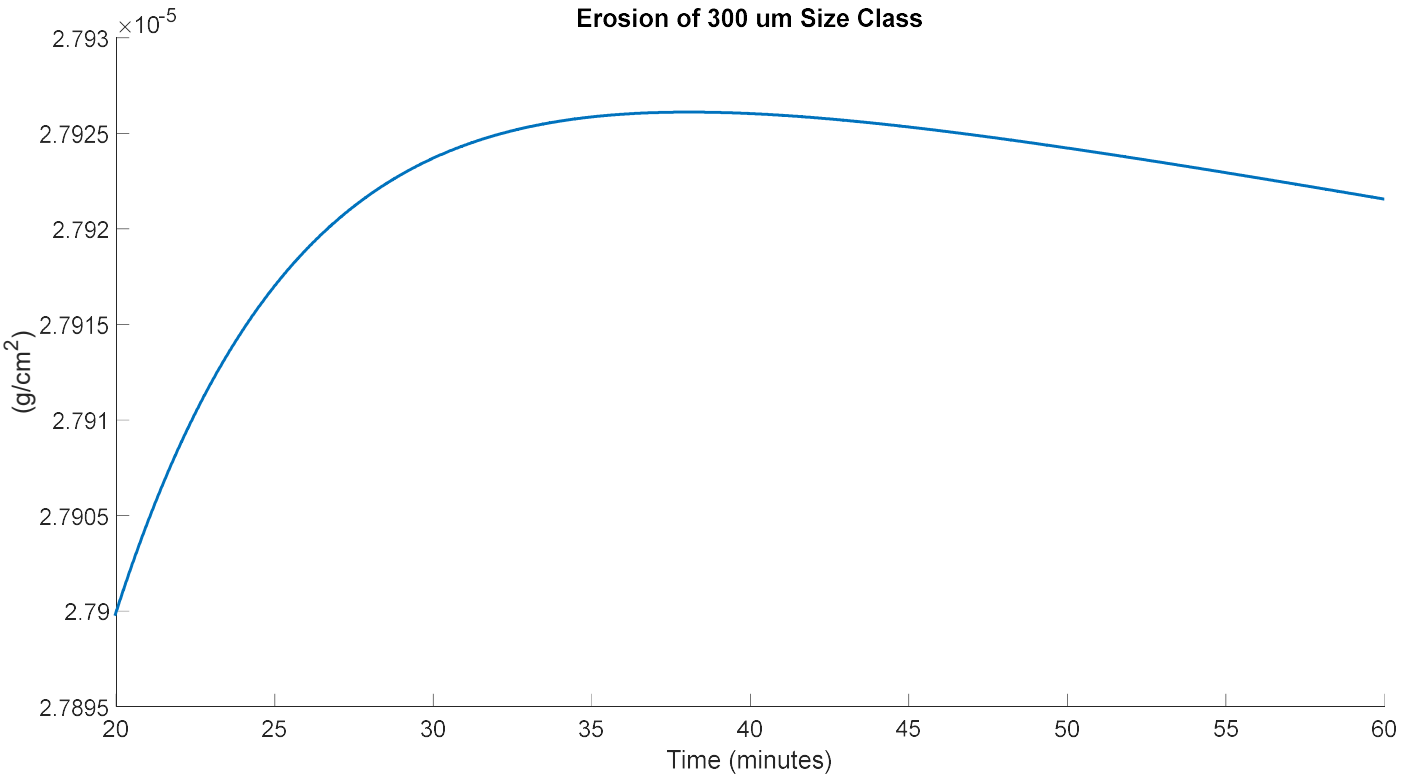

Figure 4.7: Mass Eroded per Unit Area of 300 µm Size Class at Node 5

The suspended sediment concentration time series for the 80 µm size class, shown in Figure 4.8, resembles the suspended sediment concentration plots of the 300 µm size class as the suspended load concentration was smaller at the end of the simulation when abrasion was being simulated. Due to simulation of abrasion of the 300 µm size class that was moving as bedload, mass was added to the 80 µm size class being transported in suspension, but it was not enough mass to account for the loss of mass due to the decreasing erosion rate caused by the decreasing median aggregate diameter in the bed, hence the decrease in suspended load concentration when abrasion was being simulated.

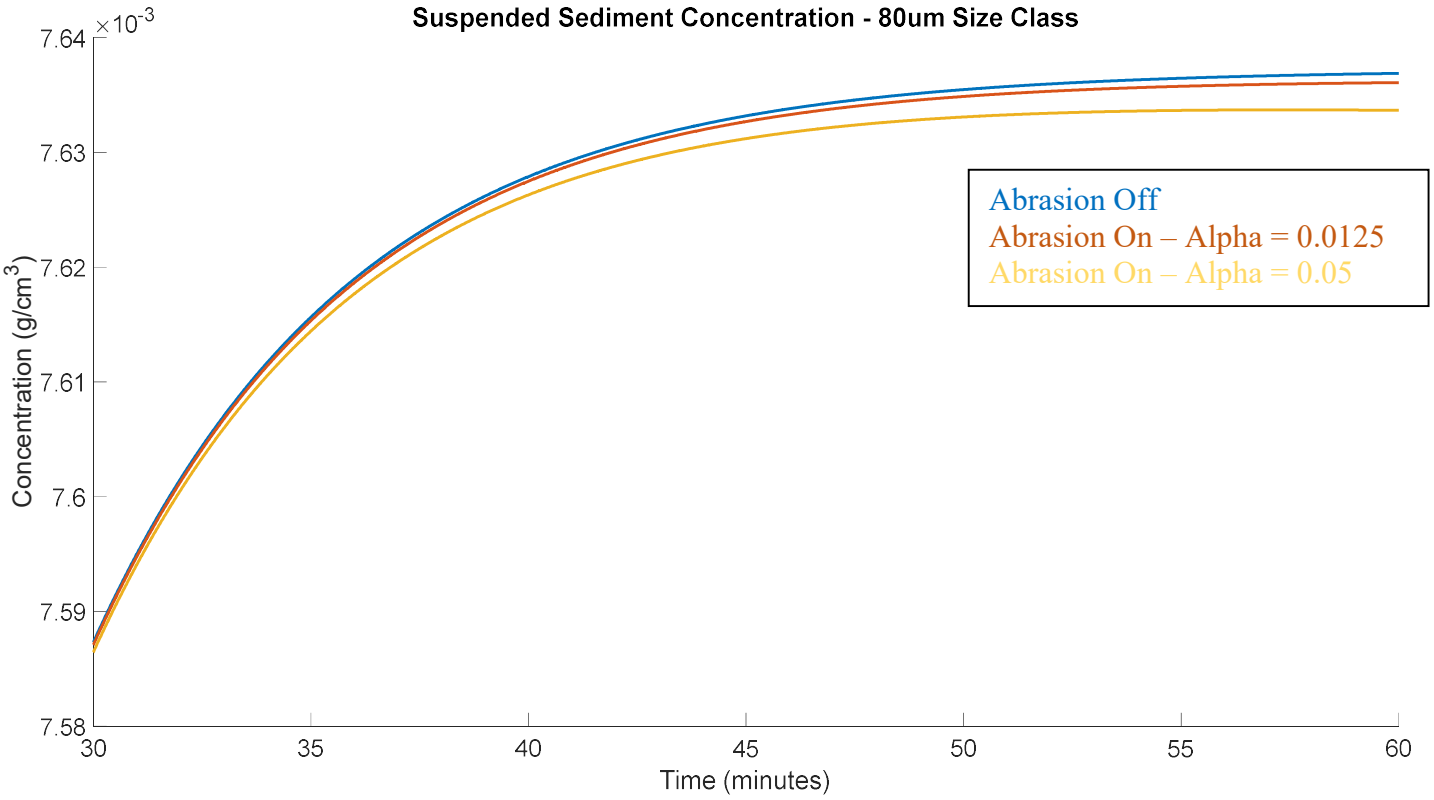

Figure 4.8: Suspended Sediment Concentration for 80 µm Size Class at Node 5

The 20 µm size class time series, shown in Figure 4.9, only had non-zero concentration values when abrasion was being simulated. This was because there was not initially any 20 µm sized aggregates in the bed, and, in this model, the only process to produce these aggregates was through abrasion of the larger size classes. As expected, the higher abrasion coefficient produced a larger concentration of the smallest aggregate size class. This size class was only transported in suspension due to its very small settling velocity.

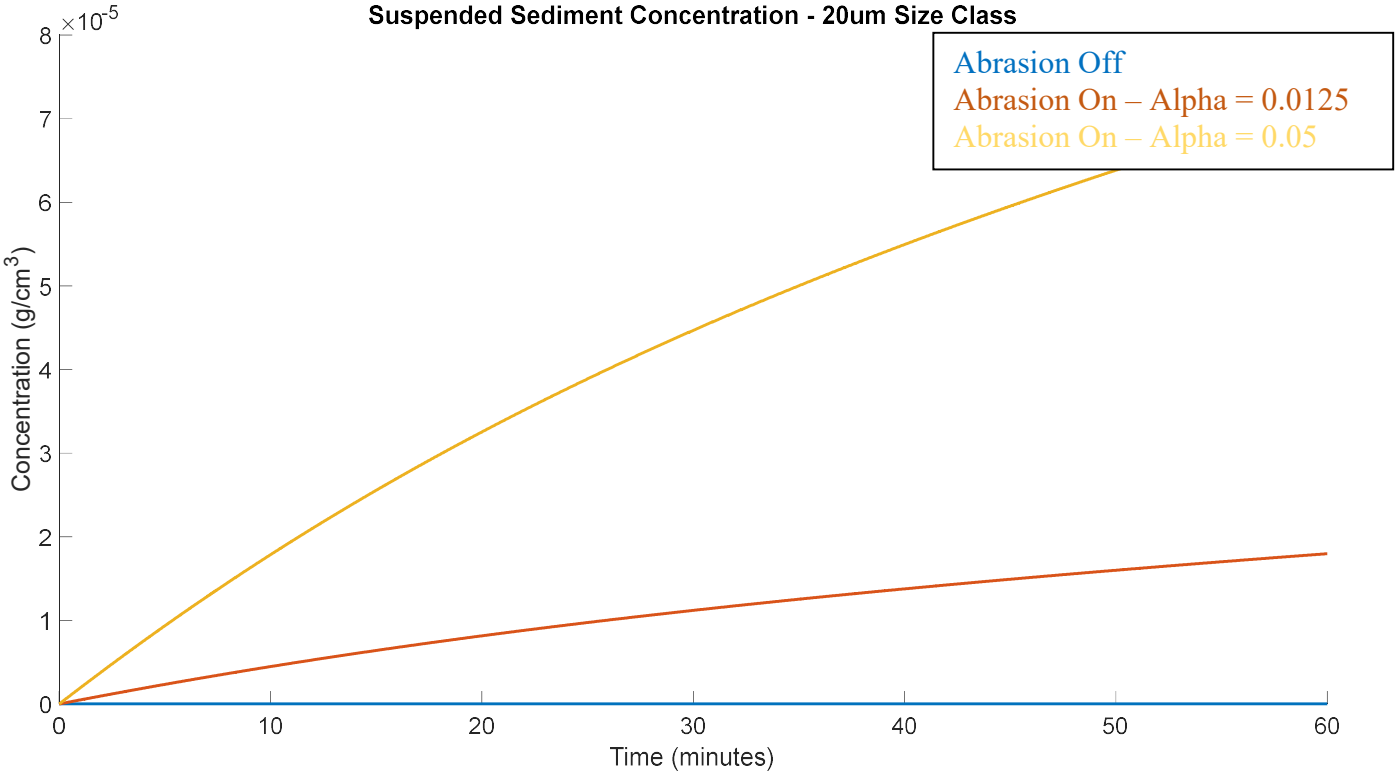

Figure 4.9: Suspended Sediment Concentration Time Series for 20 µm Size Class at Node 5

Figure 4.10 shows the total mass of aggregates being transported as bedload in the flume during the hour-long simulation. Figure 4.10 confirms that simulating abrasion decreased the amount of mass that was being transported as bedload as given by Equation (3.7) and Equation (3.18). It also confirmed, as given by the same two equations, that increasing the abrasion coefficient increased the amount of mass that was lost from aggregates being transported as bedload. The simulation with the $0.05\frac{1}{m}$ abrasion coefficient had approximately 0.5% less bedload mass than the simulation without

abrasion and the simulation with the $0.0125\frac{1}{m}$ abrasion coefficient had approximately 0.1% less bedload mass than the simulation without abrasion after the hour-long simulation.

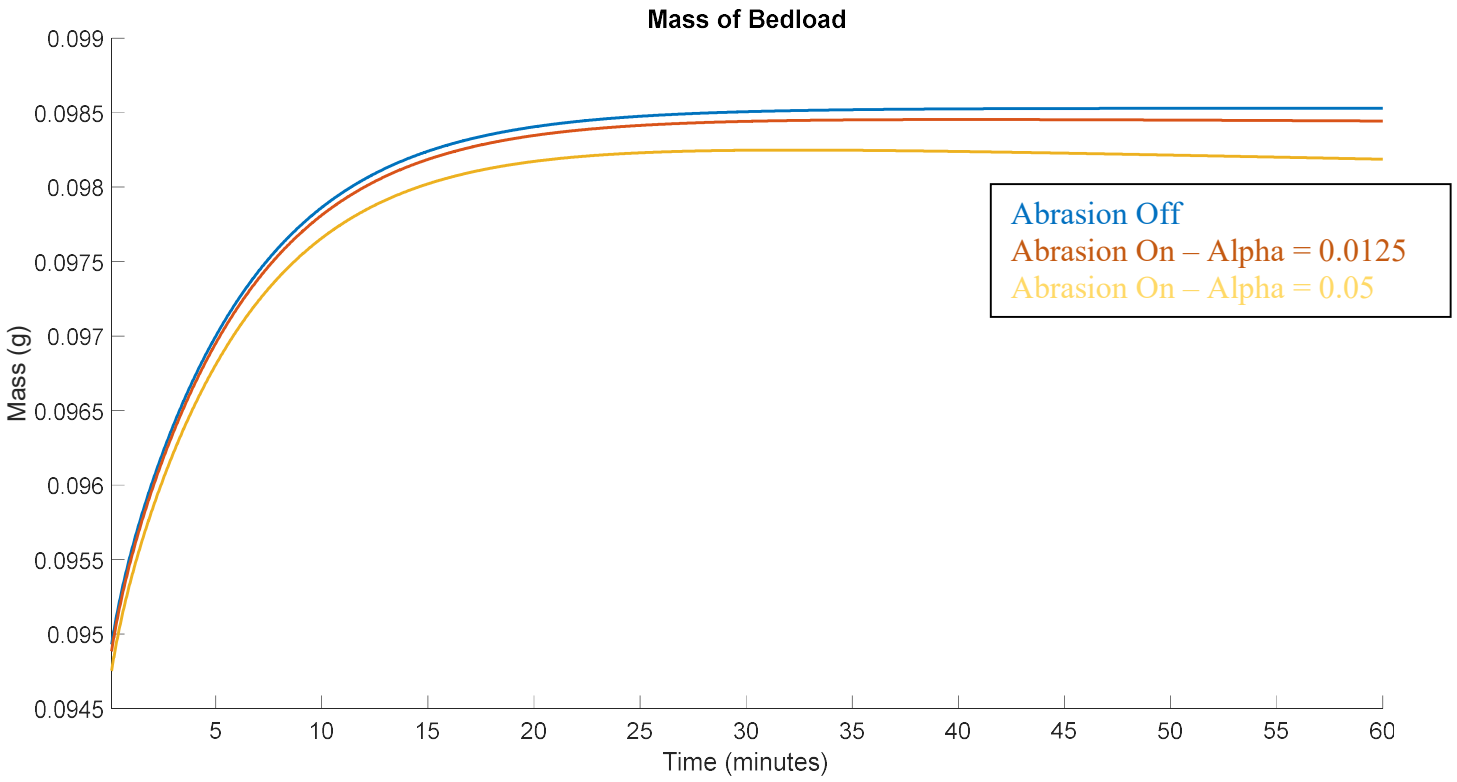

Figure 4.10: Mass of Bedload in Flume

Figure 4.11 shows the total mass of suspended sediment in the flume for the hour-long simulation. The increase in mass when abrasion was being simulated was primarily due to the increase in mass of the 20 µm size class which was accumulating mass being abraded from aggregates in bedload as calculated by Equation (3.7). Figure 4.10 confirms that simulating abrasion will increase the mass of sediment being transported in

suspension as given by Equation (3.7) and Equation (3.18). After one hour, the simulation with the abrasion coefficient of $0.05\frac{1}{m}$ had approximately 0.8% more suspended mass than the simulation without abrasion and the simulation with the abrasion coefficient of $0.0125\frac{1}{m}$ had approximately 0.3% more suspended mass than the simulation without abrasion

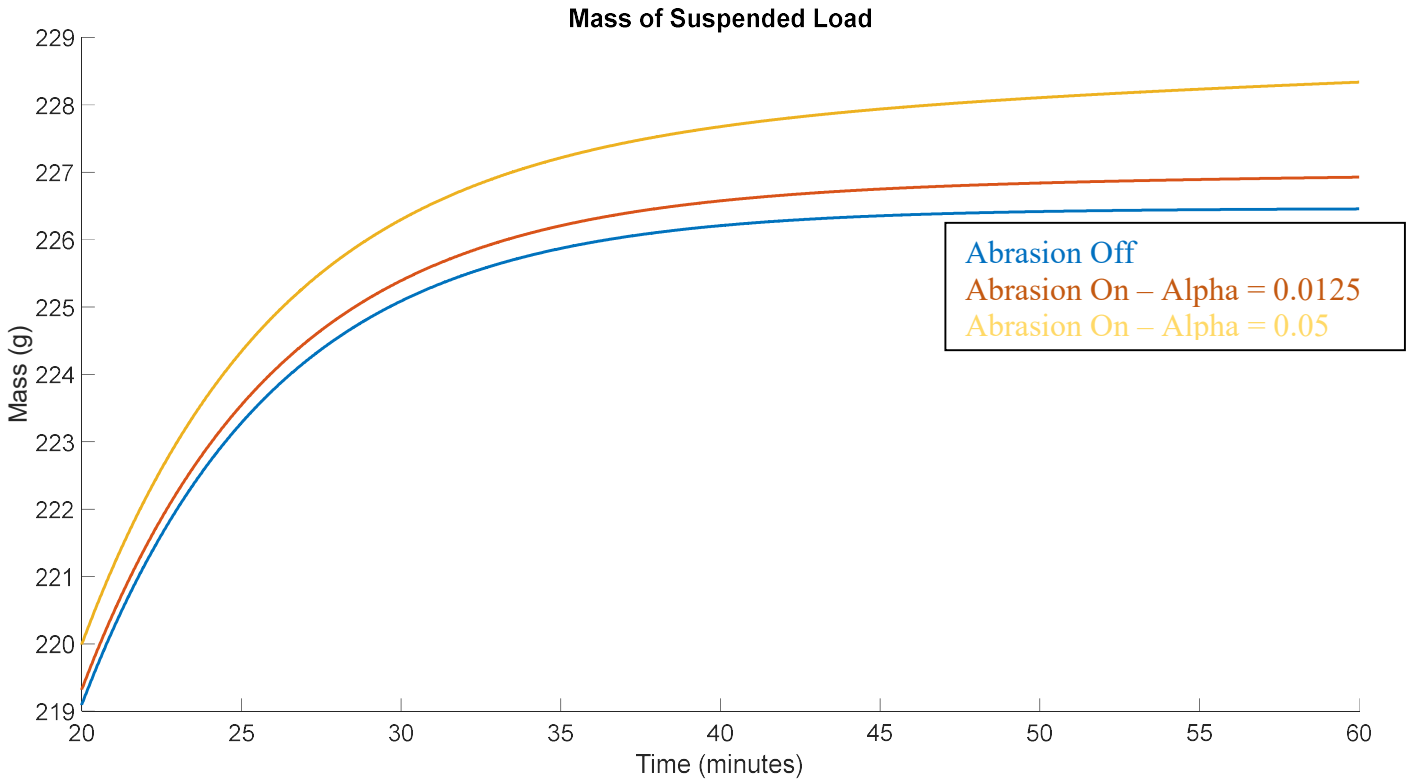

Figure 4.11: Mass of Suspended Load in Flume

Figure 4.12 shows how the total mass of all the aggregates in the bed and in transport were conserved during the hour-long simulation. The results in Figure 4.12 show that the model does conserve mass very well. Figure 4.12 also shows that increasing the abrasion coefficient does increase the amount of mass lost during the hour-long simulation. Errors in mass conservation can be attributed to rounding errors and the simplicity of the sediment transport model.

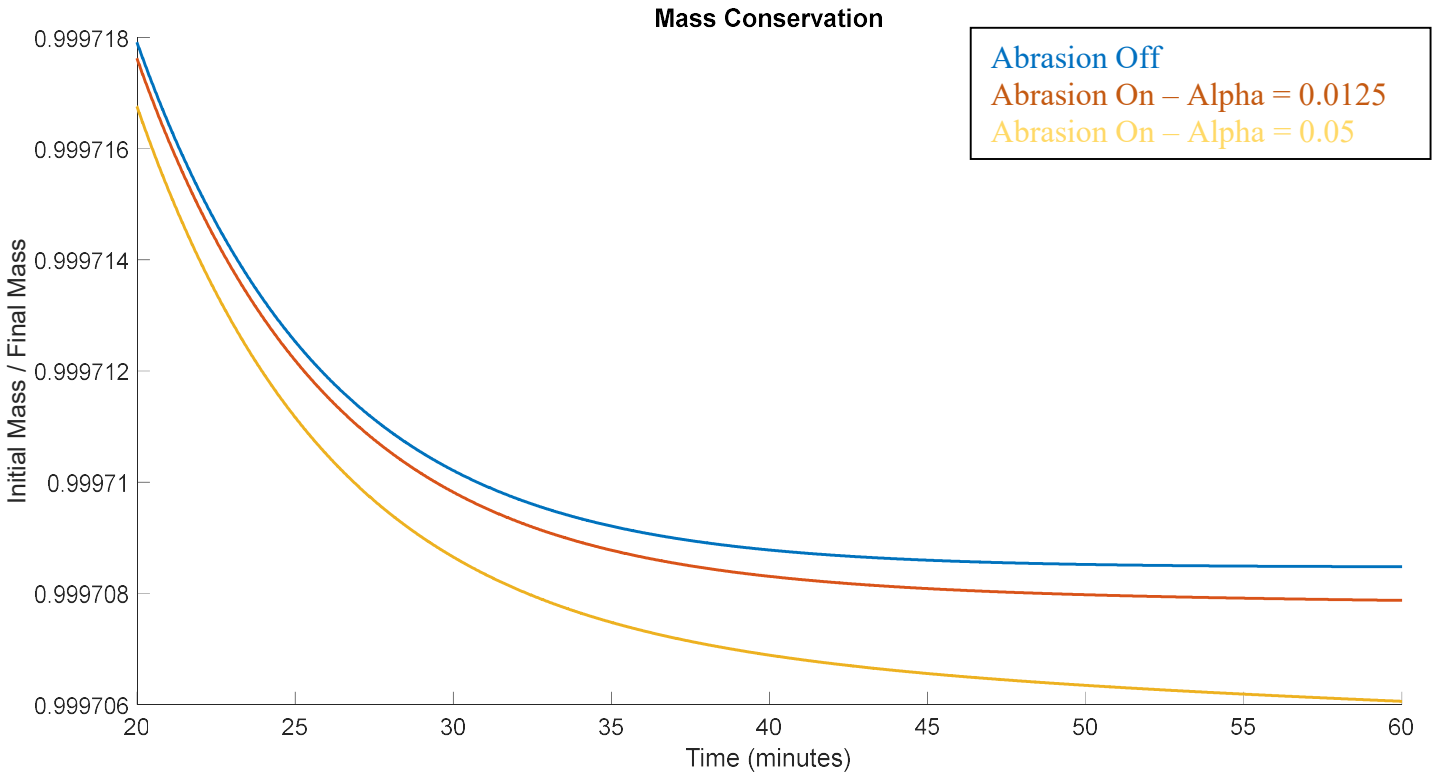

Figure 4.12: Mass Conservation

CHAPTER 5

SIMULATION OF ABRASION IN THE JAMES RIVER

AREA OF INTEREST AND INITIAL CONDITIONS

After developing an abrasion routine that simulates abrasion of mud aggregates and confirming its effectiveness in a 1-D sediment transport model, the routine was included in an existing GSMB model of the James River Estuary in Chesapeake Bay. Figures 1.1, 1.2, and 1.3 from Chapter 1 show the location of the area of interest. The existing GSMB model in the James River estuary was created to model, among other factors, the effects from adding a new dredged material placement site in the James River (Hayter *et al.,* 2020). The location of the dredged material placement site can be seen in Figure 5.1.

Figure 5.1: Potential Dredged Material Placement Site is Shown in the Red Polygon

To replicate the dredged material located in the placement site, the sediment property data, described in Chapter 3, was input in the grid cells which overlap the location of the placement site. The grid used for the entire James River and Chesapeake Bay GSMB model was shown in Figure 2.9 and Figure 2.10. Figure 5.2 shows the grid at the placement site location shown in Figure 5.1. Specifically, grid block 8, shown in the middle of Figure 5.2, was the location of the placement site.

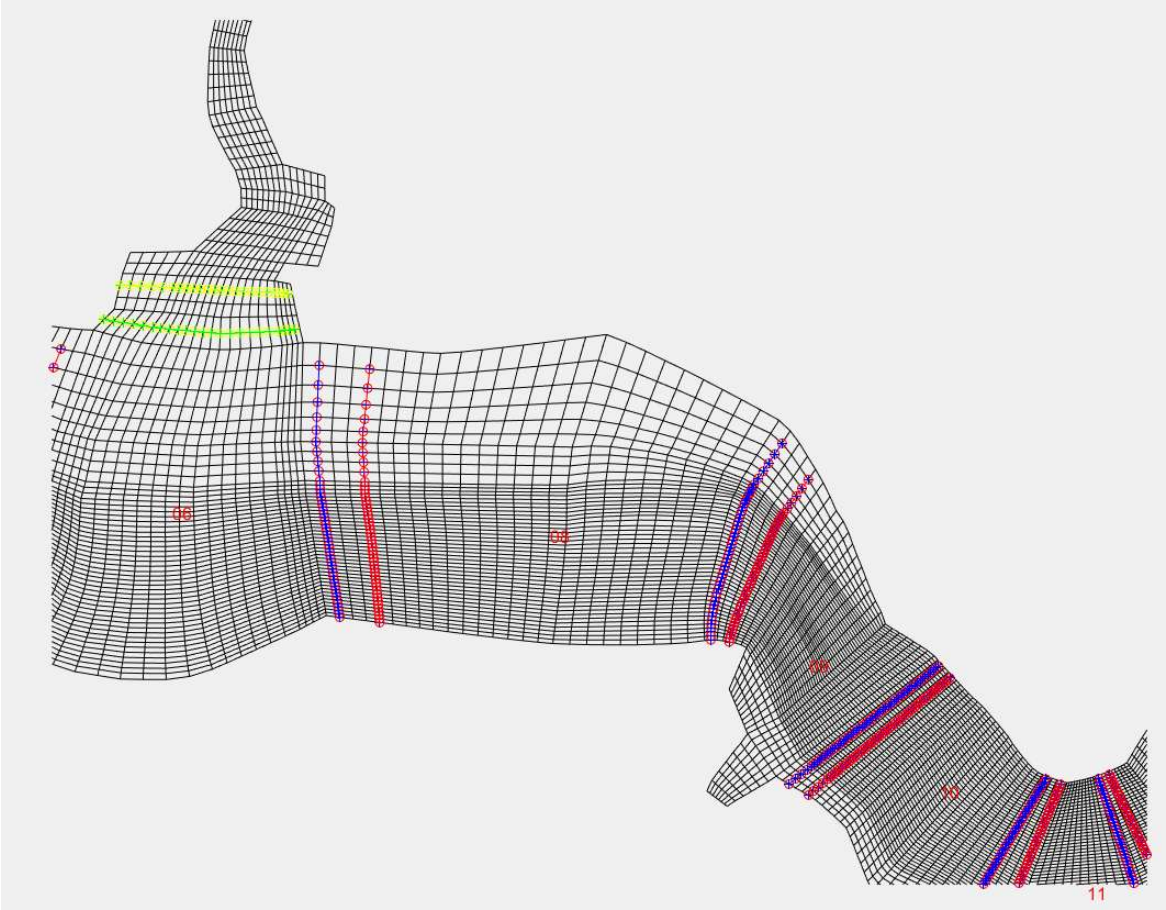

Figure 5.2: Grid Blocks Including and Surrounding Placement Site Which is Located in Grid Block 8

Figure 5.3 shows the specific grid cells that was given dredged material sediment properties to represent the potential dredged material placement site. The total area of the cells that encompass the placement site is approximately 0.91 km^2.

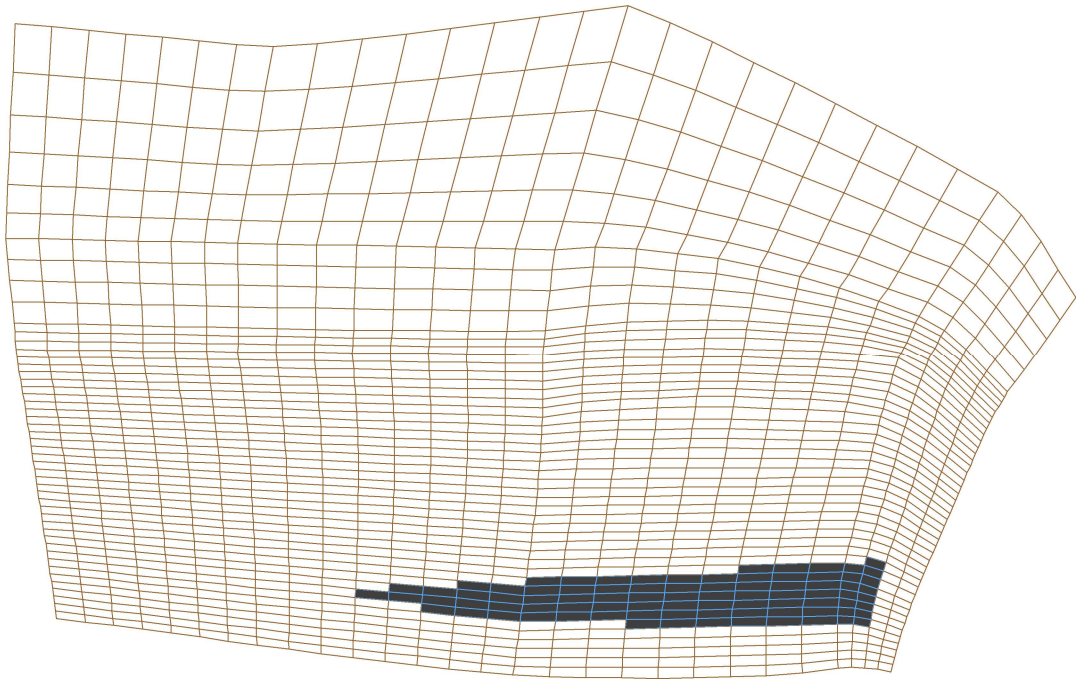

Figure 5.3: Location of Dredged Material Placement Site in Grid Block 8

The placement area shown in Figure 5.3 contains the placed dredged material and was represented by three different sized aggregates. As previously described, a fourth aggregate size class is created due to the process of abrasion when abrasion was included in the simulation. The four aggregates have the same sizes and properties as the aggregates used in the 1-D sediment transport model as given in Table 3.1. The 3,500

μm, 300 μm, and 80 μm aggregates each made up 13% of the third layer of the bed at the placement site, totaling 39%. The third layer is considered to be the top layer of the sediment bed at the beginning of the simulation. The other 61% consisted of other sediment in the sediment bed. It is important to note that in the initial GSMB model of the James River, there was 12 sediment size classes to fully represent the different material in the James River and Chesapeake Bay being modeled. In the current GSMB model of the James River, three mud aggregate size classes were added to represent the dredged material and one other mud aggregate size class, the 20 μm aggregate size class, was added to represent the silt created as a byproduct of abrasion. The placement site shown in Figure 5.3 is the only location where the three largest mud aggregate size classes are present at the start of the simulation, but that changed after the mud aggregates were eroded and transported.

The hydrodynamic model in GSMB, CH3D, was hot started, meaning that conditions at the last time step of a previous model was used for the initial conditions. The sediment transport model in GSMB, SEDZLJ, was cold started, meaning that initially there was no suspended sediment concentrations or no bedload concentrations at any of the 33 grid blocks in the model domain.

RESULTS FROM 3-D GSMB JAMES RIVER MODEL

In a model of an estuary, factors such as tidal cycles, salinity transport, and morphological changes can all effect the results of a sediment transport simulation. This had to be considered when interpreting the results of the GSMB model simulations with

and without the simulation of abrasion. To interpret the effects of adding abrasion to the sediment transport model, the results that needed to be produced had to be specific.

The first result that was analyzed was how the total mass of mud aggregates in the placement site changed by using a 15-day, 3-D GSMB model simulation when abrasion was and was not being simulated. A 15-day simulation was used to simulate the aggregate transport in the James River estuary over numerous tidal cycles and allow plenty of time for the aggregates to be transported throughout the estuary. The entire 15-day simulation took two and a half days to run. As stated in Chapter 1, the most efficient method to dispose of dredged material from the navigation channel in the James River is to place the dredged material at a placement site close to the channel. Analyzing the sediment transport of placed dredged material from these placement sites helps the USACE with planning how long placement sites can be used and finding the best locations for future placement sites. Therefore, if adding the simulation of abrasion to the current GSMB model in the James River effects how much mass of mud aggregates leaves the placement site, it could potentially help the USACE in more accurately planning for future placement sites (Hayter *et al.,* 2020).

Figure 5.4 shows the total mass of the mud aggregates in the placement site over the 15-day simulation as well as two plots of bed shear stress from two different cells. The middle plot in is from a cell on the downstream side of the placement site shown in Figure 5.3 and the bottom plot is from a cell on the upstream side of the placement site shown in Figure 5.3. Each side of the placement site in Figure 5.3 is exposed to slightly different magnitude of bed shear stresses, hence a plot from each side is shown in Figure

5.4. The sinusoidal nature of the magnitude of the bed shear stresses in Figure 5.4 is due to the flow of the river changing directions between flowing upstream and downstream. The two instantaneous losses of mass of the mud aggregates in each cell can be explained by the two bed shear stress plots. Just as individual aggregates have critical shear stresses for erosion, the bed layers also have a critical shear stress for erosion. When the mud aggregates were initially input in the chosen cells, they were placed in layer three. The critical shear stress for layer three was 2.5 dyne/cm^2. The top bed shear stress plot shows the bed shear stress at a single cell and it is shown that when the bed shear stress reaches 2.5 dyne/cm^2, there is a loss in the mass of mud aggregates in the bed due to the process of mass erosion. A group of cells in the right side of the placement site, which were exposed to bed shear stresses similar to that of the middle plot in Figure 5.4, were exposed bed shear stress that exceeded the critical bed shear stress for erosion approximately 0.5 days into the simulation. The remainder of the cells in the left side of the placement site, which experienced similar bed shear stresses as the bottom plot in Figure 5.4, did not experience the 2.5 dyne/cm^2 shear stress until approximately 4.5 days into the simulation.

At the end of the 15-day simulation over 99% of the initial mass had left the placement site in both runs with and without abrasion. When comparing the difference between when abrasion is being simulated and when abrasion is not being simulated, it is shown in Figure 5.4 that simulating abrasion in the GSMB model decreases the amount of mass of mud aggregates in the bed. This was expected because when abrasion was occurring, mass was being transferred from larger aggregate size classes moving as

bedload to the next smallest aggregate size class as well as to the 20 μm aggregate size class. The smaller mud aggregate size classes were less likely to deposit, hence there was less overall mass of mud aggregates in the bed over the 15-day simulation.

At the end of the 15-day simulation there was 233 kg of mud aggregates in the placement site when abrasion was being simulated and 12,050 kg of mug aggregates in the placement site when abrasion was not being simulated. Both masses are less than 1% of the initial 7 million kg of mug aggregates initially in the placement site.

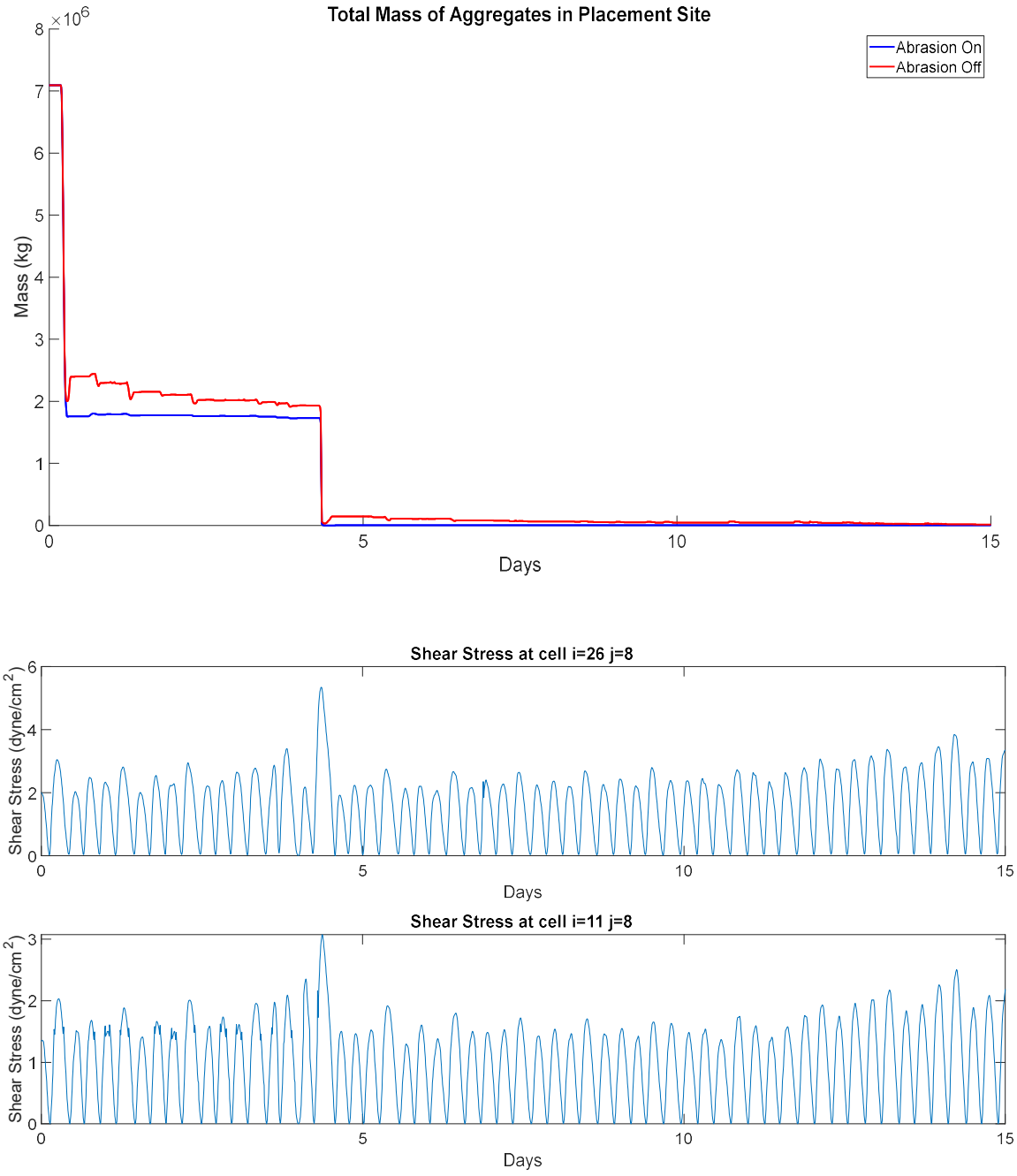

Figure 5.4: Mass of Aggregates in Placement Site and Bed Shear Stresses

While placing dredged material in along navigation channel placement sites is an efficient way to dispose of dredged material, the subsequent erosion and transport of this material can potentially bring the material back into the navigation channels that the material was once dredged from. For this reason, it was important to determine how much mass of mud aggregates that eroded from the placement site were subsequently deposited back into the channel by the end of the 15-day simulation. The mass of mud aggregates at four locations in the navigation channel with the deepest relative depths were chosen to be analyzed during the 15-day simulation. Two of the four locations chosen are upstream of the placement site and the other two locations are downstream of the site.

The four locations chosen were in grid blocks 5, 6, 9, 10. Figure 5.5 shows these grid blocks in relation to the placed dredged material site in grid block 8.

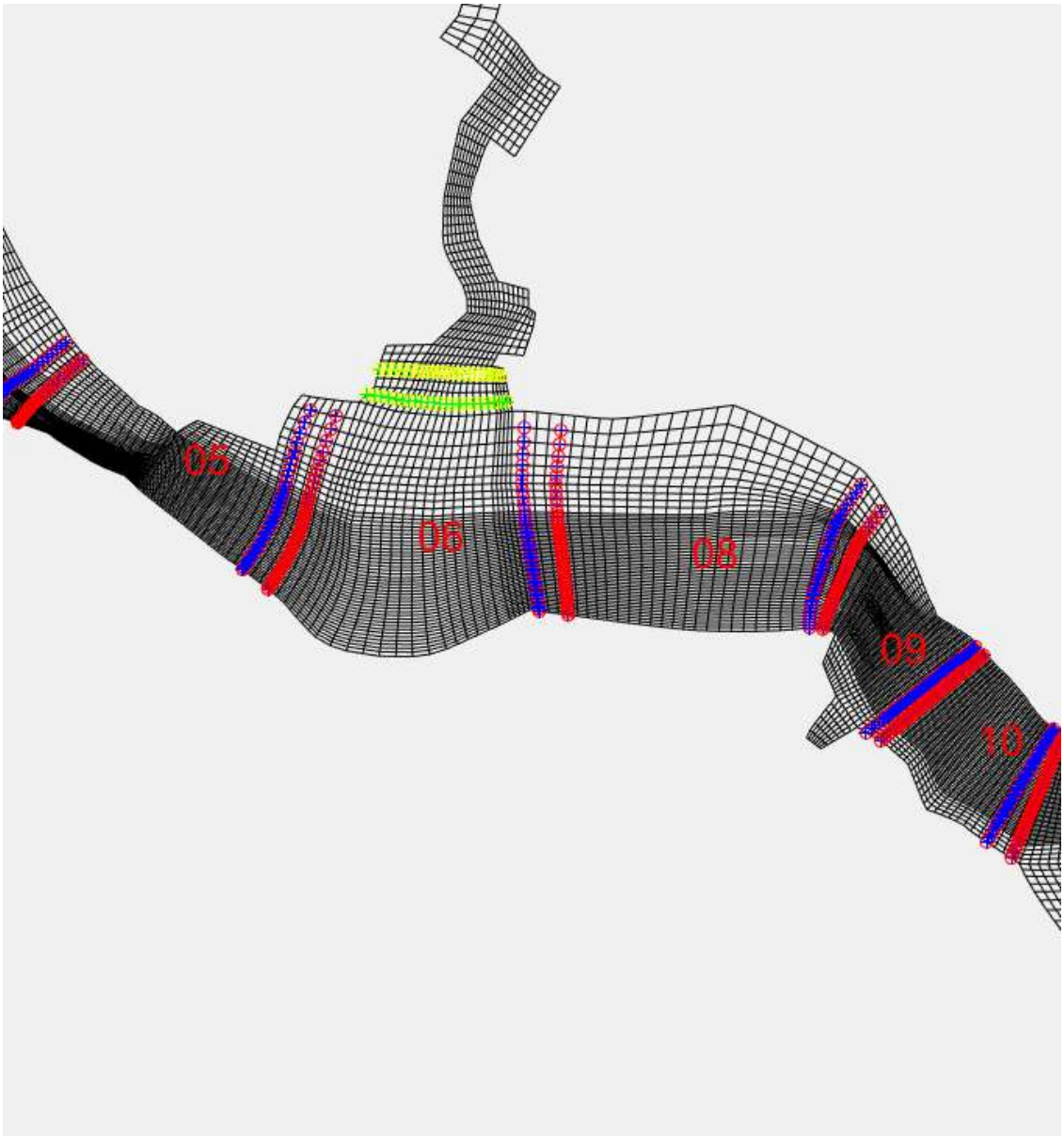

Figure 5.5: Grid Blocks 5, 6, 9, and 10 in Relation to Grid Block 8, the Location of the Dredged Material Placement Site

Starting in grid block 5, the farthest upstream grid block analyzed, the section of the navigation channel chosen is indicated by the orange highlighted cells shown in

Figure 5.6. The depths shown in Figure 5.6 are the initial water depths at the beginning of the model simulation. Table 5.1 gives the area of the section of the navigation channel and the distance from the dredged material placement site to the section of the navigation channel. The distance given for grid block 5, and all remaining grid blocks, is the shortest distance along the river from the navigation channel to the dredge material placement site.

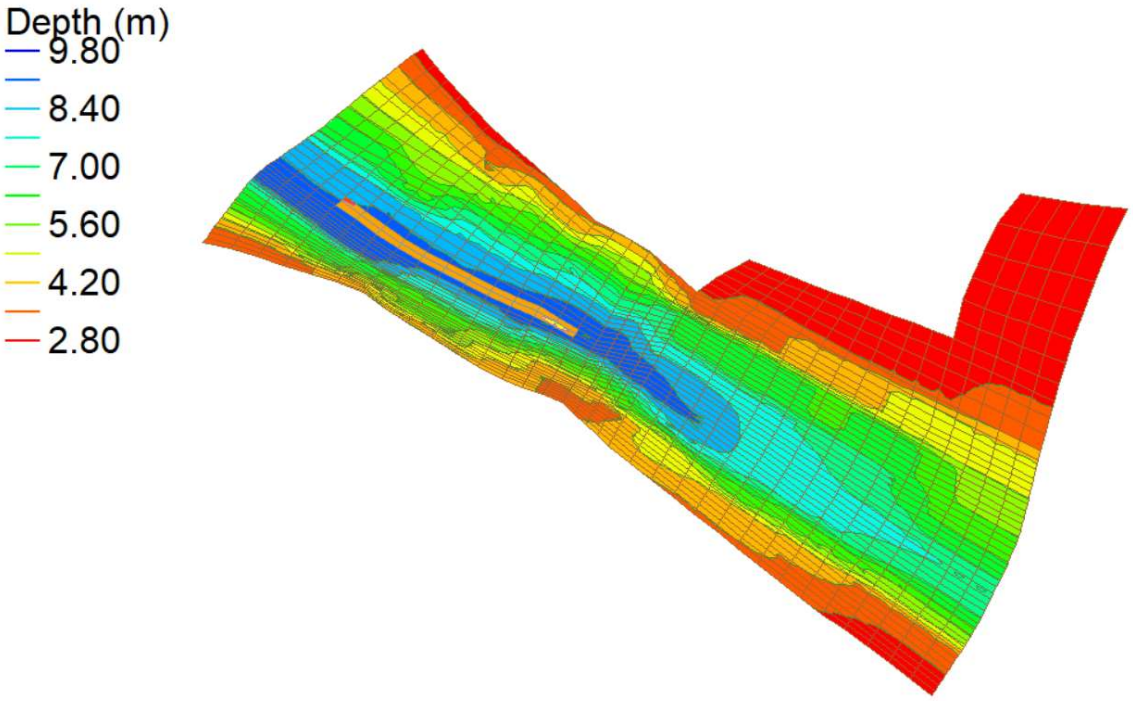

Figure 5.6: Section of the Navigation Channel Represented by the Orange Highlighted Cells in Grid Block 5

Table 5.1: Parameters of Cells Representing the Navigation Channel in Grid Block 5

	Navigation Channel in Grid Block 5
Area (m^2)	157,000
Shortest Distance from Placement Site (km)	10.5

Figure 5.7 shows the time series of total mud aggregate mass in the highlighted cells representing the navigation channel, as shown in Figure 5.6, as well as the average bed shear stress in the highlighted cells representing the navigation channel. Figure 5.7 also indicated it took between three to four days for the mud aggregates to be transported to the analyzed sections. As expected, the amount of mass of mud aggregates in the channel is consistently less when abrasion is being simulated than when abrasion is not being simulated. As defined by the developed abrasion routine, the 3,500 μm and 300 μm aggregate size classes are transported as bedload, mass is transferred from the larger aggregate size class to the next smallest aggregate size class and to the 20 μm aggregate size class. The smaller aggregate size classes are less likely to deposit on the sediment bed, so as the abrasion of aggregates in bedload results in a decrease in mass of larger sized aggregates in bedload and an increase of mass of smaller sized aggregates in suspension, the combined mass of all four aggregate size classes in the sediment bed decreases. During high and low tides in the 15-day simulation, the mass of mud aggregates in the sediment bed decreased an average of approximately 63% when abrasion was being simulated.

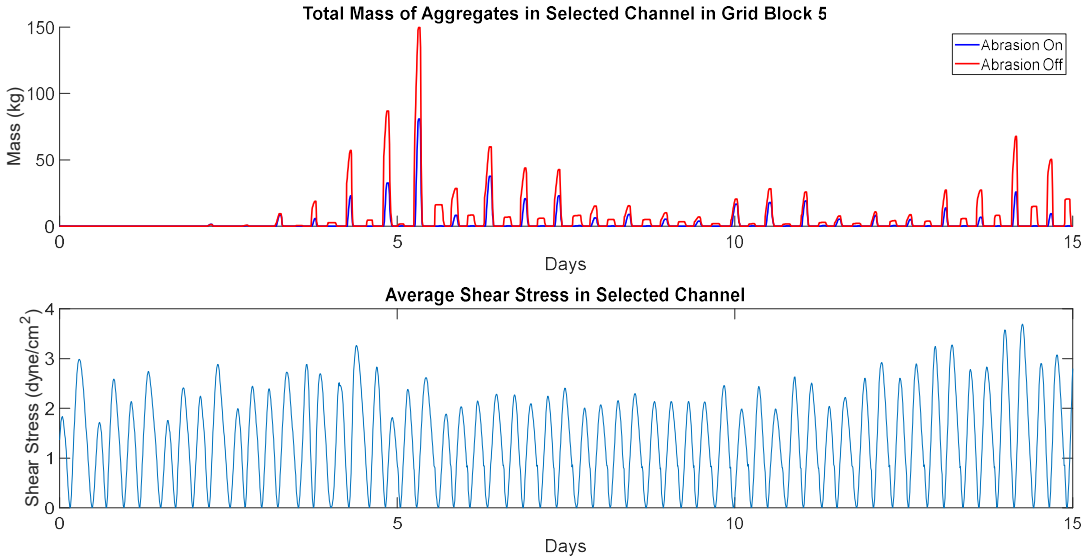

Figure 5.7: Total mass in Cells Representing Navigation Channel and Average Bed Shear Stress of Cells Representing Navigation Channel in Grid Block 5

Figure 5.8 shows the relationship between the tidal and riverine hydrodynamics in the James River and the mass of mud aggregates in the bed at the selected cells in grid block 5. The oscillation of the bed shear stress is due to the tidal cycles. As can be seen, at high tide and low tide the bed shear stresses are at a minimum. When the bed shear stress is at a minimum, the sediment that is being transported as bedload or suspended load deposits on the sediment bed. Figure 5.8 confirms that at the times when the mass of aggregates in the bed is at a maximum, the bed shear stress is at or near a minimum. This relationship between the hydrodynamics in the James River and the mass of aggregates in the bed is consistent with the remaining results, so Figure 5.8 is the only example given of this relationship.

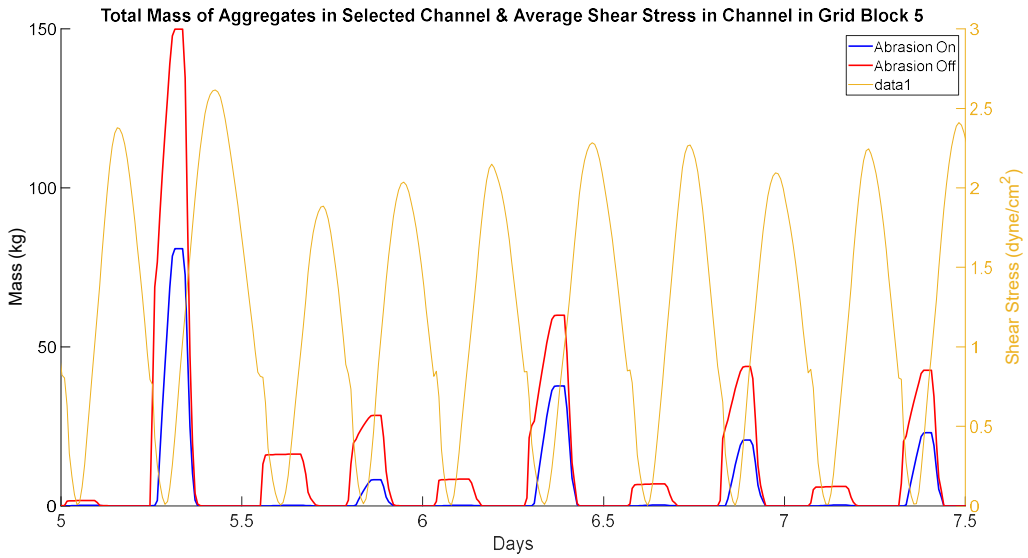

Figure 5.8: Total Mass of Aggregates in Cells Representing Navigation Channel and Average Shear Stress in Cells Representing Navigation Channel in Grid Block 5

The second upstream portion of navigation channel analyzed was in grid block 6 and is represented by the red highlighted cells in Figure 5.9. Table 5.2 gives the area of the highlighted cells and their shortest distance from the placement site.

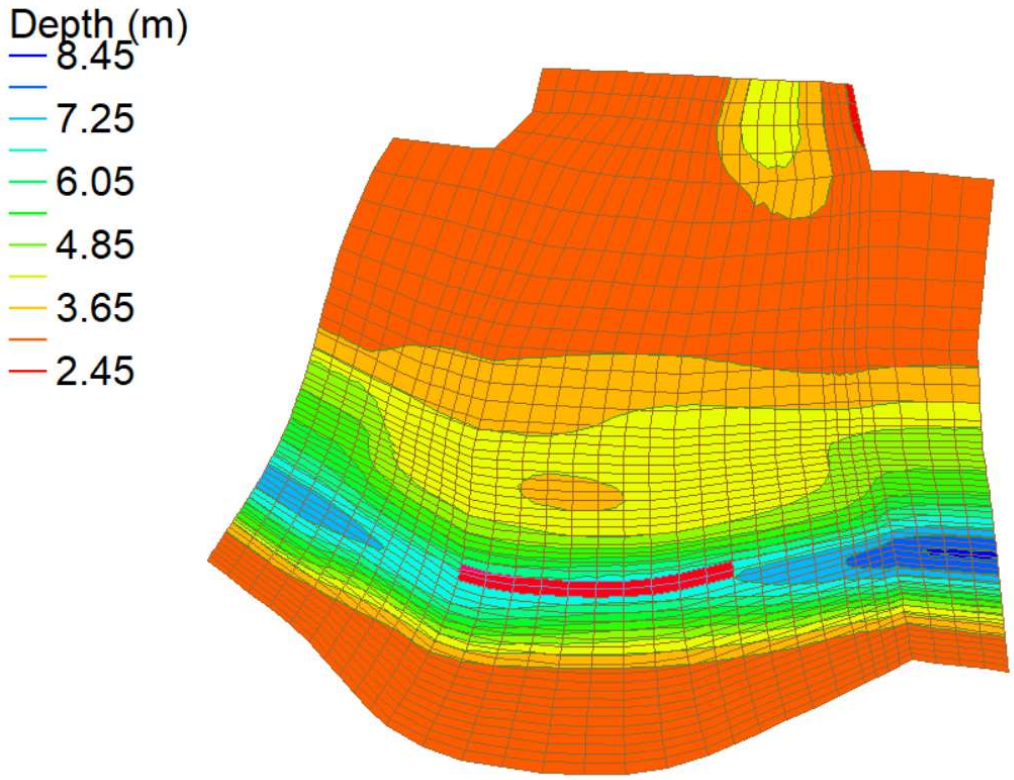

Figure 5.9: Section of the Navigation Channel Represented by the Red Highlighted Cells in Grid Block 6

Table 5.2: Parameters of Cells Representing the Navigation Channel in Grid Block 6

	Navigation Channel in Grid Block 6
Area (m^2)	255,300
Shortest Distance from Placement Site (km)	3.7

Figure 5.10 shows the amount of mud aggregate mass in the cells highlighted in Figure 5.9 as well as the average bed shear stress over the 15-day simulation. Figure 5.10 shows that it took around one day for the mud aggregates to be transported to the

analyzed cells. Consistent with previous results, the amount of mud aggregate mass in the sediment bed of the analyzed cells is smaller when abrasion is being simulated compared to when abrasion is not being simulated. As the largest two aggregate size classes were transported at bedload, mass was lost due to abrasion and was transferred to the next smallest aggregate size class as well as the 20 µm aggregate size class. Smaller aggregates were less likely to deposit, therefore there was less overall mass of the four mud aggregates size classes in the sediment bed in the highlighted cells due to the transfer of mass from the largest two aggregate size classes in bedload to smaller aggregates size classes. Throughout the 15-day simulation, abrasion attributed to the loss of an average of approximately 54% of the mass of the four mud aggregate size classes in the sediment bed when measured at high and low tides.

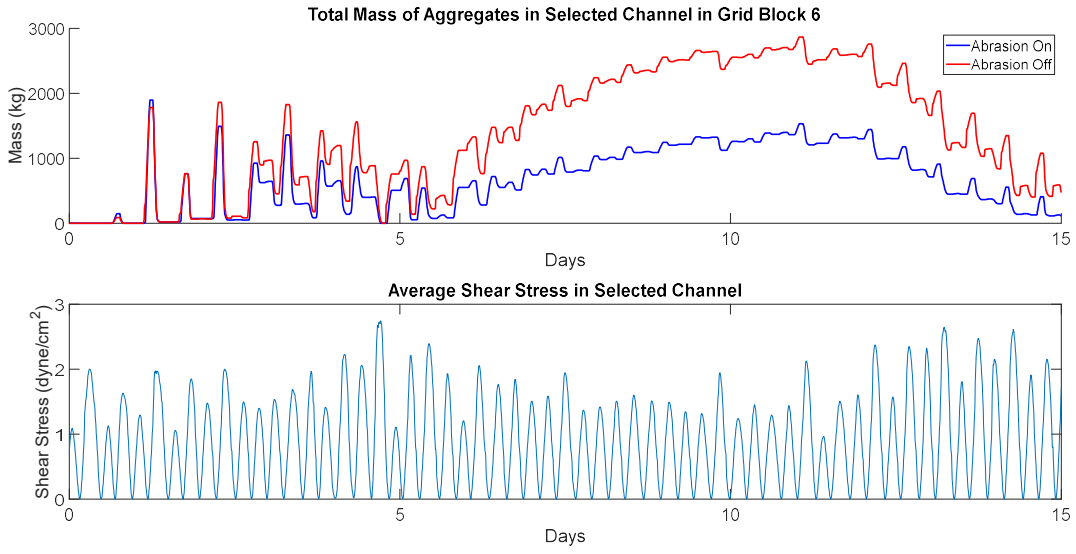

Figure 5.10: Total mass in Cells Representing Navigation Channel and Average Bed Shear Stress of Cells Representing Navigation Channel in Grid Block

The first portion of the navigation channel analyzed downstream of the placement site is in grid block 9 and is indicated by the highlighted orange and red cells shown in Figure 5.11. Table 5.3 gives the area of the highlighted channel and its shortest distance from the placement site.

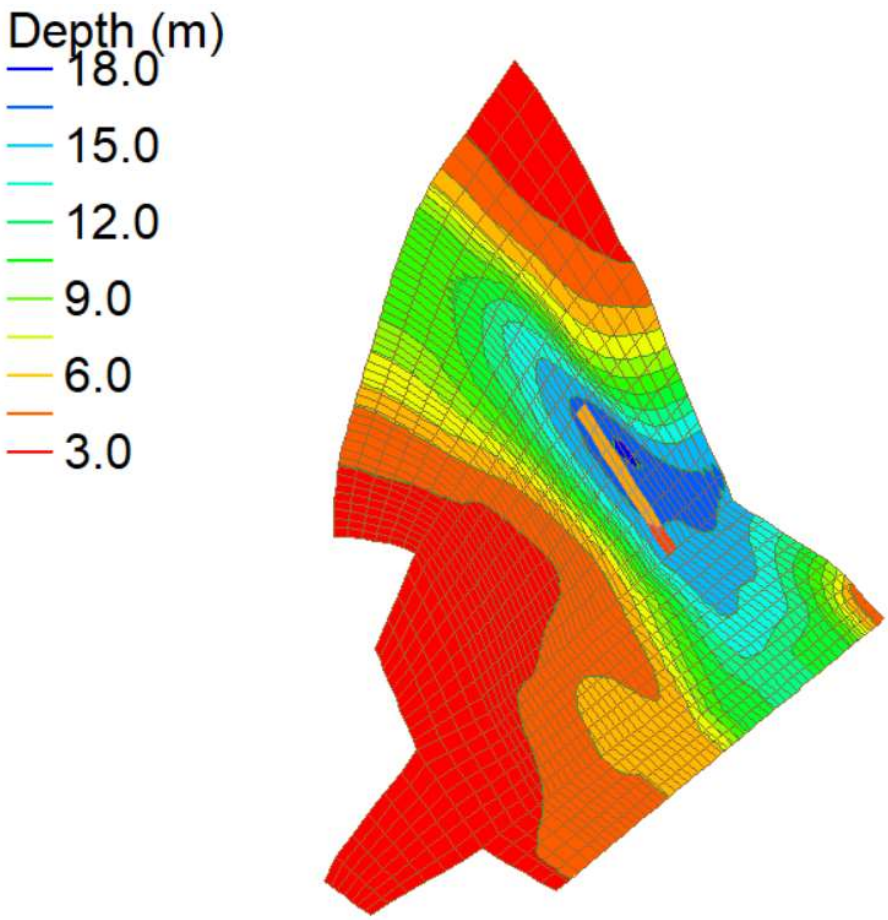

Figure 5.11: Section of the Navigation Channel Represented by the Orange and Red Highlighted Cells in Grid Block 9

Table 5.3: Parameters of Cells Representing the Navigation Channel in Grid Block 9

	Navigation Channel in Grid Block 9
Area (m^2)	88,000
Shortest Distance from Placement Site (km)	1.3

Once again, as expected, the total mass of mud aggregates in the highlighted grid cells in the navigation channel in grid block 9 was less when abrasion was being simulated than when abrasion was not being simulated (see Figure 5.12). It took the mud aggregates less than a day to reach the analyzed cells. Another observation is that while simulating abrasion caused a decrease of approximately 50% to 65% of the mass of the four mud aggregate size classes in the sediment bed for the upstream grid cells when measured at high and low tides, the channel in grid block 9, which is downstream of the placement site, the mass of the four mud aggregate size classes decreases an average of approximately 75% when abrasion is being simulated. As shown in Figure 5.13, the bed shear stress and average velocity was greater downstream of the placement site which did not allow for as much deposition to occur. The deposition of suspended load is a function of flow velocity and the probability of deposition of bedload is a function of bed shear stress, therefore higher flow velocities and higher bed shear stress resulted in less deposition downstream of the placement site.

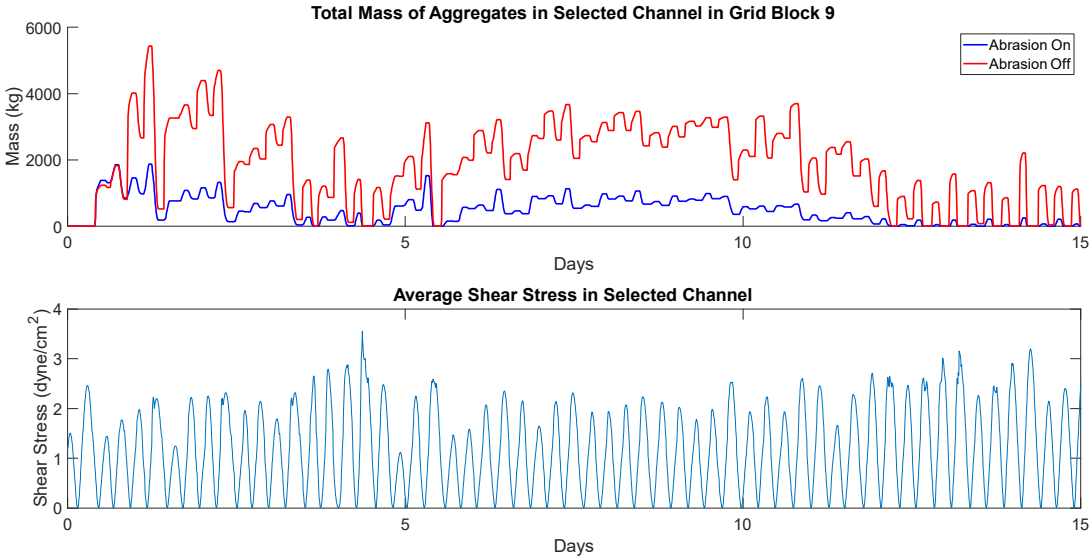

Figure 5.12: Total mass in Cells Representing Navigation Channel and Average Bed Shear Stress of Cells Representing Navigation Channel in Grid Block 9

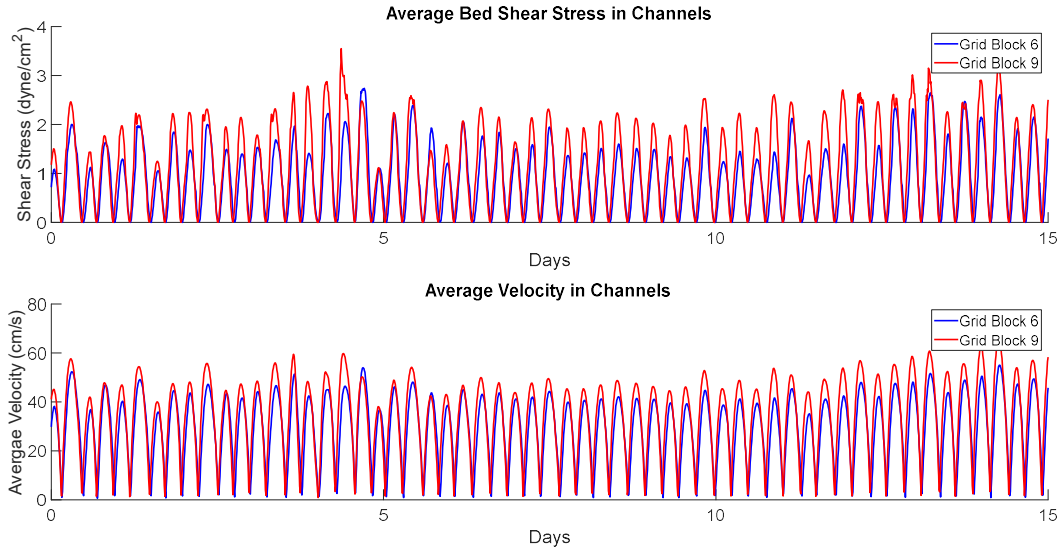

Figure 5.13: Average Shear Stress and Velocities in Grid Block 6 and Grid Block 9

The last portion of the navigation channel that was analyzed was located in grid block 10, and is highlighted orange, red and pink as shown in Figure 5.14. Table 5.4 gives the area of the highlighted channel and its distance from the placement site.

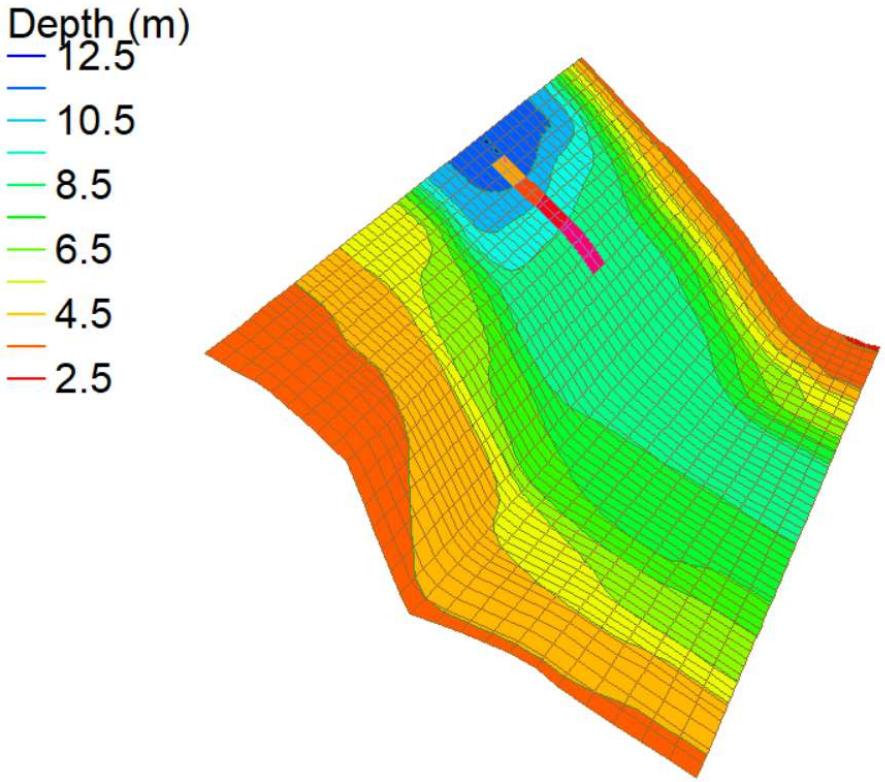

Figure 5.14: Section of the Navigation Channel Represented by the Orange and Pink Highlighted Cells in Grid Block 10

Table 5.4: Parameters of Cells Representing the Navigation Channel in Grid Block 10

	Navigation Channel in Grid Block 10
Area (m^2)	71,600
Shortest Distance from Placement Site (km)	8.7

Similar to previous results, when abrasion was being simulated there was less mud aggregate mass in the bed compared to when abrasion was not being simulated. This was again due to the trasnfer of mass from aggregtaes in bedload to smaller aggregates that were less likely to deposit. Even when the analzyed portion of the channel was a far distance downstream, 8.7 km, the results were consistent with previous findings. During high and low tides in the 15-day simulation, the mass of mud aggregates in the sediment bed decreased an average of approximately 76% when abrasion was being simulated.

An area farther downstream than these analzyed cells will be analzyed later in this thesis.

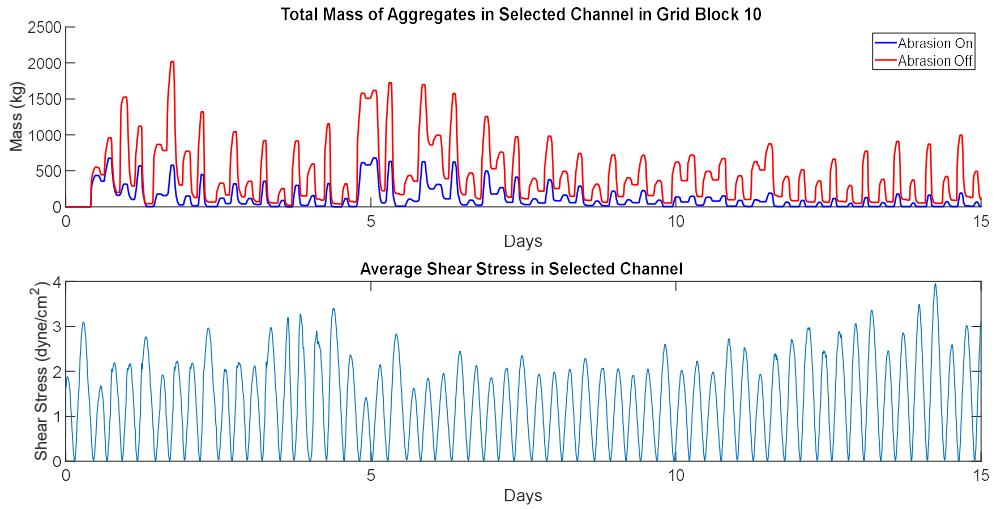

Figure 5.15: Total mass in Cells Representing Navigation Channel and Average Bed Shear Stress of Cells Representing Navigation Channel in Grid Block 10

Like the 1-D sediment transport model, simulated bed shear stresses in the James River GSMB model were never strong enough to transport the 3,500 µm aggregate size class in suspension. However, the 300 µm aggregate size class was transported in suspension and as bedload. Neither the 80 µm nor 20 µm aggregate size class were transported as bedload. Since the 3,500 µm aggregate size class was only located in the placement site initially, and was only transported as bedload, then when abrasion was being simulated, the aggregate should not be able to travel more than a few kilometers before being losing over 95% of its mass. The same observation could be made for the 300 µm aggregate size class but note that not all of the 300 µm aggregate size class was transported as bedload, meaning it could be transported as suspended load and detected many kilometers form the placement site. By analyzing the bedload concentration of

mud aggregates within a few kilometers of the placement site, it can be shown that a high percentage, more than 95%, of mass is lost by aggregates in bedload within the first few kilometers of transport.

Figure 5.16 shows the dredged material placement site in grid block 8 along with two yellow boundaries. The bedload concentrations for the 3,500 μm and 300 μm aggregate size classes were measured at these two boundaries to prove that these aggregates being transported as bedload loses over 95% its mass close to the placement site. The average distance to the upstream boundary is 2.2 km and the average distance to the downstream boundary is 1.2 km. The distances were measured from the center of area of the placement site to each boundary.

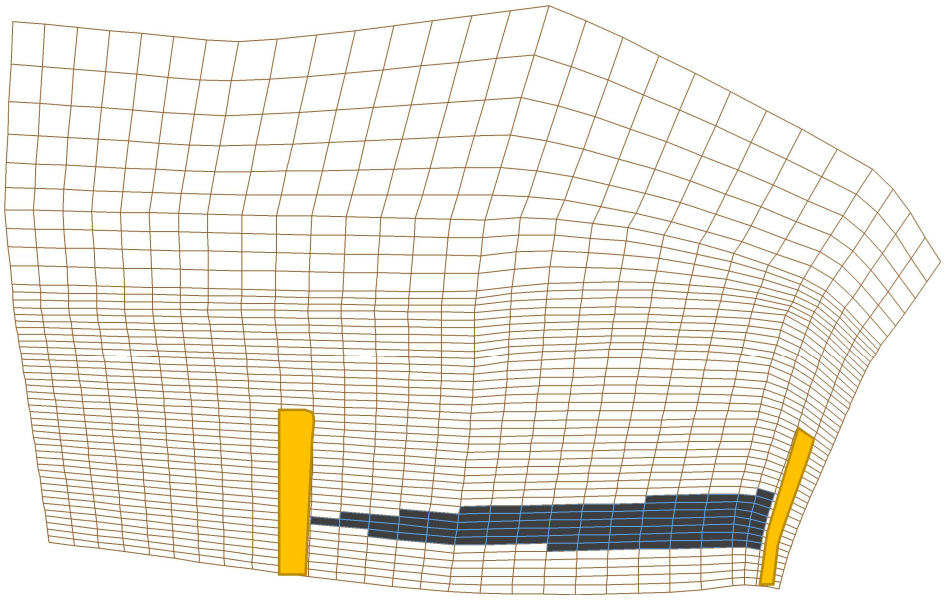

Figure 5.16: Dredge Material Placement Site and Two Boundaries

Figure 5.17 shows the average bedload concentration of the 3,500 µm size class at the left boundary as shown in Figure 5.16. There is little to no concentration at the left boundary because the bed shear stress only reaches the critical shear stress for erosion of the 3,500 µm aggregate size class twice during the 15-day simulation. Even so, the bedload concentration for the 3,500 µm size class is decreased by 20% when abrasion is being simulated compared to when abrasion is not being simulated. The explanation for the relatively small decrease in bedload concentration is that while the left boundary is 2.2 km from the center of area of the placement site, the cells on the far left of the placement site experienced bed shear stresses high enough to erode and transport the 3,500 µm mud aggregate size class less than a few hundred meters to the left boundary.

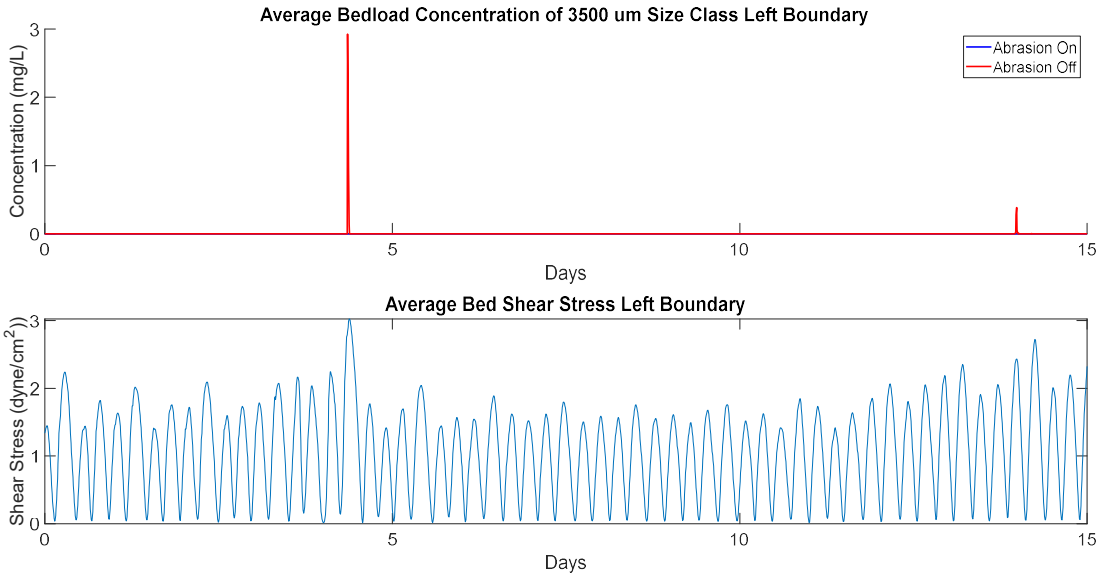

Figure 5.17: Average Bedload Concertation of 3,500 µm Aggregate Size Class and Average Shear Stress at Left Boundary

Figure 5.18 shows the average bedload concertation of the 300 µm size class along the left boundary. The bedload concentration of the 300 µm size class when abrasion is being simulated is decreased by an average of over 95% compared to when abrasion is not being simulated. The average distance from the placement site to the left boundary was 2.2 km, so the results shown in Figure 5.18 infers that after a few kilometers, over 95% of the mass of 300 µm mud aggregates is abraded to smaller aggregate size classes which are always transported in suspension, which was expected based on the mud aggregate abrasion experiments, with results shown in Figure 3.2, and the simple abrasion simulation shown in Figure 3.5.

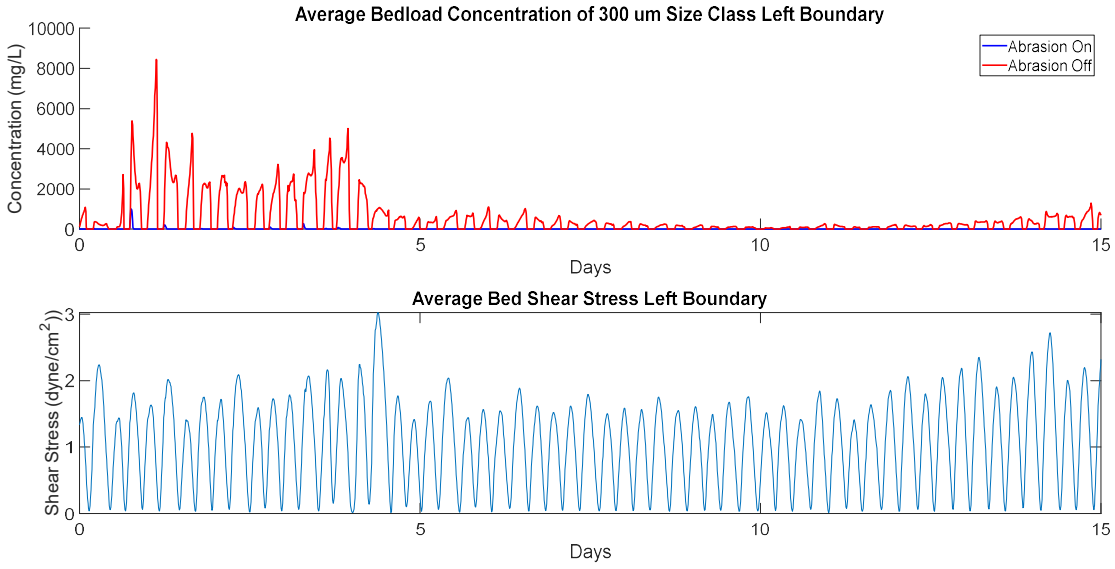

Figure 5.18: Average Bedload Concertation of 300 µm Aggregate Size Class and Average Shear Stress at Left Boundary

At the right boundary, Figure 5.19 shows once again there were very few occasions when the bed shear stress was great enough to transport the 3,500 µm size class as bedload. When abrasion was being simulated the concentration of the 3,500 µm aggregate size class was decreased by an average of over 99% than when abrasion was not being simulated.

Figure 5.19: Average Bedload Concertation of 3,500 µm Aggregate Size Class and Average Shear Stress at Right Boundary

The 300 µm aggregate size class bedload concentration at the right boundary shows similar results to what was seen at the left boundary. The average distance to the right boundary from the dredged material placement site was 1.2 km, and Figure 5.20 shows that an average of over 95% the mass of the 300 µm aggregate size class in bedload had been lost due to abrasion before reaching the right boundary.

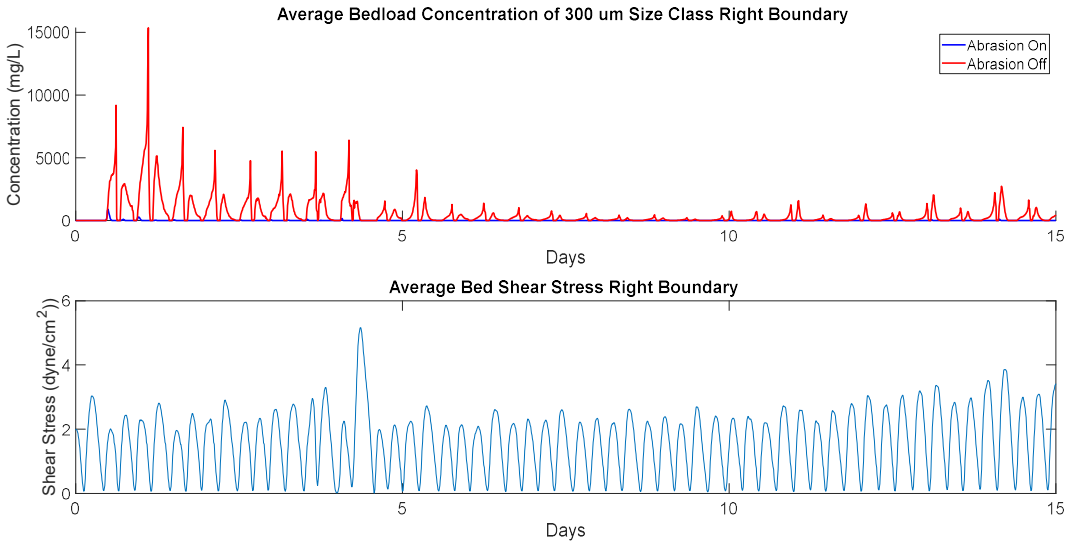

Figure 5.20: Average Bedload Concertation of 300 µm Aggregate Size Class and Average Shear Stress at Right Boundary

The last analysis performed using the output of the GSMB model run with both abrasion and no abrasion compared the mass of aggregates transported at a distance approximately 15 km downstream of the placement site. The area that was analyzed was also the location of a group of oyster leases. An oyster lease is issued for a section of riverbed where oysters are located. Another analysis performed on this area was if the suspended sediment concentration of the 20 µm aggregate size class, the byproduct of the abrasion process, was large enough to be detrimental to the oysters 15 km from the dredged material placement site. The group of oyster leases closest to the dredged material placement site were chosen, and this area shown in the red rectangle in Figure 5.21.

Figure 5.21: Satellite View of Oyster Leases

The location of this group of oyster leases is in grid block 14, which is shown in relation to the placement site, grid block 8, in Figure 5.22.

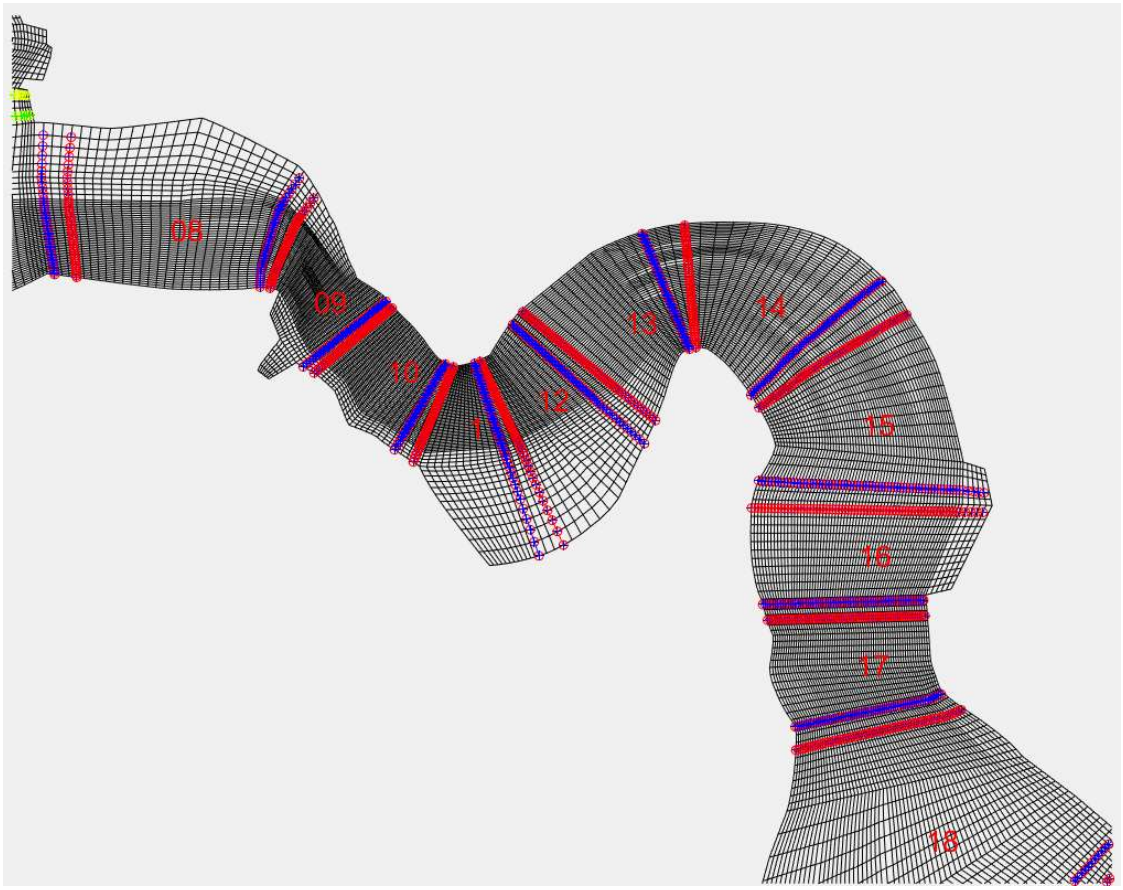

Figure 5.22: Grid Blocks near Oyster Leases

Figure 5.23 shows the specific cells that will be considered a part of the oyster leases. The total area of these cells is 7.22 km^2. The analysis performed on these cells will consist of finding the total mass of mud aggregates in the bed as well as finding depth averaged suspended sediment concentrations over the 15-day simulation.

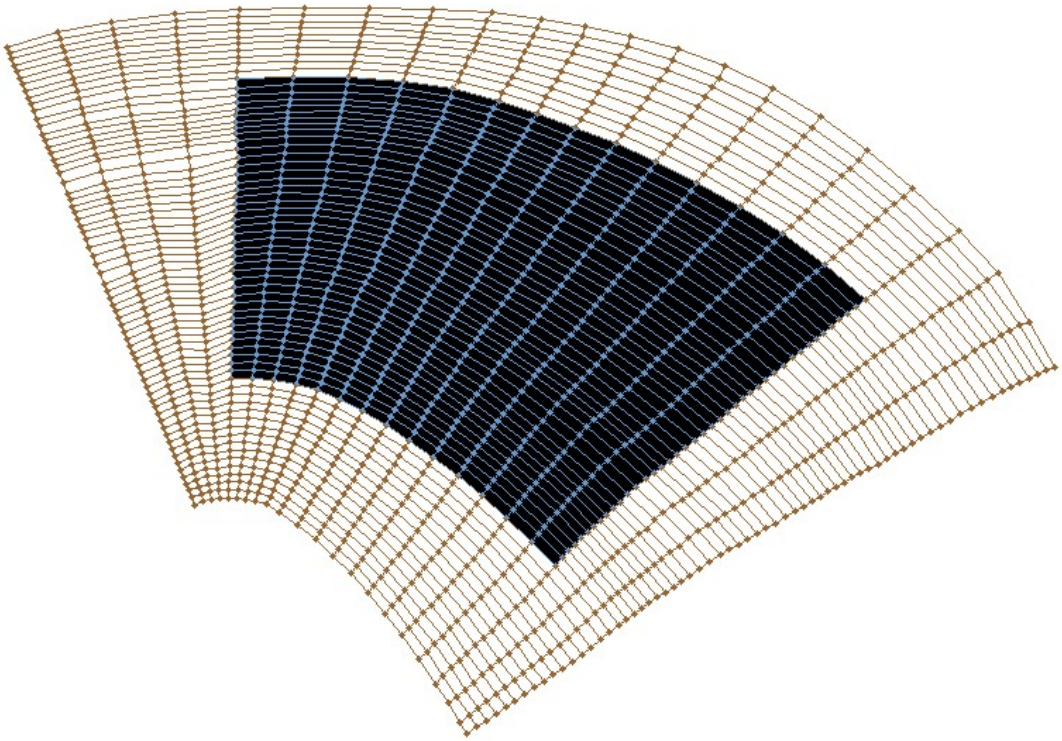

Figure 5.23: Cells in Grid Block 14 Associated with the Oyster Leases

The first result determined was how the simulation of abrasion effected the total mass of aggregates in the area of interest. Figure 5.24 shows how adding abrasion to the simulation decreased the total mass of aggregates in the bed by an average of approximately 60%. These results are consistent with the findings from the analysis of the aggregate mass in the channels. As explained earlier, the abrasion routine simulates abrasion by transferring mass from larger aggregate size classes transported as bedload to smaller aggregate size classes primarily transported in suspension. Since smaller aggregate size classes are less likely to deposit, there is an overall decrease of mass of aggregates in the bed.

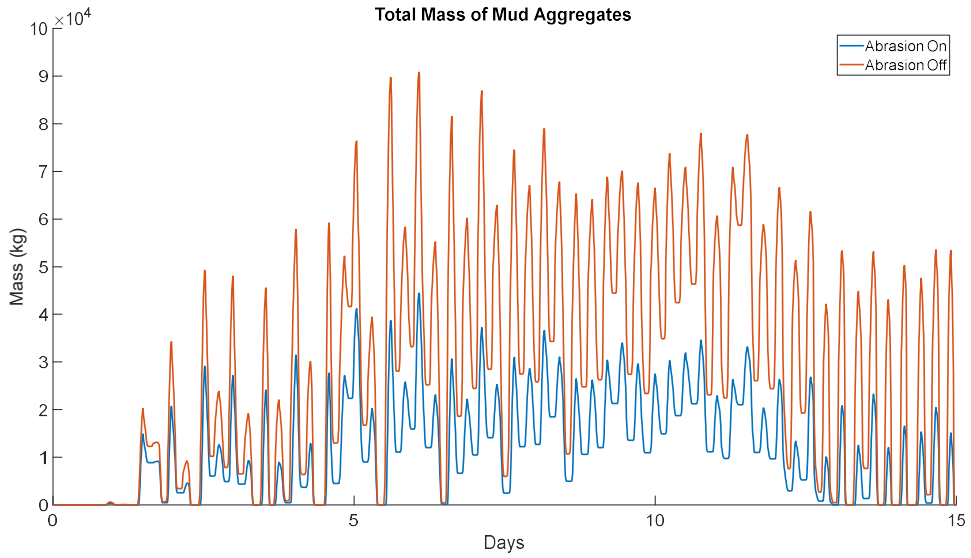

Figure 5.24: Mass of Mud Aggregates in Bed in Area of Interest

To better show the effects of adding an abrasion routine to the sediment transport model, the mass of individual size classes in the sediment bed in the area of interest were analyzed. Figure 5.25 shows the mass of the 300 µm size class in the bed in the cells defined in Figure 5.23. As concluded earlier, the 300 µm aggregate size class only traveled a few kilometers before mostly being abraded to smaller aggregate size classes. At approximately 15 km away from the placement site, there is substantially less mass of the 300 µm aggregate size class in the sediment bed when abrasion is being simulated than when abrasion is not being simulated. This is because at 15 km away from the placement site, most of the 300 µm aggregate size class had undergone abrasion during transport. Figure 5.25 shows that at distances far away from the dredge material placement site, aggregates that travel as bedload are not abundant because they

underwent abrasion during transport. For the case of the 300 µm aggregate size class, there is still a small amount of mass in the bed 15 km from the placement site because some of this sized aggregate can travel in suspension.

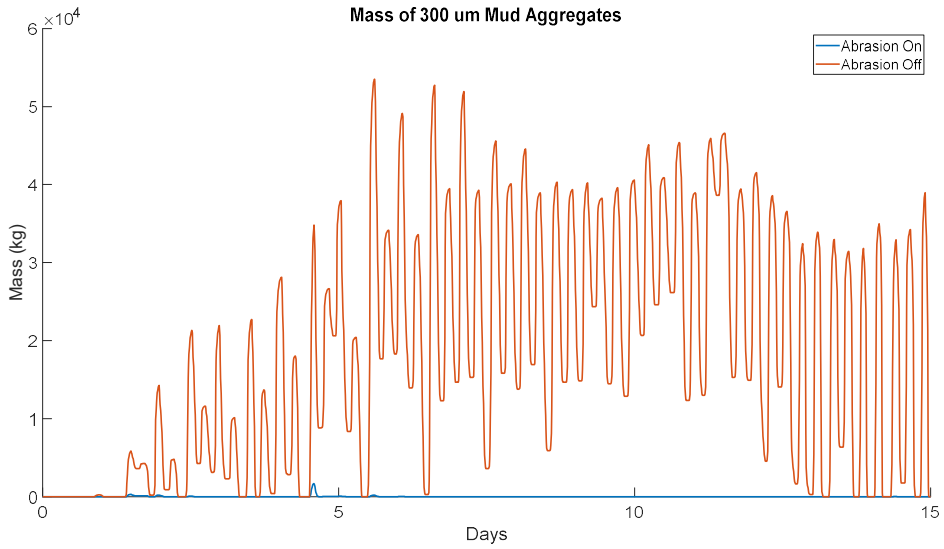

Figure 5.25: Mass of 300 µm Aggregate Size Class in Bed in Area of Interest

Figure 5.26 shows the mass of the 80 µm aggregate size class in the bed for the area defined in Figure 5.23. Since the 80 µm aggregate size class only travels in suspension, it never loses mass due to abrasion. The 80 µm aggregate size class does however gain mass due to abrasion of the 300 µm aggregate size class defined by the sink and source terms in Equations (3.17) and (3.18). Therefore, in Figure 5.26, there is an approximately 5% increase in mass in the bed for the 80µm aggregate size class when abrasion is being simulated then when abrasion is not being simulated, which is not a significant increase.

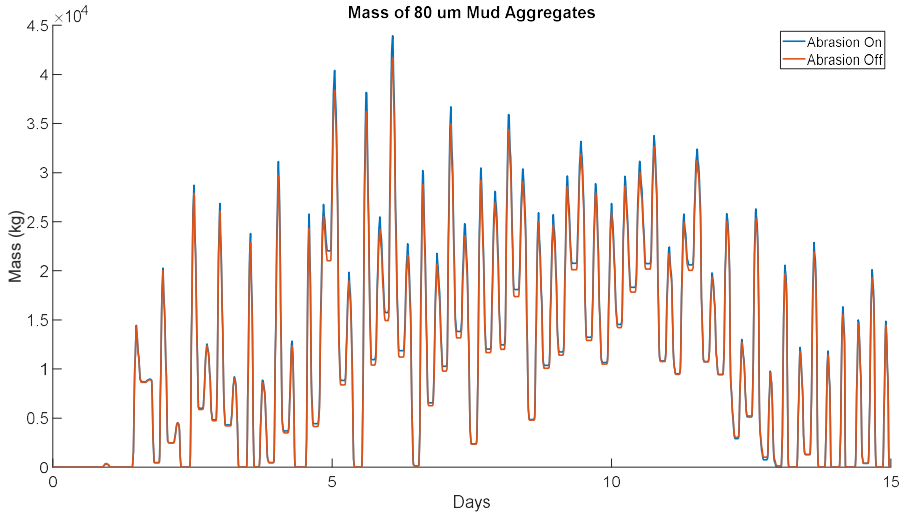

Figure 5.26: Mass of 80 µm Aggregate Size Class in Bed in Area of Interest

The above analysis shows specifically how abrasion effects the mass of mud aggregates in the sediment bed at distances such as 15 km away from the placement site. Simulating abrasion in the model consistently showed that aggregates transported as bedload lost over 95% of its mass due to abrasion within a few kilometers of the dredged material placement site. As abrasion caused a decrease in mass of larger sized aggregates and an increase in mass of smaller sized aggregates, there was a decrease in mass of aggregates deposited in the bed because smaller aggregates were less likely to deposit.

The effects of suspended sediment concentration on oysters in the James River was studied by Suedel *et al.* (2014). Suedel *et al.* tested oysters at different suspended sediment concentrations to determine if exposure to high concentrations effects oyster survival, growth and condition index. Condition index is a way to measure oyster meat

quality. Suedel *et al.* experimented with suspended sediment concentrations up to 500 mg/L and found that oysters in the James River can withstand this concentration for a few days with no effects on the oysters (Suedel *et al.,* 2014). The 500 mg/L concentration gives a reference for what the suspended sediment concentration of the 20 µm aggregate size class would have to be to adversely affect oysters in the James River.

Figure 5.27 shows the depth averaged and area averaged suspended sediment concentration for the 20 µm aggregate size class in the oyster leases as well as the suspended sediment concentration for the bottom most water column layer for the 20 µm aggregate size class in the area shown in Figure 5.23.

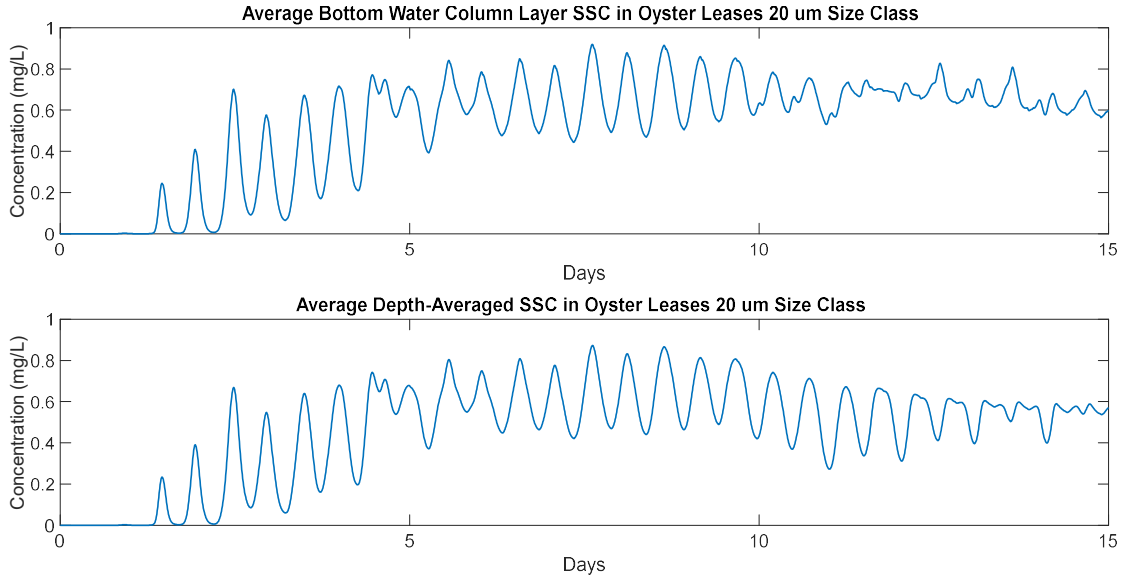

Figure 5.27: Average SSC of 20 µm Aggregate Size Class in Oyster Leases

As seen in Figure 5.27, the suspended sediment concentration of the 20 μm size class never approaches the 500 mg/L concentration needed to adversely affect oysters in the James River. Even if suspended sediment concentration of other dredged material aggregate size classes or native material sediment size classes to the James River was close to 500 mg/L, adding the abrasion routine to the model would not increase the suspended sediment concentration around the oyster leases to a concentration that would be harmful to the oysters.

Figure 5.28 shows the depth averaged and area averaged suspended sediment concentration of the 80 μm aggregate size class as well as the suspended sediment concentration for the bottom most water column layer of the 80 μm aggregate size class for the area shown in Figure 5.23. When abrasion was simulated there was a slight increase in suspended sediment concentration of the 80 μm aggregate size class due to the abrasion of the 300 μm aggregate size class in bedload, but the increase in concentration was not significant. Like the 20 μm aggregate size class, adding the abrasion routine to the sediment transport model does not increase suspended sediment concentration enough to adversely affect the oysters in the area defined in Figure 5.23.

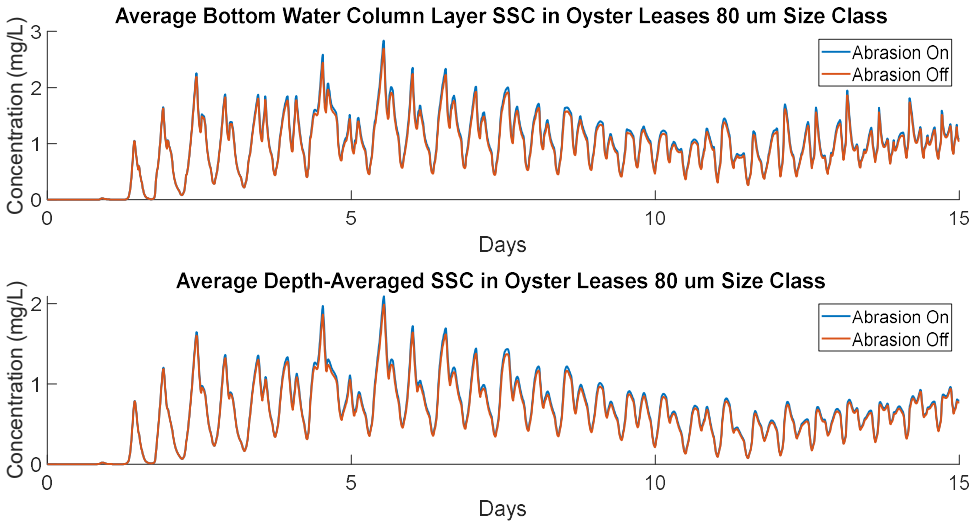

Figure 5.28: Average SSC of 80 µm Aggregate Size Class in Oyster Leases

CHAPTER 6

CONCLUSIONS AND RECOMENDATIONS

Previous research revealed that placed dredge material was frequently eroded as mud aggregates as opposed to individual particles (Perkey *et al.,* 2019). Mud aggregates collected in the James River, VA estuary were tested in the sediment laboratory at the U.S. Army Coastal and Hydraulics Laboratory in Vicksburg, MS and found to undergo abrasion when being transported as bedload (Perkey *et al.,* 2019). Abrasion is not currently simulated in sediment transport models as very little research had been performed on this process and it was not considered to significantly alter the simulation results. As shown in the results from Chapter 4 and Chapter 5, simulating the abrasion of aggregates in sediment transport models effects the bedload and suspended load concentrations of mud aggregates and the total mass of mud aggregates in the sediment bed in waterways such as estuaries, rivers, and reservoirs where they are commonly found.

CONCLUSIONS

1) When the abrasion routine was included in the developed 1-D sediment transport model and the existing GSMB model of the James River, the overall mass of mud aggregates in bedload decreased while the overall mass mud aggregates in suspended load increased. As the mud aggregates in bedload transport were undergoing abrasion, mass was transferred to the next smallest aggregate size

class and a 20 μm aggregate size class. This was significant because the smaller mud aggregate size classes were less likely to deposit, therefore there was less mass of mud aggregates in the sediment bed when abrasion was being simulated. In analyzed sections of the navigation channel, both upstream and downstream of the placement site, the use of the abrasion routine in the 3-D sediment transport model included in the GSMB model of the James River decreased the mass of mud aggregates in the sediment bed, compared to the simulation without abrasion, by the average percentages given in Table 6.1.

Table 6.1: Average Percent Decrease in Mass of Mud Aggregates in Sediment Bed When Abrasion was Being Simulated at Analyzed Portions of the Navigation Channel (Measured from Closest Distance from Placement Site to Analyzed Cells)

	10.5 km upstream	3.7 km upstream	1.3 km downstream	8.7 km downstream
Percent Decrease	63%	53%	75%	76%

As shown in Table 6.1, the effect that abrasion has on the simulation of mud aggregates transported from the placement site are greater downstream of the placement site, as higher flow velocities downstream of the placement site

decreased the amount of deposition into the analyzed portions of the navigation channels.

2) Prior research showed that mud aggregates could only travel a few kilometers before losing over 95% of their effective diameter due to abrasion (Perkey *et al.* 2019). This research was confirmed in the results from the 3-D model of the James River when comparing a loss of mass instead of a loss of effective diameter. At distances of 1.2 km and 2.2 km from the center of area of the placement site, adding abrasion of mud aggregates to the simulation caused a decrease of over 95% of the bedload concentrations of the 3,500 μm and 300 μm mud aggregate size classes at both distances when observed at each time step compared to the simulation without abrasion.
3) At the end of a 15-day simulation of sediment transport in the James River using a 3-D sediment transport model, there was 233 kg of mud aggregates in the dredged material placement site when abrasion was added to the sediment transport model and 12,050 kg when abrasion was not being simulated. Both masses were less than 1% of the initial mass of mud aggregates in the placement site, indicating that after the 15-day simulation, there was not a significant difference, relative to the initial mass, between the mass of mud aggregates in the placement site during the simulation with and without abrasion. However, one day into the simulation, the difference between the mass of mud aggregates in the placement area during the simulations with and without abrasion of mud aggregates was approximately

25%. This indicates that the percent difference between the two simulation can be significant at certain times and conditions.

4) The addition of the abrasion routine did not increase the suspended sediment concentration to the magnitude that it would harm the oysters located approximately 25 km from the dredged material placement site

RECOMMENDATIONS

1) While the research by Perkey and Smith provided abrasion coefficients for the James River and other locations around the United States, more research needs to be completed to ensure the accuracy of the abrasion coefficients. Continued research similar to Perkey *et al.* (2019) also needs to be completed to explore the correlations between abrasion coefficients and sediment characteristics. The abrasion coefficients that are available from their research, along with future experimentally found abrasion coefficients from other locations, need to be validated using specialized equipment that can measure the changes of aggregates due to abrasion to calibrate the abrasion coefficients used in the abrasion routine. Ideally, in the future, there will be a database of abrasion coefficients for a variety aggregates in rivers and estuaries across the country. Continued research to determine accurate abrasion coefficients is essential to the future accuracy and use of the abrasion routine.
2) There needs to be coordination with the USACE to determine if the decrease in predicted mass of mud aggregates in navigation channels when the abrasion

routine is included in existing sediment transport models is significant. In the 15-day simulation completed in this thesis, the mass of mud aggregates transported from the dredge material placement site into the sediment bed of the navigation channel decreased by as much as 75%. This information needs to be given to the USACE for them to determine if it useful.

3) There needs to be coordination with the USACE to determine if the results from the simulation including the abrasion routine more accurately portrayed the mass of mud aggregates in the navigation channel compared to the results of the simulation without abrasion. For instance, the USACE could determine if the mass dredged from the navigation channel was more or less than what they prepared for based on existing sediment transport models without the simulation of abrasion of aggregates. This information along with the first recommendation can help calibrate the abrasion routine to provide more accurate results.

REFERENCES

ADCIRC. Retrieved from adcirc.org

Engineering Research and Development Center (ERDC). (2014). CE-QUAL-ICM (ICM). Retrieved from https://www.erdc.usace.army.mil/Media/Fact-Sheets/Fact-Sheet-Article-View/Article/547416/ce-qual-icm-icm/

Fettweis M, Baeye M, Francken F, Lauwaert B, Van den Eynde D, Van Lancker V, Martens C, Michielsen T. (2011). Monitoring the effects of disposal of fine sediments from maintenance dredging on suspended particulate matter concentration in the Belgian nearshore area (southern North Sea).

Guillou, S., Thiebot, J., Romuald Verjus, J. C., Besq, A., Hau, D., & Se, K. (2011). The Filling Dynamics of an Estuary: From the Process to the Modelling. In *Sediment Transport in Aquatic Environments*. InTech. http://dx.doi.org/10.5772/19933

Hayter, Earl. (2013). *Fundamentals and Modeling of Cohesive Sediment Transport*

Hayter, E., Kim, S., Lackey, T. (2020). *Life Cycle Analysis of Dancing Point-Swann Point, Goose Hill Shoal, and Tribell Shoal Placement Sites*

Jones, Craig., Lick, William. (2001). SEDZLJ: A Sediment Transport Model.

Mehta, A., 2014. *An Introduction To Hydraulics Of Fine Sediment Transport*. New Jersey, N.J.: World scientific.

Parker, Gary. (1991). Selective Sorting and Abrasion of River Gravel. *Journal of Hydraulic Engineering, 117(2)*

Perkey, D. W., Smith, S. J., Fall. (2019). Cohesive Sediment Field Study: James River, Virginia. *ERDC Coastal and Hydraulics Laboratory Data Report*

Perkey, D. W., Smith, S. J. (2020). Impacts of Mud Aggregate Processes in Sediment Transport Studies. *ERDC Coastal and Hydraulic Laboratory Technical Note*

Perkey, D. W., Smith, S. J., Fall, K. A., Massey, G. M., Friedrichs, C. T., & Hicks, E. M. (2020). Impacts of Muddy Bed Aggregates on Sediment Transport and Management in the Tidal James River, VA. *Journal of Waterway, Port, Coastal, and Ocean Engineering, 146*(5)

Perkey, D. W., Smith, S. J., Fall, K. A., Massey, G. M., Friedrichs, C. T., & Hicks, E. M. (2020). *Physical Factors that Influence Muddy Bed Aggregate Production, Size and Durability*

Smith, S. J. (2020) Personal Communication [Personal Interview].

Smith, S.J., Fall, K.A. (2020). *Weathering of Cohesive Mud Aggregates by Bedload Trasnport.* AGU Ocean Sciences Meeting.

Suedel, B. C., Clarke, J. U., Wilkens, J., Lutz, C. H., & Clarke, D. G. (2014). The Effects of a Simulated Suspended Sediment Plume on Eastern Oyster (Crassostrea

virginica) Survival, Growth, and Condition. *Estuaries and Coasts*, *38*(2), 578–589. https://doi.org/10.1007/s12237-014-9835-0

van Rijn, L. C. (1987). Sediment Transport, Part I: Bed Load Transport ” (October, 1984, Vol. 110, No. 10). *Journal of Hydraulic Engineering*, *9*, 1189–1190.